Technical Report Documentation Page

1. Report No.	2. Government Accession No.	3. Recipient's Catalog No.
FHWA/TX-08/0-5798-1		

4. Title and Subtitle	5. Report Date
A REVIEW OF PERFORMANCE MODELS AND TEST PROCEDURES WITH RECOMMENDATIONS FOR USE IN THE TEXAS M-E DESIGN PROGRAM	October 2007 Resubmitted: June 2008 Published: September 2008
	6. Performing Organization Code

7. Author(s)	8. Performing Organization Report No.
Fujie Zhou, Emmanuel Fernando, and Tom Scullion	Report 0-5798-1

9. Performing Organization Name and Address	10. Work Unit No. (TRAIS)
Texas Transportation Institute The Texas A&M University System College Station, Texas 77843-3135	11. Contract or Grant No. Project 0-5798

12. Sponsoring Agency Name and Address	13. Type of Report and Period Covered
Texas Department of Transportation Research and Technology Implementation Office P. O. Box 5080 Austin, Texas 78763-5080	Technical Report: September 2006-August 2007
	14. Sponsoring Agency Code

15. Supplementary Notes

Project performed in cooperation with the Texas Department of Transportation and the Federal Highway Administration.

Project Title: Develop Test Procedures to Characterize Material Response Behavior and Transfer Functions for TxDOT M-E Design

URL: http://tti.tamu.edu/documents/0-5798-1.pdf

16. Abstract

In the first year of this project, a comprehensive review was made of the available models for predicting the major distresses in flexible pavements, including cracking of asphalt layers and chemically bound layers, permanent deformation of asphalt layers, and permanent deformation of granular base and subgrade layers. In conducting these reviews, the latest models under consideration in both national efforts and various state development efforts were reviewed. The models identified for each of the major distresses are described in this report. Additionally, the associated laboratory test procedures, which can be used to provide TxDOT with the material properties needed as inputs to both the pavement response and performance prediction models, were also identified and discussed. Finally, a detailed laboratory testing plan was proposed for Year 2 study.

17. Key Words	18. Distribution Statement
Flexible Pavement Design, Overlay Test, Repeated Load Test, Rutting, Fatigue Cracking, Tex-ME	No restrictions. This document is available to the public through NTIS: National Technical Information Service Springfield, Virginia 22161 http://www.ntis.gov

19. Security Classif.(of this report)	20. Security Classif.(of this page)	21. No. of Pages	22. Price
Unclassified	Unclassified	142	

Form DOT F 1700.7 (8-72) **Reproduction of completed page authorized**

A REVIEW OF PERFORMANCE MODELS AND TEST PROCEDURES WITH RECOMMENDATIONS FOR USE IN THE TEXAS M-E DESIGN PROGRAM

by

Fujie Zhou
Assistant Research Engineer
Texas Transportation Institute

Emmanuel Fernando
Research Engineer
Texas Transportation Institute

and

Tom Scullion, P.E.
Senior Research Engineer
Texas Transportation Institute

Report 0-5798-1
Project 0-5798
Project Title: Develop Test Procedures to Characterize Material Response Behavior and Transfer Functions for TxDOT M-E Design

Performed in cooperation with the
Texas Department of Transportation
and the
Federal Highway Administration

October 2007
Resubmitted: June 2008
Published: September 2008

TEXAS TRANSPORTATION INSTITUTE
The Texas A&M University System
College Station, Texas 77843-3135

DISCLAIMER

The contents of this report reflect the views of the authors, who are responsible for the facts and the accuracy of the data presented herein. The contents do not necessarily reflect the official views or policies of the Texas Department of Transportation or the Federal Highway Administration. This report does not constitute a standard, specification, or regulation. The engineer in charge was Tom Scullion, P.E. (Texas, #62683).

ACKNOWLEDGMENTS

This project was made possible by the Texas Department of Transportation (TxDOT) in cooperation with the Federal Highway Administration. In particular, the guidance and technical assistance provided by the project director (PD) Joe Leidy, P.E., of TxDOT and the program coordinator (PC) Darrin Grenfell, P.E., proved invaluable. The following project advisors also provided valuable input throughout the course of the project, and their technical assistance is acknowledged: Mark McDaniel, P.E., Construction Division, TxDOT; Billy Pigg, P.E., Waco District; and Ricky Boles, P.E., Lufkin District.

TABLE OF CONTENTS

LIST OF FIGURES

LIST OF TABLES

CHAPTER 1

INTRODUCTION

The objective of Texas Department of Transportation (TxDOT) Project 0-5798 is to develop the framework for the development and implementation of the next level of Mechanistic-Empirical Pavement Design Guide (MEPDG) for TxDOT (Tex-ME). As specified in the project statement, this initial project, which is in the development process, will focus on the following areas:

- Identify and evaluate test procedures that characterize material properties needed to predict pavement response.
- Assemble existing performance prediction models (transfer functions), and evaluate their feasibility of being implemented in Texas. Key considerations will be the models' performance in basic sensitivity analysis, the practicality of the data input requirements, and their performance at simulating results from accelerated pavements tests (APT).
- Calibrate the selected transfer functions with available performance data from the LTPP databases, various test track studies, and whatever performance data is available from the databases being assembled in Texas.

In the first year of this project, a comprehensive review was made of the available models for predicting the major distresses in flexible pavements, including cracking of hot-mix asphalt (HMA) layers, permanent deformation of HMA layers, and permanent deformation of granular base and subgrade layers. In conducting these reviews the latest models under consideration in both national efforts and various state development efforts were reviewed. The models identified for each of the major distresses are described in next three chapters of this report.

Another very important aspect of this project is to identify laboratory testing procedures, which can be used to provide TxDOT with the material properties needed as inputs to both the pavement response and performance prediction models. As stated in the Texas Transportation Institute (TTI) proposal, the eventual Tex-ME program (as being proposed in other ME programs) will provide the user with various levels of flexibility when selecting material properties. At the lowest level, default values will be available for all of the design items used by TxDOT. However, Level 2 will be properties derived from the current specification and acceptance/design tests that are run on a routine basis by TxDOT. Level 1 will be the highest level where advanced materials characterization techniques will be used on all layers in the pavement structure.

In Chapters 2, 3, 4, and 5, the models most appropriate for potential inclusion in the future Tex-ME will be identified. Chapter 6 will provide a summary of laboratory test procedures proposed to provide materials inputs for these models. The recommended material characterization protocols for Level 1 inputs are provided in Appendix A, B, and C. Chapter 7 describes the detailed laboratory testing plan. Additionally, performance data is being assembled

from the National Center for Asphalt Technology (NCAT) test track and from the California Heavy Vehicle Simulator (HVS) program, and response and performance data will be generated on the instrumented sites currently being constructed in Texas. Materials from each of these projects will be characterized later in the TTI laboratory.

CHAPTER 2

MODELS FOR PREDICTING FATIGUE CRACKING OF HMA LAYERS

This chapter is divided into the following major sections:

- Section 2.1 provides a description of the concept of fatigue cracking.
- Section 2.2 discusses the existing models available to predict fatigue cracking.
- Section 2.3 recommends models to be considered for inclusion in the Tex-ME.

2.1 BACKGROUND OF FATIGUE CRACKING

As noted by Suresh, the word *fatigue* originated from the Latin expression *fatigare* which means "to tire" (*1*). Although commonly associated with physical and mental weariness in people, the word *fatigue* has also become a widely used terminology in engineering vocabulary for the damage and failure of materials under cyclic loads. Fatigue is defined as a term which "applies to changes in properties which can occur in a metallic material due to the repeated application of stresses or strains, although usually this term applies specially to those changes which lead to cracking or failure." This definition is also valid for fatigue of HMA concrete, because asphalt pavements do not crack immediately after the traffic starts, and it usually takes many years and millions of load applications.

For asphalt pavement fatigue cracking, two phases of the degradation process are generally considered: crack initiation and crack propagation. During the process of the crack initiation, microcracks grow from microscopic size until, as some research indicates, a critical length of about 7.5 mm is reached (*2*). In the crack propagation process, a single crack or a few cracks grow until the crack(s) reaches the pavement surface. Researchers noted that both microcracks and macrocracks can be propagated by tensile or shear stresses or combinations of both. Thus, in a pavement structure, microcracks can form and grow in any location where tensile or shear stresses generated by traffic or environmental variations are sufficiently large. Any tensile or shear stress applied to a field where microcracks exist may cause them to grow, to reach critical size, and then to propagate as macrocracks.

The number of traffic load repetitions, N_f, to cause a crack to penetrate through the full depth of the pavement surface layer is the sum of the number of load repetitions for crack initiation, N_i, and the number of load repetitions required for macrocrack to propagate to the pavement surface, N_p.

$$N_f = N_i + N_p \tag{1}$$

It should be noted that all existing asphalt pavement thickness design programs do not directly consider the N_p, but indirectly consider it through the field calibration.

The physical evolution law governing each of the two phases (crack initiation and crack propagation) may be quite different so that different approaches have been proposed to model these two phases. More information is provided below.

2.2 FATIGUE CRACKING MODELING

Fatigue cracking is one of the major distress modes considered in asphalt pavement designs and has been studied for several decades. In 1955, Hveem demonstrated the concept that fatigue cracking has a higher propensity to occur on an asphalt pavement when the pavement experiences a larger deflection and a higher loading frequency (*3*). Since then, different types of fatigue cracking models have been proposed. Generally speaking, these models can be classified into three categories: crack initiation models, crack propagation models, and crack initiation and propagation models. The following subsections discuss these models.

2.2.1 Crack Initiation Models

Most of existing fatigue cracking models actually only describe the crack initiation phase of asphalt pavement cracking, and the crack propagation is taken into account through field calibration. These types of models can be further classified as strain-based fatigue model, energy-based fatigue model, and damage-based fatigue model. Detailed discussion for each type of models is provided below.

Strain-Based Fatigue Models

This type of model has been implemented in many of the existing asphalt pavement design procedures. The most commonly used model form to predict the number of load repetitions to fatigue cracking, as shown in Equation 2, is a function of the tensile strain and mix stiffness (modulus).

$$N_f = k_1\left(\frac{1}{\varepsilon_t}\right)^{k_2}\left(\frac{1}{S_{mix}}\right)^{k_3} \quad (2)$$

where:

Nf = number of repetitions of load to cause fatigue cracking,
ε_t = tensile strain at the critical location,
S_{mix} = stiffness of the material, and
k1, k2, k3 = regression coefficients obtained from laboratory testing.

Four examples of the strain-based fatigue models were developed by Shell Oil (*4*), the Asphalt Institute (MS-1) (*5*), the SHRP A-003A-Berkeley model (*6*), and the MEPDG fatigue model (*7*). These are shown below:

- *Shell Oil fatigue cracking model*

Because of the known impact between stress state and damage mechanism for different thicknesses of asphalt layers, Shell Oil Company has developed fatigue damage prediction equations for the two major forms of laboratory fatigue testing (*4*). In practice, the constant stress equation would be recommended for thick asphalt layer design, whereas the constant strain would be for thinner layers, although the transition from thick to thin is somewhat arbitrary. The

equations developed are presented as follows:

$$\text{Constant strain: } N_f = A_f\left[0.17PI - 0.0085PI\left(V_b\right) + 0.0454V_b - 0.112\right]^5 \varepsilon_t^{-5} E^{-1.8} \quad (3)$$

$$\text{Constant stress: } N_f = A_f\left[0.0252PI - 0.00126PI\left(V_b\right) + 0.00673V_b - 0.0167\right]^5 \varepsilon_t^{-5} E^{-1.4} \quad (4)$$

where:

N_f = number of repetitions to fatigue cracking,
ε_t = tensile strain at the critical location,
E = stiffness of the material,
V_b = effective asphalt content in volume (%),
A_f = laboratory to field adjustment factor (default =1.0), and
PI = penetration index.

- *Asphalt Institute (MS-1) model*

$$N_f = 0.00432 * 10^{4.84\left(\frac{V_b}{V_b + V_a} - 0.69\right)} \varepsilon_t^{-3.291} E^{-0.854} \quad (5)$$

where:

N_f = number of repetitions to fatigue cracking,
ε_t = tensile strain at the critical location,
E = stiffness of the material,
V_b = effective asphalt content in volume (%), and
V_a = air voids (%).

Note that this MS-1 fatigue equation is based upon modifications to constant stress laboratory fatigue criteria. The Asphalt Institute Ninth Edition of the MS-1 design manual uses a field calibration factor of 18.4 so that predictions from the model can be matched to observed field performance (*5*). This correction factor was developed for a 20 percent level of wheelpath cracking; it was recommended by Finn in his classic NCHRP 1-10 study (*8*).

- *SHRP A-003A-Berkeley fatigue model*

$$N_f = 2.738 * 10^5 * e^{0.077 * VFB} \varepsilon_t^{-3.624} * S_o''^{-2.720} \quad (6)$$

where:

N_f = number of repetitions to fatigue cracking,
ε_t = tensile strain at the critical location,
VFB = percentage of voids filled with asphalt, and
S_o'' = initial loss-stiffness of mix as measured in flexure (psi).

The SHRP A-003A research team established an integrated asphalt mix and asphalt thickness design system based on the research results from the SHRP A-003A program. This model has been recalibrated based on the HVS tests (*9*).

- *MEPDG fatigue cracking model*

The NCHRP 1-37A research team examined the Shell Oil and the MS-1 models for the recently developed MEPDG. It was found that the Shell Oil models possessed more scatter and did not possess any definite trends (*10*); also, the MS-1 model had much less scatter and resulted in a definite trend. Thus, the MS-1 model was selected and implemented in the MEPDG. In contrast to the models described above, the MEPDG fatigue cracking model actually includes the following three models:

- *The number of the load repetitions fatigue model*

$$N_f = 0.00432 * k_1 * C \left(\frac{1}{\varepsilon_t}\right)^{3.9492} \left(\frac{1}{E}\right)^{1.281} \tag{7}$$

where:

N_f = number of repetitions to fatigue cracking,
ε_t = tensile strain at the critical location,
E = stiffness of the material,
h_{ac} = asphalt layer thickness (inches), and
$k1, C$ = correction factors.

$$C = 10^{4.84\left(\frac{V_b}{V_b+V_a}-0.69\right)}, \tag{8}$$

$$k_1 = \frac{1}{0.000398 + \frac{0.003602}{1+e^{11.02-3.49*h_{ac}}}} \tag{9}$$

- *Fatigue damage model*

Fatigue damage caused by different traffic loads is calculated as the ratio of the applied number of traffic repetitions to the allowable number of load repetitions (to some failure level) as shown in Equation 10.

$$D = \sum_{i=1}^{T} \frac{n_i}{N_i} \tag{10}$$

where:

D = damage,
T = total number of periods,
n_i = actual traffic for period *i,* and
N_i = allowable failure repetitions under conditions prevailing in period *i*.

- *Fatigue cracking amount model*

Finally, another transfer function is used to calculate the fatigue cracking from the fatigue damage, which was developed and calibrated using the LTPP data. The final fatigue damage versus cracking amount model in the MEPDG is as follows:

$$FC = \left(\frac{6000}{1+e^{C_1 - C_2 * \log D}}\right) * \left(\frac{1}{60}\right) \quad (11)$$

where:

FC = percentage of fatigue cracking of total lane area,
D = damage (Equation 10),
C_1 = $-2*C_2$,
C_2 = $-2.40874-39.748*(1+h_{ac})^{-2.85609}$, and
h_{ac} = asphalt layer thickness (inches).

Energy-Based Fatigue Models

Since the early work done by Van Dijk, the energy-based fatigue models have been widely investigated (*11*). Various representations and applications of dissipated energy concepts have been proposed and are presented below.

- *Initial dissipated energy approach*

Initial dissipated energy (IDE) is the area under the stress-strain curve between the loading and unloading cycle measured during the initial loading cycles. Typically, in fatigue testing, the first 50 cycles are regarded as the conditioning cycles, and the dissipated energy at the 50th loading cycle is considered as the initial dissipated energy. Initial dissipated energy can be a good indicator of fatigue performance for similar mix types (*12*). Baburamani and Porter (*13*) also showed a good correlation between the initial dissipated energy and fatigue life. Additionally, Ghuzlan in his thesis found the initial dissipated energy is one of the most important factors that affect fatigue behavior of HMA mixes (*14*). Based on extensive bending beam fatigue testing data, Tayebali et al. proposed the following as a surrogate model to relate initial dissipated energy to fatigue life (*6*):

$$N_f = 6.72e^{0.049VFB}(w_0)^{-2.047} \quad (12)$$

where:

N_f = number of repetitions to failure,
VFB = percentage of voids filled with bitumen, and
w_0 = initial dissipated energy.

One disadvantage of the initial dissipated energy approach is that it is not appropriate for the whole loading range, especially when dealing with low strain fatigue tests. Shen and Carpenter did not find any good correlation between the initial dissipated energy and fatigue life (*15*).

- *Cumulative dissipated energy approach*

The cumulative dissipated energy is the summation of the dissipated energy experienced by the material during the fatigue test, which relates the fatigue behavior to both initial and final test cycles. A relationship between the cumulative dissipated energy and the number of loading cycles to failure is characterized as:

$$W_N = A\left(N_f\right)^z \tag{13}$$

where:

W_N = cumulative dissipated energy to failure,
A, z = experimentally derived mix coefficient, and
N_f = number of load cycles to failure.

Van Dijk was one of the earliest researchers who did an extensive study on fatigue of HMA materials based on the dissipated energy concepts (*11, 16*). He found that there is a strong relationship between the cumulative dissipated energy and the number of loading cycles to failure. This relationship is not affected by the loading mode (controlled-stress or controlled-strain), the effects of frequency (between 10Hz and 50Hz) and temperature (between 10ºC to 40ºC), and the occurrence of rest periods. However, it is highly material dependent and has to be mix specific to be applied.

Pronk and Hopman suggested the dissipated energy per cycle/period is responsible for the fatigue damage (*17*). The total dissipated energy combined with Wöhler's curve was used to develop the fatigue equation. Additionally, Tayebali et al. introduced two terms: the stiffness ratio, which is the ratio of the stiffness at load cycle (i) to the initial stiffness; and the dissipated energy ratio, which is defined as the ratio of cumulative dissipated energy up to load cycle (i) to the cumulative dissipated energy up to fatigue life (*18*). Their work showed there is a unique relationship between the stiffness ratio and the dissipated energy ratio, but not necessarily between cumulative dissipated energy and fatigue life, which is also verified by SHRP A-404 (*6*) and later by Fakhri (*19*). This relation was also found to be mix and temperature dependent.

- *Work ratio approach*

This approach was first introduced by Van Dijk and Visser (*16*) and further developed by Rowe (*12*). The work ratio, ψ_{N1}, is defined as the ratio between the product of the initial dissipated energy in cycle 1 and N1 divided by the cumulative dissipated energy, as shown in Equation 14.

$$\psi_{N1} = \frac{w_0 N1}{W_{N1}} \tag{14}$$

where:

w_0 = initial dissipated energy,
N_1 = number of load cycles to crack initiation, and
W_{N1} = cumulative dissipated energy at cycle N1.

Work ratio can be calculated in terms of the initial rheological property of the HMA mix and the mode of loading factor, Γ, as follows:

$$\psi_{N1} = \left\{ \frac{2Sin\phi_0}{Sin\phi_0 + \Gamma Sin\left[a\left(E_{60}^*\right)^{(0.224-0.222\log a)} \right]} \right\} \quad (15)$$

where:

$\Gamma = \left[\frac{100 - A - B}{100} \right]$ = mode of loading,

$A = \left[\frac{\varepsilon_0 - \varepsilon_{60}}{\varepsilon_{60}} \right] \times 100$ = percent change in strain,

$B = \left[\frac{\sigma_0 - \sigma_{60}}{\sigma_{60}} \right] \times 100$ = percent change in stress,

$a = 10^{\left[\frac{\log \phi_0 - 0.244 \log E_0^*}{1 - 0.222 \log E_0^*} \right]}$

$ø_0$ = initial phase angle,
E_0^* = initial extensional complex modulus (equivalent to bending stiffness),
E_{60}^* = 60 percent reduction in initial extensional complex modulus,
ε_{60} = 60 percent reduction in the initial strain, and
σ_{60} = 60 percent reduction in the initial stress.

Rowe (*12*) found that the work ratio can be used effectively to predict the fatigue life to crack initiation through Equation 13. The crack initiation (Equation 16) is assumed to occur at 60 percent reduction of original extensional complex modulus.

$$N1 = 205 V_b^{6.44} w_0^{-2.01} \psi_{N1}^{1.64} \quad (16)$$

where:

$N1$ = number of load cycles to crack initiation,
V_b = volume of binder (%),
w_0 = initial dissipated energy, and
ψ_{N1} = work ratio.

- *Dissipated energy ratio approach*

Carpenter and Jansen first initiated an improved implementation of the dissipated energy concept for HMA fatigue analysis, in which a dissipated energy ratio was used as a parameter to relate to fatigue life (*20*). This approach believes that not all the dissipated energy is responsible for material damage. For each cycle, the loss of energy due to material mechanical work and

other environmental influence remains almost unchanged. Therefore, if the dissipated energy starts to change dramatically, it could be explained as the development of damage. Later, this approach was examined and refined by Ghuzlan and Carpenter (*14, 21*), and Carpenter et al. (*22*). It is found that the relationship between dissipated energy ratio and fatigue life is fundamental in that it is independent of loading level, loading mode, and mix type (*22*).

This dissipated energy ratio approach was further improved by Shen and was renamed as the ratio of dissipated energy change (RDEC) approach considering the fact that it is using the ratio of the amount of dissipated energy change between different loading cycles to represent the damage propagation (*23*). The distinctiveness of the RDEC approach is the relationship between the energy parameter, plateau value (*PV*), and the fatigue life (N_f). This relation, as presented in Equation 17, is unique for all HMA mixes, all loading modes (controlled stress and controlled strain), all loading levels (normal and low damage levels), and various testing conditions (frequency, rest periods, etc.) (*23*).

$$N_f = 0.4801(PV)^{-0.9007} \tag{17}$$

where:

N_f = fatigue life, and

PV = plateau value.

Furthermore, Shen also developed the following equation to estimate the energy parameter, PV.

$$PV = 2.612\times10^{-10}(IDE)^{2.758}S^{2.493}(VP)^{3.055}(GP)^{-2.445} \tag{18}$$

where:

PV = plateau value,
IDE = initial dissipated energy,
S = the flexural stiffness of HMA mix from the laboratory fatigue test, MPa,
VP = volumetric parameter, $VP = \frac{AV}{AV + V_b}$,
AV = air voids, %,
V_b = the asphalt content by volume, $V_b = 100 \times \frac{G_{mb} \times P_{ac}}{G_b}$,
G_{mb} = bulk density, %,
P_{ac} = percent of asphalt by total weight of mix,
G_b = bulk specific gravity of the asphalt binder, assuming G_b=1.03,
GP = aggregate gradation parameter, $GP = \frac{P_{NMS} - P_{PCS}}{P_{200}}$,
P_{NMS} = percent of aggregate passing the nominal maximum size sieve,
P_{PCS} = percent of aggregate passing the primary control sieve, and
P_{200} = percent of aggregate passing #200 (0.075mm) sieve.

As an energy-based approach, the RDEC is fundamental and has been demonstrated valid for different testing methods such as flexural bending beam fatigue testing (*14, 15, 21, 22*) and

uniaxial tension testing (*24*), and various materials including both HMA materials and Portland cement concrete materials (*25*). While it is more fundamentally correct to use dissipated energy rather than tensile strain, current design systems are based on multi-layer elastic system and the viscoelastic dissipated energy cannot be easily estimated. Recognizing this limitation, Shen also developed an alternative equation, which is a strain-based fatigue prediction equation, as presented in Equation 19 (*23*).

$$PV = 61.336\varepsilon^{5.052} S^{2.749} (VP)^{1.643} (GP)^{-0.094} \quad (19)$$

where:

ε = tensile strain, and
all other parameters are the same as those in Equation 18.

Damage-Based Models

Two types of damage-based fatigue models have been proposed: viscoelastic continuum damage mechanics model and CalME damage-based fatigue model. The main difference between these two approaches is how to interpret the load reduction and fatigue damage during the fatigue test. The CalME damage-based fatigue model interprets the load reduction as fatigue damage, but for the visco-elastic continuum damage mechanics approach, the load reduction is caused by both viscoelastic property of the HMA mix and fatigue damage. Thus, the viscoelastic continuum damage mechanics approach uses the concept of "pseudo-stiffness" to define fatigue damage. Note that the pseudo-stiffness is defined as the ratio of a stress value to a pseudo-strain value at the peak pseudo-strain of each cycle. More discussion is presented below for each model.

- *Viscoelastic continuum damage mechanics approach*

Continuum damage theory was originally developed by R.A. Schapery for analyzing the response of solid rocket fuels and similar viscoelastic materials (*26, 27, 28*). Lytton, Kim, and Little later applied Schapery's work to asphalt concrete (*29*). Their work was extended and refined by Y. Richard Kim, Daniel, Lee, and Yong-Rak Kim (*30, 31, 32, 33, 34, 35*). Practical application of this continuum damage theory has been made by Lee et al. (*35*), and Christensen and Bonaquist (*36*). The brief discussion presented below largely follows the development of Christensen and Bonaquist (*36*).

Schapery defined uniaxial pseudo-strain as follows:

$$\varepsilon^R(t) = \frac{1}{E_R} \int_0^t E(t - t') \frac{\partial \varepsilon}{\partial t'} dt' \quad (20)$$

where:

ε = strain,
$\varepsilon^R(t)$ = pseudo-strain at time t,
E = relaxation modulus,
t′ = time at which loading begins, and

E^R = an arbitrary reference modulus, often set at unity.

The above definition is very similar to that for linear viscoelastic (LVE) stress:

$$\sigma(t) = \int_0^t E(t-t')\frac{\partial \varepsilon}{\partial t'}dt' \tag{21}$$

where σ(t) is stress at time t.

From Equations 20 and 21, under LVE conditions, we have:

$$\varepsilon^R(t) = \frac{\sigma(t)}{E_R} \tag{22}$$

That means that the pseudo-strain is equal to the stress resulting from an applied strain history. To quantify damage accumulation, Kim et al. used the concept of pseudo-stiffness defined by Equation 23 (*33*):

$$C = \frac{\sigma_{\max}}{\varepsilon^R_{\max}} \tag{23}$$

where *C* is the normalized pseudo-stiffness; normalization meaning that adjustments are made in the calculation of *C* for individual specimens so that the initial value (undamaged) is always unity.

For fatigue testing, a specimen is subjected to a given strain-controlled loading. With the damage accumulating during the fatigue test, the resulting stress σ_{max} for every cycle will gradually decrease compared to the pseudo-strain. Thus, Equation 23 simply defines pseudo-stiffness as the ratio of the non-linear modulus to the initial LVE modulus. The constitutive equation for uniaxial loading of a viscoelastic material with damage is given below (*31*):

$$\sigma_{\max} = C\varepsilon^R_{\max} \tag{24}$$

The applicable stress-pseudo-strain relationship is as follows (*36*):

$$\sigma_{\max} = \left(\frac{\partial W^R}{\partial \varepsilon^R_{\max}}\right)^{\alpha} \tag{25}$$

where W^R is the pseudo-strain energy density function. The time dependent growth of damage can be given by the following equation (*36*):

$$\frac{dS}{dt} = \left(-\frac{\partial W^R}{\partial S}\right)^{\alpha} \tag{26}$$

where *S* is a variable characteristic of the amount of internal damage in a material, and α is a material constant, which usually has a value close to 2.0. Equations 24 and 25 can be combined and integrated to yield the following relationship (*36*):

$$W^R = 0.5C\left(\varepsilon_{\max}^R\right)^2 \tag{27}$$

Regarding the relationship between pseudo-stiffness C and the internal damage parameter S, Lee and Kim proposed a form of generalized power law (*32*):

$$C = C_{10} - C_{11}(S)^{C_{12}} \tag{28}$$

where C_{10}, C_{11}, and C_{12} are constants describing the rate of damage accumulation of a specimen under cyclic loading. It should be noted that this equation would become negative at some value of S, which means that the damaged modulus would also be negative, and an applied tensile strain would result in a compressive stress. Knowing the limitation of Equation 28, Christensen and Bonaquist suggested a better function in a simple exponential form (*36*):

$$C = \exp(C_2 S) \tag{29}$$

where C_2 is a constant indicative of the rate of damage accumulation in a specimen under cyclic loading. Now, substitute Equation 29 into Equation 27, and differentiate with respect to S; the following relationship results:

$$\frac{\partial W^R}{\partial S} = 0.5C_2 \exp(C_2 S)\left(\varepsilon_{\max}^R\right)^2 \tag{30}$$

Then, substitute Equation 30 into Equation 26 and integrate to solve for t:

$$t = \frac{2^{\alpha}\exp(-\alpha C_2 S)}{\alpha(-C_2)^{1+\alpha}\varepsilon_{\max}^R}_{S=0}^{S=t} \tag{31}$$

Now, if the reference modulus $E^R = 1$, then, $\varepsilon^R(t) = \sigma(t)$. In addition, for sinusoidal loading, the maximum tensile stress is equal to:

$$\frac{|\sigma_{\max} - \sigma_{\min}|}{2} = \sigma_0 = \varepsilon_0 \times |E|_{LVE} \tag{32}$$

where:

$|E|_{LVE}$ = LVE complex modulus,
σ_0 = maximum tensile stress (or stress amplitude), and
ε_0 = maximum tensile strain (or strain amplitude).

Note that the number of loading cycles N is loading time t times frequency f (Hz).

Equation 30 can then be solved over the given integration limits and given in the following form:

$$N_f = \frac{2^{\alpha} f\left[\exp(-\alpha C_2 S_f) - 1\right]}{\alpha(-C_2)^{1+\alpha}|E|_{LVE}^{2\alpha}}\left(\frac{1}{\varepsilon_0}\right)^{2\alpha} \tag{33}$$

where S_f is the value of internal damage variable S at failure. It is clear that fatigue life (N_f) is a

function of the damage evolution characteristics of the material (C_2), viscoelastic material properties (α, $|E|$), fatigue test conditions (f, ε_0), and a failure criterion (S_{1f}).

The main advantage of using continuum damage mechanics to predict fatigue behavior of HMA mixes is that the time-temperature superposition principle can be employed to shift the characteristic curve determined at one temperature to different temperatures. In that way, it is possible to save considerable testing time and materials. The disadvantage of this approach is that it needs sophisticated laboratory tests and data analysis techniques. Generally, this approach is still under development. Application of this approach to predict fatigue cracking of asphalt pavement has not been seen yet in the literature.

- *CalME damage-based fatigue cracking model*

Another approach of considering fatigue damage caused by repeated loading is through the stiffness ratio (SR) proposed by Tsai, Harvey, and Monismith (*37*). Different from viscoelastic continuum damage approach, this approach assumes that stiffness (or load) reduction is caused by fatigue damage. This approach has been used in the CalME design program. In the present version of CalME, the SR is predicted in the following equation (*38*):

$$SR = \exp\left(-\alpha \times N^{\beta}\right) \tag{34}$$

where:

SR = stiffness ratio, defined as the ratio of stiffness at repetition *n* over the initial stiffness (taken at about 50 repetitions),
N = number of load applications, and α and β are assumed on the format:

$$\alpha = \exp\left(\alpha A + \alpha B \times t + \alpha C \times \ln(w) + \alpha D \times t \times \ln(w)\right)$$
$$\beta = \beta A + \beta B \times t + \beta C \times \ln(w)$$

where:

t = temperature in ºC,
w = internal energy density (½×ε^2×E), and
αA, αB, αC, αD, βA, βB and βC = constants determined from 4-point bending beam fatigue tests under controlled strain.

The use of *SR* damage-based approach has several advantages: 1) stiffness is easy to measure both in the laboratory and in the field, and 2) stiffness is often utilized as an input for linear layered-elastic programs for pavement analysis, thus making it useful for programming fatigue performance prediction. However, it is worth noting that no asphalt thickness design program but the CalME program used this approach. Actually, Monismith and his associates are continuously developing this model. More research is still needed to refine this model (*38*).

2.2.2 Crack Propagation Models

Different types of models have been developed to characterize fatigue crack propagation. Models reviewed here include the classical fracture mechanics model, the cohesive crack model,

and the non-local continuum damage model.

Classical Fracture Mechanics Model

Since Majidzadeh et al. introduced fracture mechanics concepts into the field of asphalt pavements, the fracture mechanics approach has been widely used in predicting pavement cracking (*39*). In contrast to continuum mechanics, the fracture mechanics approach focuses on crack propagation. The crack propagation process can be caused by Modes I, II, III, or a combination of the three modes of loading (Figure 1):

- Mode I loading (opening mode, K_I) results from loads that are applied normally to the crack plane (thermal and traffic loading).
- Mode II loading (sliding mode, K_{II}) results from in-plane shear loading, which leads to crack faces sliding against each other normal to the leading edge of the crack (traffic loading).
- Mode III loading (tearing mode, K_{III}) results from out-of plane shear loading, which causes sliding of the crack faces parallel to the crack leading edge. Compared to Modes I and II, Mode III is rare and is often neglected for simplicity.

The fact that the mechanisms of fatigue cracking (bending and shearing) discussed previously can be exactly modeled by fracture Modes I and II makes the fracture mechanics approach very attractive for modeling fatigue crack propagation.

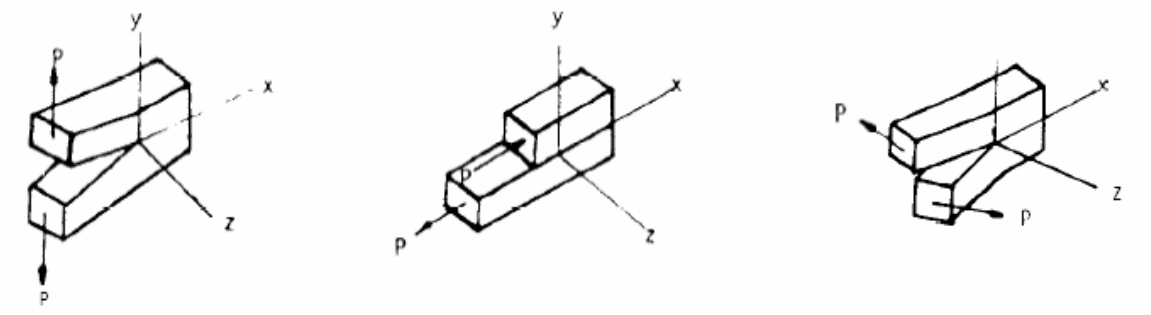

(a) (b) (c)

Figure 1. Three Modes of Crack Opening Displacement: (a) Mode I − Opening Mode, (b) Mode II − Shearing Mode, (c) Mode III − Tearing Mode (*40*).

The generally accepted crack propagation law was proposed by Paris and Erdogan in the form of Equation 35 (*41*). It has successfully been applied to asphalt concrete by many researchers for the analysis of experimental tests and prediction of reflection cracking and low temperature cracking.

$$\frac{dc}{dN} = A * (\Delta K)^n \tag{35}$$

where:

c = crack length,
N = number of loading cycles,
A, n = fracture properties of asphalt mixture determined by the experimental test, and
ΔK = stress intensity factor (SIF) amplitude, depending on the geometry of the pavement structure, fracture mode, and crack length.

The number of load cycles N_f needed to propagate a crack through an asphalt layer of thickness h can be estimated by numerical integration in the form of Equation 36.

$$N_f = \int_0^h \frac{dc}{A(\Delta K)^n} \tag{36}$$

The use of Paris' law (Equation 35) for the description of the crack growth process in viscoelastic materials, such as HMA mixes, has been theoretically justified by Schapery (*42, 43, 44*). However, it is apparent that both SIF and HMA fracture properties (A and n) must be known in order to predict fatigue crack propagation. In the following paragraphs, the focus will be placed on the SIF calculation and HMA fracture properties determination.

- *Calculation of SIF*

Since there is a singularity at the crack tip in the stress field, a finite element (FE) program is needed to compute the SIF. Two special SIF computation programs for pavements have already been developed for crack propagation. The first one named CRACKTIP was developed for thermal cracking by Lytton and his associates at TTI in 1976 (*45*). The CRACKTIP is a two dimensional (2-D) FE program, and it models a single vertical crack in the asphalt concrete layer via a crack tip element (*45*). This program has been successfully used to develop the SIF model and predict the cracking propagation. Figure 2 shows the SIF of bending (SIF_b) and SIF of shearing (SIF_s) versus crack length relationship. It is interesting to note that there is a "neutral axis" where bending stresses no longer cause crack propagation. Its location depends on the level of load transfer and the moduli of the pavement layers. This neutral axis must be considered in order to accurately predict reflection cracking.

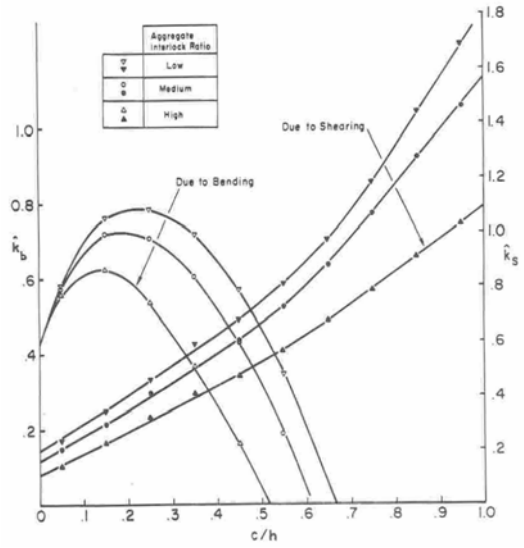

Figure 2. Non-dimensionalized Bending and Shearing SIF vs. Non-dimensionalized Crack Length (*46*).

Although 2-D FE programs run much faster than the three dimensional (3-D) FE programs, it is common knowledge that the SIFs computed from 2-D plane strain conditions are overestimated because of the difference between plane strain conditions and the 3-D nature of a cracked geometry and loading conditions. In order to balance the accuracy of 3-D FE (3-D nature of the cracked pavement geometry and the loading condition) and fast running time of 2-D FE, a semi-analytical FE program named *SA-CrackPro* was recently developed at TTI by Zhou et al. (*47*). This *SA-CrackPro* provides for adequate accuracy and efficient analysis of crack propagation in an asphalt layer. The *SA-CrackPro* program uses a single quarter-point triangular singular element to produce the stress singularity at the crack tip as shown in Figure 3 (*48*). The SIFs (K_I and K_{II}) can then be elegantly determined based on Equations 37 and 38 proposed by Ingraffea and Manu, if the displacements of the crack tip nodes computed by FE analysis are correlated to those predicted by theory (*49*).

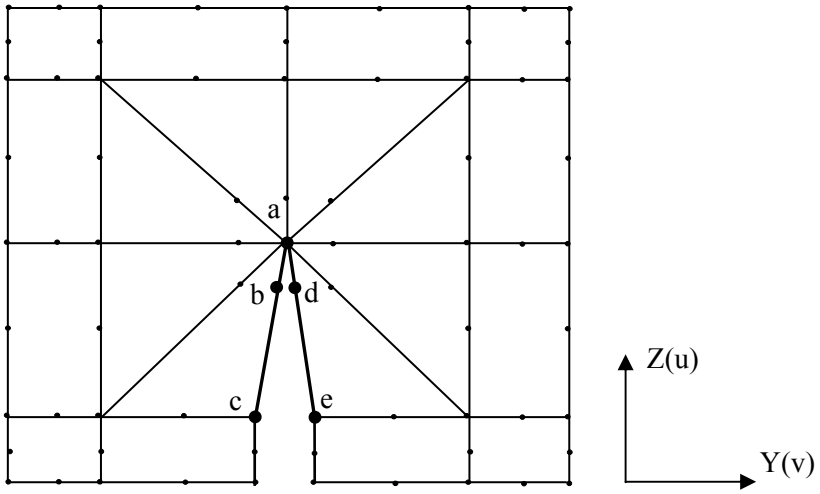

Figure 3. 8-node Quadrilateral and Quarter-point Triangular Elements.

$$K_I = \sqrt{\frac{2\pi}{L}}\frac{G}{\kappa+1}\left[4(v_B - v_D) + v_E - v_C\right] \quad (37)$$

$$K_{II} = \sqrt{\frac{2\pi}{L}}\frac{G}{\kappa+1}\left[4(u_B - u_D) + u_E - u_C\right] \quad (38)$$

where:

G = shear modulus,
κ = $(3-\upsilon)/(1+\upsilon)$ for plane stress,
κ = $3-4\upsilon$ for plane strain, and
L = element length.

The inputs to the *SA-CrackPro* program are the same as those used in the multilayer elastic program for calculating tensile strain at the bottom of asphalt layer. Furthermore, regression equations for bending and shearing SIFs are under development. Once SIF regression

equations are developed, it becomes possible to practically consider crack propagation in the structural design of asphalt pavement.

- *HMA fracture properties: A, n*

Laboratory tests characterizing HMA fracture properties (*A* and *n*) have been conducted for a long time (*39, 50, 51, 52, 53, 54, 55, 56, 57, 58*). Among them, the most systematic laboratory studies on fracture properties *A* and *n* were conducted by Molenaar and his associates (*53, 54, 55, 56, 57, 58*). The most often used test to quantify these parameters is the repeated direct tension test. However, this test method is relatively complicated and has not been widely accepted in the field of asphalt pavement. Recently, Zhou et al. developed a very simple, quick test procedure to determine fracture properties of HMA mixes (*A* and *n*) using the TTI overlay tester (OT) (*47*). This procedure can be routinely used to determine HMA fracture properties. More information about using the OT to determine fracture properties of HMA mixes is presented in Appendix A.

In summary, the classical fracture mechanics-based fatigue crack propagation model is conceptually sound, and the mechanisms of fatigue cracking (bending and shearing) can be easily described with a fracture mechanics-based model. Furthermore, this type of model, as discussed previously, has been successfully employed to predict the reflection cracking in asphalt overlays by different researchers. Moreover, the two difficult aspects of application of fracture mechanics: SIF calculation and fracture properties (*A* and *n*), as noted above, have been solved. Thus, a fracture mechanics-based crack propagation model is mature enough to be implemented in any mechanistic-empirical structural pavement design system.

Cohesive Crack/Zone Model

It is a well known fact that asphalt concrete is a non-linear elastic material, and its fracture behavior is very complicated. Uzan and Levenberg discussed the phenomenology of asphalt concrete fracture and provided an overview of the cohesive crack model (CCM) (*59*). There is a strongly non-linear fracture process zone (FPZ) around the crack tip in asphalt concrete as shown in Figure 4. It is important to mention that in some situations, for HMA mixes, the FPZ can extend to considerable lengths, up to a few centimeters (*60*). In order to account for a relatively large plastic yield zone ahead of a crack tip, Dugdale (*61*) and Barenblatt (*62*) proposed a "correction" for the classical linear elastic fracture mechanics. Their model approximated an elastic-plastic material behavior by applying closure stresses at the crack's tip. Hillerborg et al. proposed a similar model to account for the relatively large FPZ that have been encountered in concrete failure (*63*). The above models are generally considered cohesive cracking models, because the models employ cohesive closure stresses near the crack tip region.

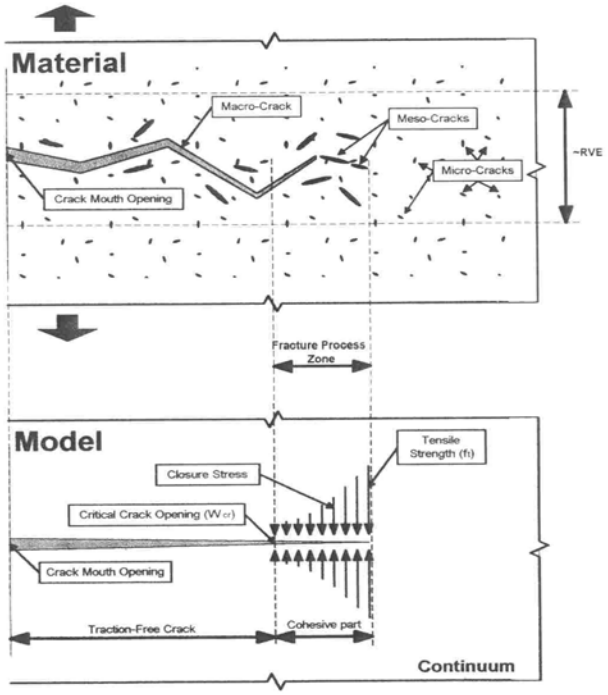

Figure 4. Cohesive Cracking Model Analogy (*59*).

The three fundamental hypotheses of the standard cohesive crack model are as follows:

- The properties of the materials outside the process zone are governed by the undamaged state.
- A crack length can be divided into two separate regions (see Figure 4): a traction free length and a cohesive part. In the cohesive part, crack opening resisting tractions exist, and there is still stress transfer between its faces, which is done by introducing closure stresses. The CCM postulates that the cohesive part of the crack begins to form at a "point" when the maximum principal stress at that "point" reaches the tensile strength of the material (and the crack propagation perpendicular to the maximum stress direction) (*64*). Actually, this postulation is a crack initiation criterion.
- Meanwhile, the stress transfer capability of the cohesive part follows a descending path, from full transfer capability (when the cohesive crack faces just begin to depart [say peak stress conditions]) down to zero transfer capability as the displacement between the two cohesive crack faces reach a critical opening. This representation constitutes the CCM's crack propagation criterion. During the crack propagation analysis, the traction free crack is incrementally advanced whenever the calculated displacement reaches the critical opening in size. The stress transferred between the faces of the crack is described by a post-peak function (softening function). In the case of the opening mode, the function is:

$$\sigma = f(w) \tag{39}$$

where σ is the tensile stress and *w* is the crack opening displacement. This softening curve of the material is considered to be a main component of the cohesive crack model. Although each material has its unique softening curve, determined only by experiments, Petersson first found that the softening curve is similar in shape for different mixtures of Portland cement concrete when the softening curves are plotted in a non-dimensional form (*65*).

Jenq and his associates first applied the CCM to simulate crack initiation and propagation in asphalt concrete mixtures (*60, 66*). However, their work got little attention until the Superpave model team started to develop an advanced asphalt concrete mixture material characterization model (*67*). Then, Uzan and Levenberg developed a laboratory experimental test (direct tension test) to determine the CCM parameters (*59*). Similar work was later done by Seo et al. (*68*). Soares et al. considered the heterogeneity in crack modeling of asphalt concrete mixtures (*69*). The latest research in this field is being led by Buttlar and their associates (*70, 71, 72, 73*). Their research focus was on developing a laboratory test such as a disk-shaped compact tension test to determine the CCM parameters and associated numerical simulation.

In general, the application of the CCM to HMA mixes is still in the preliminary stage. All studies discussed above only applied the CCM to cracking under monotonic loading. To extend the CCM to repeated loading (such as reflection cracking), additional material parameters describing damage accumulation under unloading and reloading are needed. However, no work on this has been done yet. Therefore, the CCM is very promising, but it is not mature yet. More research is still needed.

Non-Local continuum Damage Mechanics Model for Crack Propagation (74)

Wu et al. proposed another approach for modeling crack propagation (*74*). Continuum damage mechanics (CDM) allows one to describe the heterogeneous microprocesses involved during the straining of materials and structures at the macroscale. The basic theory of CDM can be found in papers by Chaboche (*75, 76*). However, the application of CDM to asphalt concrete mixes was pioneered by Lee and Kim (*77, 78*), followed by many other researchers, and it is still under development. The ultimate state of local CDM corresponds generally to macroscopic crack initiation upon which it becomes a crack propagation problem and should be considered in the framework of fracture mechanics. If local CDM is used to describe crack propagation, the spurious mesh dependency then comes into play. Fortunately, this mesh-dependency can be avoided by introducing non-local mechanics. A non-local continuum is a continuum in which the stress at a point depends not only on the strain history of the same point, but also on the strain history of the point's neighbor. Bazant and Jirasek gave a comprehensive, state-of-the-research review of non-local formulations and provided a series of causes as well as motivations for introducing non-local continuum (*79*).

Non-local CDM is essentially an "enhancement" of local-CDM. Thus, the local-CDM is the first to be introduced below.

- *Local CDM*

The stress-strain relationship for a linear elastic material with isotropic damage can be written as:

$$\sigma = (1-\omega)\mathbf{C} : \varepsilon \tag{40}$$

where $C_{ijkl} = \lambda\delta_{ij}\delta_{kl} + \mu(\delta_{ik}\delta_{jl} + \delta_{il}\delta_{jl})$ with $\lambda = \frac{E\nu}{(1+\nu)(1-2\nu)}$ and $\mu = \frac{E\nu}{2(1+\nu)}$ is the elasticity tensor and the scalar $\omega \in [0,1]$ represents the damage. Damage is defined such that ω= 0 represents the initial, undamaged material, and ω= 1 represents a state of complete loss of integrity.

Equation 40 is complemented by the damage evolution law:

$$\dot{\omega} = g(\omega, \tilde{\varepsilon})\left\langle \dot{\tilde{\varepsilon}} \right\rangle_+ \tag{41}$$

where $\dot{\omega}$ is the time derivative of damage ω, $g(\omega, \tilde{\varepsilon})$ is a non-negative function to enforce the irreversibility of damage evolution, $\tilde{\varepsilon} = f(\varepsilon)$ is a measure of the strain that reflects its damaging effect due to cracking, and $\langle . \rangle_+$ denotes the Macaulay bracket, which is an average over a representative volume. A popular definition of $\tilde{\varepsilon}$ is given by Mazars and Cabot (*80*):

$$\tilde{\varepsilon} = \sqrt{\sum_{i=1}^{3} \langle \varepsilon_i \rangle_+^2} \tag{42}$$

where ε_i is the i^{th} principal strain. When dealing with loading histories composed of well-defined, discrete cycles, an evolution law in terms of the number of cycles and the loading amplitudes is often considered more practical (*81*). Such a cycle-based damage evolution law can be obtained from Equation 42 by integrating over one loading cycle resulting in a relation of the form (*82*):

$$\frac{\partial \omega}{\partial N} = G(\omega, \tilde{\varepsilon}_a) \tag{43}$$

where N is the number of load cycles, $\tilde{\varepsilon}_a$ is the amplitude of $\tilde{\varepsilon}$ for the current load cycle, and G is a non-negative function representing the damage accumulation property of the material.

- *Non-local CDM*

Numerous ways have been proposed to incorporate non-locality into the constitutive relations of materials. The most successful ones fall into two categories: integral formulation and implicit gradient formulation. The implicit gradient formulation was recommended since it is much easier to implement in the FE code, and it is a special case of the integral formulation.

Implicit gradient formulation is proposed by Peerlings et al., in which a non-local strain $\bar{\varepsilon}$ is introduced to replace the local strain measure $\tilde{\varepsilon}$ in damage evolution Equations 41 and 42 (*83*). And $\bar{\varepsilon}$ and $\tilde{\varepsilon}$ are related through an additional differential equation:

$$\bar{\varepsilon} - c\nabla^2\bar{\varepsilon} = \tilde{\varepsilon} \tag{44}$$

where $\sqrt{c}$ has a dimension of length and is related to the internal length scale, which should be approximately equal to the maximum grain size of the material, and $\nabla^2 = \sum_i \partial^2 / \partial x_i^2$ is the Laplacian operator. Physically, Equation 44 implies that $\bar{\varepsilon}$ is a spacial average of $\tilde{\varepsilon}$ and the radius of the averaging domain is in proportion to $\sqrt{c}$.

The introduction of Equation 44 leads to a coupled problem between the displacement field and the non-local strain field. The non-local strain becomes an additional degree of freedom for each node. The evaluation of a consistent algorithmic tangent at any Gauss point requires only the current strain ε, damage ω, and non-local strain $\bar{\varepsilon}$ for that same point. In this sense, the implicit gradient formulation is mathematically local and is much easier to be incorporated into existing FE codes.

After developing the non-local CDM-based crack propagation model, the SHRP beam fatigue tests were conducted to calibrate the model's parameters. Frequency sweep test was used to determine the Young's modulus master curves of two HMA mixes. Fatigue tests provided stiffness reduction curves that captured the material degradation process of the two asphalt concrete mixes under repetitive loading. FE models were established to simulate the beam fatigue test. Damage evolution law parameters were calibrated by matching the calculated and measured stiffness reduction curves. Finally, the laboratory calibrated crack propagation model was verified by simulating reflection cracking in an HVS test conducted on an asphalt concrete overlay placed on a cracked and jointed concrete pavement. The model not only recovered the most dominant crack pattern observed in the field, but it also predicted the reflection cracking life of the overlay with reasonable accuracy. Figure 5 shows damage field and crack pattern after 396,000 load repetitions. In conclusion, the implicit gradient non-local CDM, implemented in a FE program, provides a promising mechanistic model for simulating crack propagation in asphalt concrete overlays.

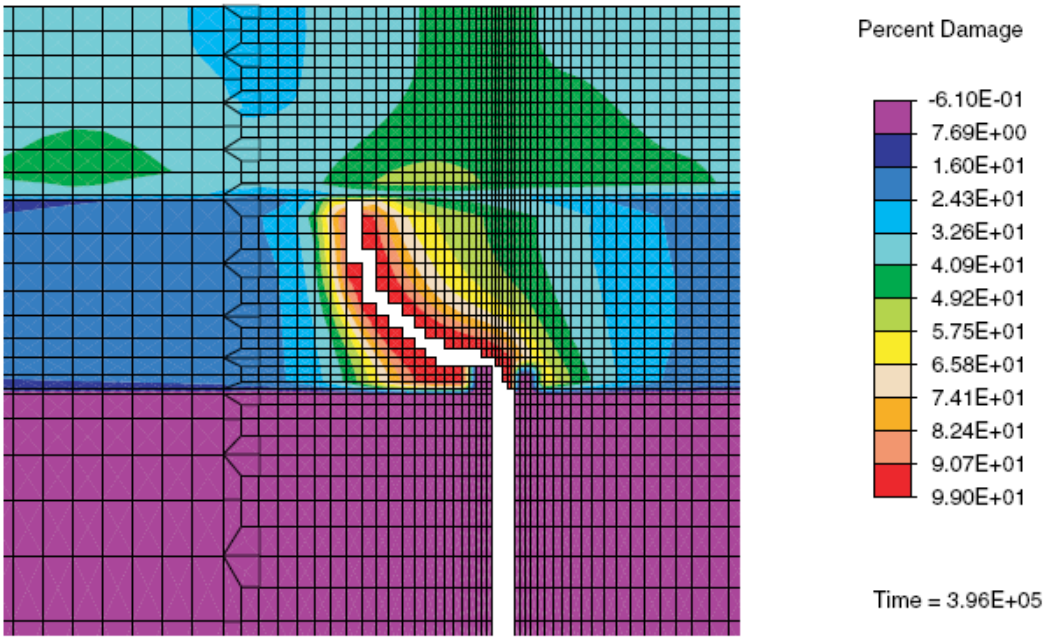

Figure 5. Case 9, Damage Field and Crack Pattern after 396,000 Load Applications (*74*).

In general, the non-local CDM reflection cracking model, similar to the CCM discussed previously, is very advanced. Wu's research results demonstrated this promising model to predict reflection cracking in asphalt overlays over existing pavements (*74*). However, this non-local CDM model is still under development and not ready for routine use.

2.2.3 Integrated Crack Initiation and Crack Propagation Model

The first integrated crack initiation and crack propagation model was proposed by Lytton et al. under SHRP A-005 study (*2*). Since then, significant research efforts led by Lytton have been made at TTI to study fatigue behavior of HMA mixes. The most comprehensive study just finished by Walubita et al. further expanded the SHRP A-005 approach (*84*). The new name for the expanded approach is Calibrated Mechanistic approach with Surface Energy (CMSE). Practically speaking, this CMSE approach is still under development, and significant work is still needed to refine and expand it in order to practically apply this approach for pavement design and analysis. Alternatively, Zhou et al. took the concept of crack initiation and propagation and developed an OT-based fatigue cracking prediction approach (*47*). Detailed information about the OT-based approach is discussed below.

As noted previously, fatigue cracking is the combination of crack initiation and crack propagation process. The number of traffic load repetitions (N_f) to cause a crack to initiate and propagate through the asphalt surface layer is the sum of the number of load repetitions needed for micro-cracks to coalesce to initiate a macro-crack (crack initiation, *Ni*) and the number of load repetitions required for the macro-crack to propagate to the surface (crack propagation, *Np*).

$$N_f = N_i + N_p \tag{45}$$

In the OT based approach, both N_i and N_p are estimated from the fracture properties (A and n), which are determined from the OT.

Estimation of N_i

It is well known that the traditional fatigue models established based on bending beam fatigue tests mainly address the crack initiation stage. Thus, the traditional fatigue model shown in Equation 46 is proposed to estimate N_i.

$$N_i = k_1\left(\frac{1}{\varepsilon}\right)^{k_2} \tag{46}$$

The key issue of estimating N_i is to establish a "bridge" between fracture properties (A and n) and fatigue parameters k_1 and k_2. Based on fracture mechanics, Lytton et al. found the following relationships between these parameters (*2*).

$$k_1 = \frac{d^{\left(1-\frac{n}{2}\right)}}{Ar^n(1-nq)E^n}\left[1-\left(\frac{c_0}{d}\right)^{(1-nq)}\right] \tag{47}$$

$$k_2 = n \tag{48}$$

Equation 47 indicates that parameter k_1 (or $\log k_1$) is a function of k_2 (= n), A, and E:

$$\log k_1 = f(k_2, E, A) \tag{49}$$

As reported by Schapery (*28*), Molenaar (*53*), Jacobs (*55*), Lytton et al. (*2*), and Erkens et al. (*57*), the fracture property A is highly related to parameters n (= k_2) and log E. Thus, it is reasonable to simplify Equation 47 as follows:

$$\log k_1 = a_1 + a_2 k_2 + a_3 \log E \tag{50}$$

where a_1, a_2, and a_3 are regression constants. It is worth noting that a very similar relationship shown in Equation 50 can also be developed based on continuum damage mechanics (*35*). Therefore, Equation 50 is theoretically sound. The key to estimating parameter k_1 is to determine regression constants a_1, a_2, and a_3.

In order to do so, the results from historical fatigue test data were reviewed. It was found that the bending beam fatigue test (BBFT) is the most often used method to characterize fatigue behavior of HMA mixes. In this project, several sources of BBFT data were assembled and used to develop the required regression parameters in Equation 50. After carefully reviewing the available BBFT data, the following data sets were selected for modeling:

- SHRP A-003A fatigue data (*6*): 218 tests,
- Harvey et al.-1996 (*9*): 211 tests,
- Sousa et al.-1998 (*85*): 129 tests,
- Tsai-2002-WesTrack fatigue data (*86*): 150 tests,
- Ghuzlan and Carpenter-2003 (*87*): 478 tests, and
- Tsai and Monisimth-2005 (*88*): 162 tests.

The total number of available BBFT data sets was 1348. The test variables covered in these 1348 sets of data include type of asphalt binder (conventional and modified), asphalt contents, type of aggregates, type of HMA mixes (dense-graded, Superpave, and SMA), air void contents, test temperatures, and aging conditions.

Using the "Solver" optimization technique in Microsoft Excel® by minimizing the sum of squared errors between the measured and the predicted k_1, the regression constants a_1, a_2, and a_3 were determined, and the final k_1 equation is presented below. Figure 6 shows the predicted and the measured logk_1.

$$k_1 = 10^{6.97001 - 3.20145 k_2 - 0.83661 \log E} \qquad R^2 = 0.99 \tag{51}$$

With Equations 46, 48, and 51, N_i can be estimated provided that tensile strain at the bottom of asphalt layer and modulus of asphalt layer are known.

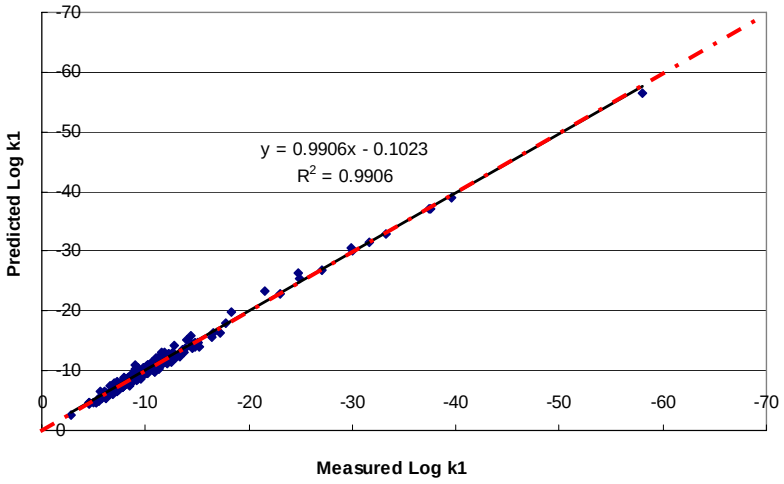

Figure 6. Predicted logk_1 vs. Measured logk_1.

Estimation of N_p

Theoretically, with known fracture properties A and n (from the OT) and SIF (from the FE program or regression equations), N_p can be estimated from Equation 52:

$$N_p = \int_{c_0}^{h} \frac{1}{A(\Delta K)^n} dc \tag{52}$$

where c_0 is the initial crack length and h is asphalt layer thickness. Based on micro-mechanics theory and laboratory test results, Lytton et al. recommended an initial macro-crack length (c_0) of 7.5 mm, which results from micro-cracks growth (*2*).

However, it is well known that one axle passing over a crack results in three loading sequences: shearing (approaching to a crack), bending (loading on the top of the crack), and shearing (leaving from the crack). These three loading sequences make it difficult to directly estimate N_p from Equation 52. In this project, an alternative approach was proposed.

Instead of estimating N_p from Equation 52, the authors recommended calculating the crack propagation length induced by one axle pass using the following form of Paris' law.

$$\Delta c = A(\Delta K)^n \times \Delta N \tag{53}$$

Note that for one axle pass, a crack should propagate three times: Δc_s, Δc_b, and Δc_s, corresponding to the shearing, bending, and shearing loading sequence, respectively. Thus, the crack propagation length (Δc) induced by one axle pass is the sum of Δc_s, Δc_b, and Δc_s.

$$\Delta c = 2 \times \Delta c_s + \Delta c_b = A \times \left[2 \times \left(\Delta K_{Shearing}\right)^n + \left(\Delta K_{Bending}\right)^n\right] \times \Delta N \tag{54}$$

Add more axle passes and repeat the above process until the accumulated crack length is equal to asphalt layer thickness (h). Then, N_p is the sum of all the number of passes.

OT-Based Fatigue Cracking Prediction Approach

Based on the information presented above, the OT-based fatigue cracking prediction approach is proposed. The key steps of this approach are summarized below:

1. Run dynamic modulus test to develop dynamic modulus master curves of HMA mixes.
2. Run the OT to determine HMA fracture properties: A and n.
3. Estimate traditional fatigue model parameters, k_1, k_2, and N_i from Equations 46, 48, and 51.
4. Compute the SIF caused by traffic load from regression equations or FE programs.
5. Estimate N_p with an initial macro-crack length (c_0 =7.5 mm) using Equation 54.
6. Calculate N_f from Equation 45.
7. Calculate the damage caused by a specified number of load repetitions (n) using Miner's law (Equation 55).

$$Damage = \sum \frac{n}{N_f} * 100\% \tag{55}$$

8. Predict fatigue crack amount using the model proposed in the MEPDG (*10*).

$$crack\ area(\%) = \frac{100}{1 + \exp(a_1 + a_2 * \log Damage)} \quad (56)$$

where a_1, a_2 = calibration coefficients.

Note that Equation 56 is a sigmoidal function form, which is bounded with 0 percent cracking as a minimum and 100 percent cracking as a maximum. Specifically, it was assumed that a fatigue cracking value of 50 percent cracking of the total area of the lane theoretically occurs at a damage percentage of 100 percent. This assumption clearly indicates the following relationship:

$$a_1 = -2 \times a_2 \quad (57)$$

In summary, based on theoretical review and 1348 sets of BBFT data, a "bridge" (equations) between crack initiation model (traditional fatigue model) and crack propagation model (Paris' law) was developed in this section. An OT-based fatigue cracking prediction approach including both crack initiation and crack propagation was then proposed.

2.3. RECOMMENDED FATIGUE MODEL FOR TEX-ME

Table 1 presents a comparison among different types of fatigue cracking models based on several parameters, such as the capability of characterizing fatigue crack initiation and propagation process and compatibility of the model to the existing TxDOT FPS framework. As noted in Table 1, both energy and strain-based fatigue models consider only crack initiation of fatigue cracking and ignore the crack propagation stage. The CalME considers the fatigue damage, but this approach still focuses on the crack initiation stage. The authors believe that the lack of focus on crack propagation is why the current "crack initiation" approaches require very large field calibration factors in the order of 15 to 300.

The viscoelastic continuum damage mechanics model, cohesive crack/zone model, and non-local continuum damage mechanics model are very advanced models, and the current status of these advanced models is that they are still under development and are many years away from implementation. Thus, the OT-based fatigue cracking model is currently thought to be the best option for better modeling fatigue cracking, and it is recommended for inclusion in a future Tex-ME program. Furthermore, this approach has proven to be a practical approach for predicting fatigue cracking under TxDOT 9-1502 pooled-fund study project (*89*).

Table 1. Comparison of Fatigue Cracking Modeling Approaches.

Fatigue Models		Development Status	Crack Propagation Mechanisms		Combined Mechanisms	Compatible with FPS	
			Crack Initiation	Crack Propagation Bending+Shear		Yes	No
Strain-based Model	Shell Oil	Finished	√			√	
	AI	Finished	√			√	
	SHRP-A-003A	Finished	√			√	
	MEPDG	Finished	√	√		√	
Energy-based Models		Finished	√	√			√
Damage-based Models	Viscoelastic Continuum Damage Model	Under development	√				√
	CalME	Under improvement	√			√	
Cohesive Cracking Model		Under development		√			√
Non-local Continuum Damage Mechanics Model		Under development		√	√		√
TTI OT-based Fatigue Cracking Model		Finished	√	√	√	√	

CHAPTER 3

MODELS FOR PREDICTING RUTTING IN HMA LAYERS

3. 1. INTRODUCTION

Rutting gradually develops with increasing number of load applications and appears as longitudinal depressions in the wheelpaths accompanied by small upheavals to the sides. Rutting is always a major concern for at least two reasons: 1) if the surface is impervious, the ruts trap water, and at depths of about 0.2 in., hydroplaning (particularly for passenger cars) is a definite threat; and 2) as the ruts progress in depth, steering becomes increasingly difficult, leading to added safety concerns. Therefore, it is important to make efforts to minimize rutting. This literature review focuses on the following aspects of asphalt rutting:

- rutting mechanisms,
- rutting prediction methodology, and
- laboratory testing to characterize rutting resistance of HMA concrete.

3.2. RUTTING MECHANISMS

Rutting occurs in flexible pavements because of the accumulation of small permanent deformations in any of the pavement layers or the subgrade. Such deformations may be caused by too much repeated stress applied to the pavement layers or by an HMA mix that is too low in shear strength. In the first case, the rutting is considered more a structural or construction problem. It is generally the result of an underdesigned or undercompacted pavement section or of an unbound base or subgrade that have been weakened by the intrusion of moisture. In the second case, the rutting is normally a mixture design or placement-related problem. When an asphalt pavement layer has inadequate shear strength, a small but permanent shear deformation occurs each time a heavy truck applies a load. A rut will then appear with enough load applications. As noted below, most pavement surface rutting, at least for reasonably stiff supporting materials, is confined to HMA layers.

Regarding HMA layer rutting, it is commonly accepted that rutting (permanent deformation) is a manifestation of two different mechanisms and is a combination of densification (volume change) and repetitive shear deformation (plastic flow with no volume change). It is difficult to determine the relative amounts of rutting occurring in each HMA layer, and the relative proportions of rut depth that can be attributed to densification and shear, because many factors, such as binder type, binder content, mix type, load level, temperature, initial compacted density, etc., have influence on rutting. The following paragraphs document field trench studies on asphalt pavement rutting.

- **AASHO Road Test-1962**: Trenching studies performed at the AASHO Road Test (*90*) and test-track studies reported by Hofstra and Klomp indicated that the shear deformation rather than densification was the primary rutting mechanism (*91*). The importance of

placing materials at high densities in order to minimize the shear deformation was emphasized.

Measurements at the AASHO Road Test indicated that the surface rut depth reached a limiting value for asphalt concrete thickness of approximately 10 in. Thicker layers did not exhibit additional rutting.

- **Hofstra and Klomp-1972** (*91*): The deformation through the asphalt-concrete layer was greatest near the loaded surface and gradually decreased at lower levels. Because rutting is caused by plastic flow, such a distribution of rutting with depth is reasonable: more resistance to plastic flow is encountered at greater depths and shear stresses are smaller there as well.
- **Uge and van de Loo-1974** (*92*): The deformation within an asphalt layer (thickness reduction under the action of pneumatic tires) no longer increased with increasing layer thickness beyond a certain threshold (130 mm in their case).
- **Eisenmann and Hilmer-1987** (*93*): The rutting was mainly caused by deformation flow without volume change, including two stages:
    - In the initial stage of trafficking, the increase of irreversible deformation below the tires is distinctly greater than the increase in the upheaval zones. In this initial phase, therefore, traffic compaction has an important influence on rutting.
    - After the initial stage, the volume decrement beneath the tires is approximately equal to the volume increment in the adjacent upheaval zones. This is an indication that compaction under traffic is completed for the most part and that further rutting is considered to be representative of the deformation behavior for the greater part of the lifetime of a pavement.
- **Brown and Cross-1989** (*94*)**:** Brown and Cross's trench results showed that permanent deformation is limited to the upper 100 mm (4 in.) of the mix. It also indicated that, at least for reasonably stiff supporting materials, most pavement rutting is confined to the asphalt pavement layer.
- **UC-Berkeley HVS study-2000** (*95*): Air-void contents of cores taken in the wheelpath after trafficking showed relatively little densification, except when the overlays were poorly compacted, despite final rut depths of 15 to 24 mm. Note that the maximum rut depth is defined for their study as the vertical distance between the bottom of the wheelpath and the highest of the adjacent humps. The average proportion of rut depth attributable to the shear flow as opposed to the densification varied between 19 to 100 percent, depending on the overlay type. The greatest shear flow occurred on the 38 mm asphalt-rubber hot mix gap-graded (ARHM-GG) sections and the least on the dense-graded asphalt concrete (DGAC) sections. These results indicated that *rutting did not consist of a process of densification to a very low air-void content followed by rapid shear flow. Instead, it appears that rutting consists of simultaneous densification and shear flow, with the rates of shearing and densification varying at different periods of rut development*. The performance of the poorly compacted ARHM-GG mixes indicated that considerable shear flow occurred at high air-void contents.

On many of these test sections, HVS trafficking was continued well beyond the failure rut depth of 12.5 mm (0.5 in.). Final rut depths ranged between 15 and 24 mm. All of the sections subjected to trafficking by highway wheels/tires had an initial period of rapid rut development, followed by a second period with a reduced rate of rutting that continued until trafficking was stopped. The aircraft wheel test section (513RF) had a slight reduction in rut rate as trafficking progressed, but much less than that of the other test sections. *None of the test sections showed any evidence of a "tertiary" period of rut development* in which the rate of rut development increases again after the second period of reduced rutting rate. *The lack of a tertiary rutting period, despite final ruts of 15 to 24 mm, suggested that the tertiary stage is either:*

- *a phenomenon that occurs only in the laboratory during triaxil repeated load testing,*
- *a phenomenon that occurs in the field when temperatures (40-55ºC) or loads exceed those previously experienced by the mix, or*
- *a phenomenon that only occurs when rut depths have already exceeded 24 mm.*

Results of trenching and profilometer measurements at the top of the base indicates that less than 5 mm of the final average maximum rut depth occurred at the surface of the aggregate base on any of the test sections. Note that the asphalt layer thicknesses of these test sections range from 7.5 to 9.0 in. The measurements are not precise because of noise caused by individual particles at the surface of the base. Disturbance at the surface of the base was minimized during sawing and slab removal, although some disturbance was inevitable due to penetration of the prime coat into the base and adhesion of particles of the base to the asphalt layers when the slabs were removed.

- **Federal Highway Administration's ALF-1999** (*96*)

  - The decreases in air voids due to trafficking indicated that when the rut depth in the asphalt pavement layer was 20 mm, the range in percent densification was approximately 20 to 55 percent, which is 4 to 11 mm.
  - Based on the rutting data from all pavements, rutting occurred in all asphalt pavement lifts. No particular lift or group of lifts consistently rutted the most. The rut depths used in this analysis consisted of both the rut depth due to densification and viscous flow.
  - By splitting the total rut depth into the percent rut depth in the asphalt pavement layer and the percent rut depth in the underlying layers, it was found that *the percentage of rutting in the asphalt pavement layer decreased with increasing total rut depth*. The percentage of rutting in the underlying layer increased as the asphalt pavement layer became thinner due to lateral shearing and flow.
  - The reductions in air voids due to trafficking (densification) in the top and bottom halves of the 200 mm thick asphalt pavement layer were not significantly different at a 95 percent confidence level for any pavement test. Based on the average densification in the top and bottom halves, it was found that the average

densification in the bottom half could be greater than, equal to, or less than the average densification in the top half.

- **TxDOT's trench on SPS1-US281 sections-2001** (*97*): The two trench profiles indicated that the rutting was coming primarily from the top 50 mm (2 in.) HMA layer. As shown in Figure 7, the deep rutting accompanied the considerable lateral shear flow.

Figure 7. Trench Profiles for 161 (Top) and 162 (Bottom).

- **National Center for Asphalt Technology (NCAT) 2000 test track-2004** (*98*): Results from NCAT 2000 test track are summarized below:
  - The amount of permanent deformation in all of the test sections was very low. Permanent deformation essentially stopped when the air temperature was less than 28ºC. The accumulation of permanent deformation in the second summer was significantly less than the first.
  - Under traffic, mixes containing PG 64-22 densified more than mixes containing PG 76-22 binder. As expected, the amount of permanent deformation was over 60 percent less in the sections that contained PG 76-22 as compared to the sections containing PG 64-22.
  - Adding an additional 0.5 percent binder above optimum to the mixes produced with PG 64-22 increased permanent deformation by approximately 50 percent. However, there was no increase when an extra 0.5 percent binder was added to mixes produced with PG 76-22. This may indicate that slightly more binder can

be added to mixes with two high temperature binder bumps to improve durability without sacrificing rut resistance.
    - The amount of permanent deformation calculated based on the pavement densification in most cases exceeded the actual permanent deformation. This supports the fact that most of the test sections had very stable mixes and that the small amount of permanent deformation observed was mainly related to densification or consolidation.
    - The performance of the coarse-graded and fine-graded mixes was about the same. Hence, this study indicates that similar performance would be expected for coarse-graded and fine-graded mixes with respect to permanent deformation.

- **NCAT 2003 test track-2006** (*99*): Results from NCAT 2003 test track are listed as follows:
    - After Phase I (2000) testing, 23 sections were left in place for Phase II. The maximum rutting in any of these sections that were left in place and subjected to 20 million total equivalent single axle loads (ESALs) was 7 mm, which means all mixes are very rut resistant.
    - The factor that most affected rutting of HMA pavements was the asphalt binder PG grade. The modified asphalt reduced the rutting by over 50 percent when compared to unmodified asphalt, which basically confirmed the observation in Phase I (2000) test track.
    - SMA sections had more rutting than the Superpave sections, but neither had significant rutting. It appears that initial rutting in the SMA was due to densification and/or aggregate reorientation. After this initial rutting, little additional rutting occurred. No cracking had occurred in any of the SMA sections.
    - SMA mixes placed in 2003 test track were designed with 50 and 75 gyrations with the Superpave Gyratory Compactor. These mixes have performed well, which indicates that this lower compactive effort can be used to increase the optimum asphalt content and produce improved durability.
    - Laboratory air voids had a significant effect on dense-graded mixes designed using an unmodified asphalt binder. However, the air voids had little effect on performance of those mixes using modified asphalts.
    - The asphalt pavement analyzer (APA) showed a good trend with rutting performance. Additional work is needed with the APA along with other performance tests to clearly develop the best relationships.
    - Coarse-graded and fine-graded mixes were compared. When fine-graded mixes were compared to coarse-graded mixes, they were equally resistant to rutting, less likely to be permeable, quieter, similar in friction, possibly easier to compact, and higher in optimum asphalt content.
- **Florida HVS study-2005** (*100*): Florida DOT studied the influence of modified asphalt binder on rutting using HVS. Figure 8 shows the pavement structures tested under HVS. As noted in Table 2, the HVS testing was conducted at two temperatures: 50ºC and 65ºC. Figure 9 shows a typical rutting development under HVS loading. The observations from Florida's HVS testing are summarized below.

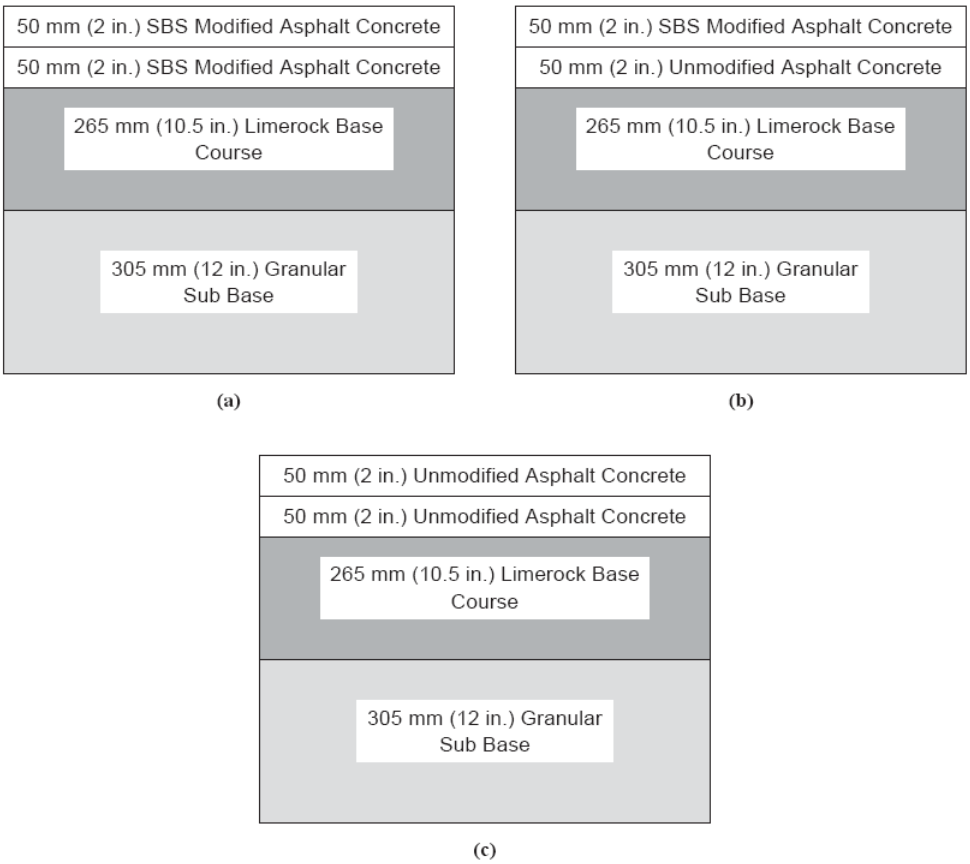

Figure 8. Pavement Cross Sections for (a) Test Tracks 1 and 2 (six test sections), (b) Test Track 3 (three test sections), and (c) Test Tracks 4 and 5 (six test sections).

Table 2. Summary of Ratios of Hump and Wheelpath Volumes.

Test Section Number	Test Temperature (°C)	Final Rut Depth (mm)	Final Number of HVS Passes	Volume Along 1-m Long Section $(m^3) \times 10^{-3}$		Percent of Rutting Attributable to	
				Within Wheelpath	Edge of Wheelpath (Hump)	Shear	Densification
1A	65	12.5	130,000	2.80	1.22	44	56
1B	50	7.8	140,060	1.64	0.69	42	58
2A	65	11.7	160,000	2.77	0.92	33	67
2B	50	9.2	240,000	1.85	0.70	38	62
3A	50	11.3	275,000	2.51	1.11	44	56
3B	50	12.0	280,032	2.37	1.26	53	47
4A	50	16.5	95,478	2.72	2.33	86	14
4B	50	17.0	65,000	2.73	2.30	84	16
5A	50	15.6	113,945	3.20	1.74	54	46
5B	50	20.7	62,935	3.11	3.20	100	0

- As expected, at the beginning of the test, densification would be the major factor in rut development, as the initial level of air voids would decrease in the wheelpath because of repeated wheel loads. However, from Figures 10 and 11, it can be seen that even after only 100 passes, approximately 40 to 50 percent of rutting can be attributed to shear flow. That is, volume of the asphalt concrete in the humps is approximately half the volume of the wheelpath. This indicates that rutting may be caused simultaneously by densification and shear flow of the asphalt concrete. Figure 10 also shows that for unmodified asphalt mixtures, the ratio of hump to wheelpath volume increases with an increasing number of HVS wheel passes. This indicates that after an initial number of wheel passes, most of the rutting occurs only because of shear flow. In comparison, for the modified asphalt mixtures, however, the ratio of hump to wheelpath volume remains somewhat constant, with approximately 40 percent of rutting caused by shear flow.
- An important factor to be noted is that during the course of this study, there was no permanent deformation within the limerock base layer as all the rutting was confined to the asphalt layers alone. This stiff base layer may have affected the formation of humps at the edge of the wheelpath.
- In conclusion, since the only variable between the two Superpave mixes considered in this study is the asphalt binder type, the rut initiation (or initiation mechanism) is primarily controlled by the stiffness of the asphalt binder.

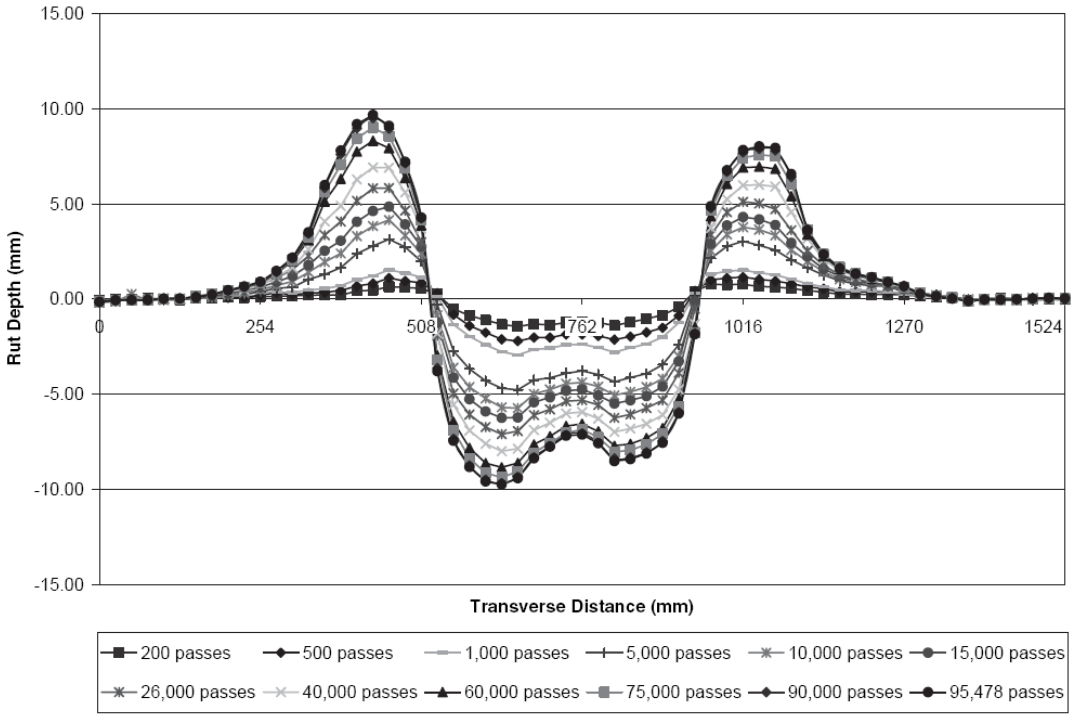

Figure 9. Typical Transverse Profiles for Section 4A.

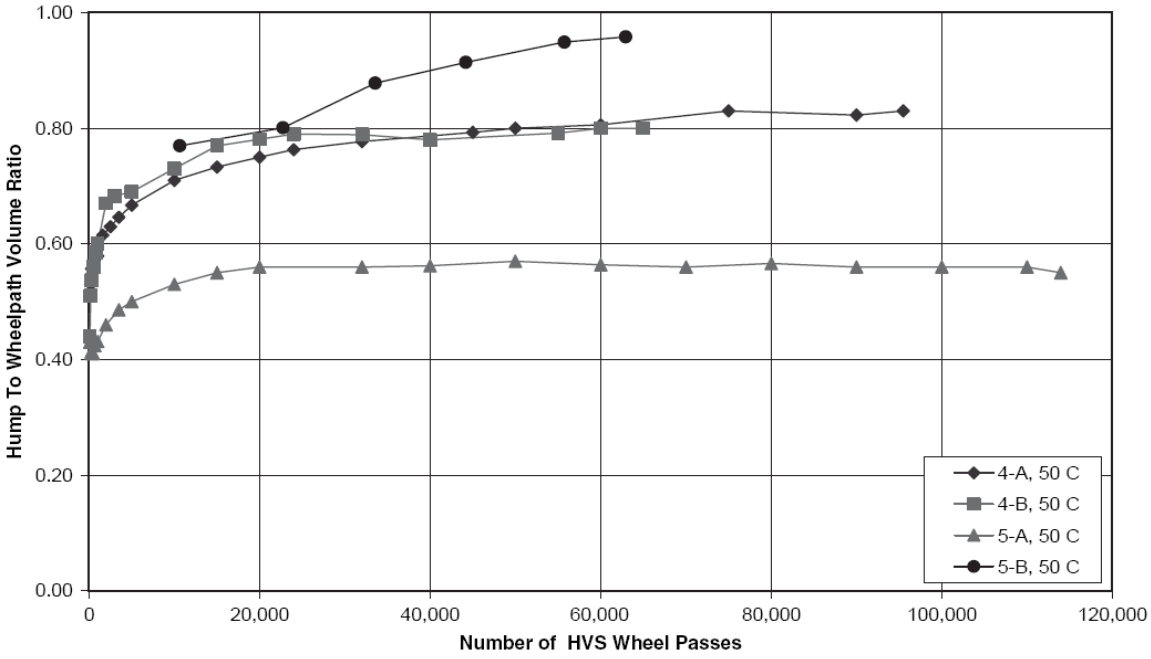

Figure 10. Progression of Hump to Wheelpath Volume Ratio: Unmodified Mixes.

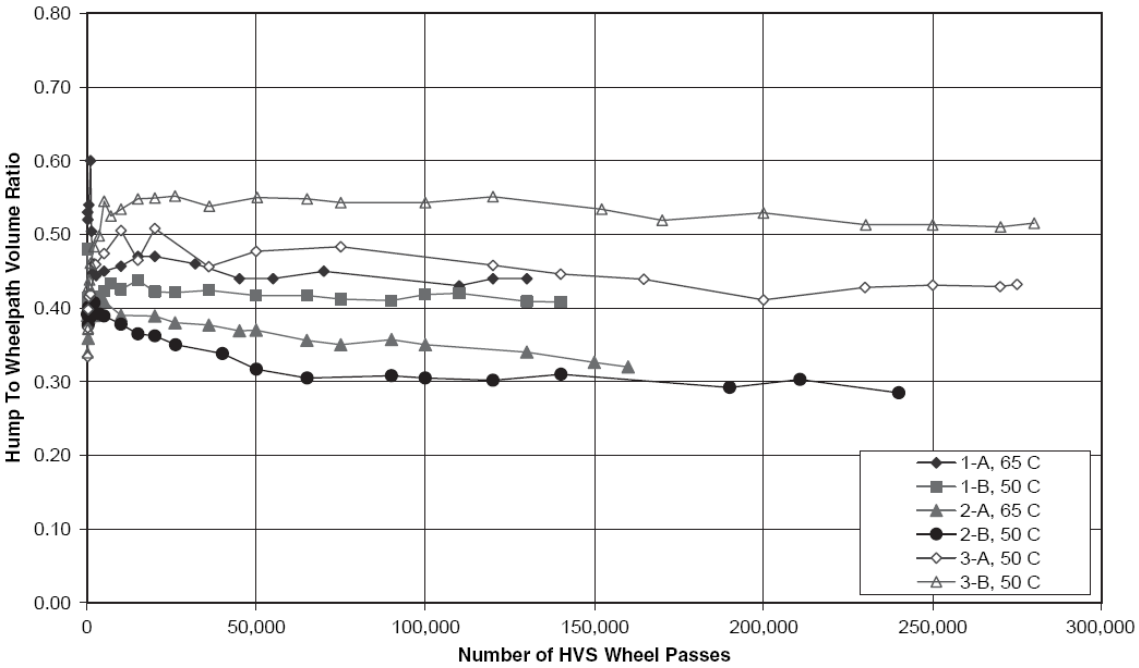

Figure 11. Progression of Hump to Wheelpath Volume Ratio: Modified Mixes.

- Summary comments on rutting mechanism:

  - Available results reviewed clearly show that, at least for reasonably stiff supporting materials, most pavement rutting is confined to the asphalt pavement layer. Furthermore, rutting or permanent deformation, in most cases, is limited to the upper 100-150 mm (4-6 in.) of an HMA layer.
  - *HVS studies at high temperature conducted by UC-Berkeley and Florida Department of Transportation indicated that rutting did not consist of a process of densification to a very low air-void content followed by rapid shear flow. Instead, it appears that rutting consists of simultaneous densification and shear flow, with the rates of shearing and densification varying at different periods of rut development*. Also, it seems that in-place density and asphalt binder type (modified and unmodified) affect the relative contribution of densification and shearing to the rutting.
  - Florida HVS test results also clearly indicated the significant effect of test temperature on rutting development, as shown in Table 2 (Sections 1A vs.1B and 2A vs. 2B).
  - Results from NCAT Phases I and II clearly showed that rutting performance of HMA mix with PG 76-22 binder is significantly different from those mixes with PG 64-22 binder. The observed differences are listed as follows:

    - Mixes designed by Superpave volumetric design method are rut resistant. This observation is also consistent with two national surveys of Superpave mix performance conducted by NCAT.
    - The modified asphalt reduced the rutting by over 50 percent when compared to unmodified asphalt, which basically confirmed the observation in the Phase I 2000 test track.
    - For rutting resistance, mixes with PG 76-22 binder are not so sensitive to asphalt binder content as those with PG 64-22 binder. Adding an additional 0.5 percent binder above optimum to the mixes produced with PG 64-22 increased permanent deformation by approximately 50 percent. However, there was no increase when an extra 0.5 percent binder was added to mixes produced with PG 76-22.
    - Similarly, laboratory air voids had a significant effect on dense-graded mixes designed using an unmodified asphalt binder. However, the air voids had little effect on performance of those mixes using modified asphalts.
  - It should be noted that the above observations are based on thick asphalt pavement and may not be applicable to thin-surfaced asphalt pavements typically used on stabilized granular base or low-volume roads.

3.3 RUTTING PREDICTION MODELS

There currently exist two broad approaches to the problem of designing against rutting or permanent deformation. One approach is design procedures based upon an empirical correlation of excessive deformations related to some predefined "failure" condition of the pavement. This group may be further subdivided into procedures based upon empirical tests used to categorize

the material strength and those designs based upon the use of a limiting subgrade strain (or stress) criteria from elastic layered theory. The major advantage of these procedures is the fact that they currently are workable design tools for pavement analysis. The major disadvantage of such an approach is that they cannot be used to *predict* the amount of deformation anticipated after a given number of load applications.

The second approach encompasses procedures based upon the prediction of accumulated deformations in each component of the pavement system. Obviously, for a more advanced or rational design method, this group is preferred due to the ability to compute cumulative deformations of any pavement system. Substantial research and development efforts have been conducted to make these approaches into rational design procedures. More information about each category is presented below.

3.3.1 Limiting Subgrade Strain

In this approach, the pavement layers are made thick enough to limit the vertical compressive strain at the top of the subgrade to a value associated with a specific number of load repetitions, this strain being computed by means of a layered-elastic analysis. The logic of this approach, first suggested by the Shell researcher (*101*), is based on the assumption that, for materials used in the pavement structure, permanent strains are proportional to elastic strains. Limiting the elastic strain to some prescribed value will also limit the plastic strain. Integration of the permanent strains over the depth of the pavement section provides an indication of the rut depth. By controlling the magnitude of the elastic strain at the subgrade surface, the magnitude of the rut is controlled. An equation of the following form is used to relate the number of load applications to vertical compressive strain at the subgrade surface:

$$N = A\left(\frac{1}{\varepsilon_v}\right)^b \tag{58}$$

where:

N = number of load applications,
ε_v = elastic vertical strain at subgrade surface, and
A, b = empirically determined coefficients.

This approach has been quantified by the back-analysis of pavements with known performance but is semi-empirical in nature since it applies to a particular range of structures with particular materials under particular environmental conditions. Values of the coefficients have been derived for different locations and circumstances. Brown and Brunton reviewed the use of this semi-empirical criterion in 1984 (*102*). While they improved its application to allow for varying rut resistance of different asphalt mixtures, they made it clear that the parameter is only an indicator of the potential for critical rutting to develop as a consequence of permanent deformations developing in all layers. ***A common misconception is that the subgrade strain criterion only refers to permanent deformation in the subgrade.*** The relationships between allowable strain and numbers of standard wheel loads were developed from linear elastic back-analysis of structures with known performance in relation to rutting. The parameter is not, therefore, fundamentally based and cannot be expected to provide reliable design guidance for

pavements with characteristics that differ significantly from those used in the back-analysis. In 1997 Brown critically reviewed this approach again, and concluded that it is out of date and should be replaced (*103*).

3.3.2 Quasi-Elastic Approach (or layer-strain method)

A rather recent approach used for the prediction of permanent deformation is based upon the use of elastic theory and the results of plastic strains determined by repeated load laboratory tests on pavement materials. This approach is termed "quasi-elastic" due to the use of elastic theory to predict a non-elastic response. The approach was initially introduced by Heukelom and Klomp (*104*). Since then, research has been conducted by others such as Monismith (*105*), McLean (*106*), Romain (*107*), Barksdale (*108*), and Morris and Hass (*109*) for soils, granular materials, and asphalt concrete.

The fundamental concept of this approach is the assumption that the plastic strain ε_p is functionally proportional to the elastic state of stress (or strain) and number of load repetitions. This constitutive deformation law is considered applicable for any material type and at any point within the pavement system. The response of any material must be experimentally determined from laboratory tests for conditions (times, temperature, stress state, moisture, density, etc.) expected to occur *in situ*.

Provided the plastic deformation response is known, elastic theory (either linear or non-linear) is then used to determine the expected stress state within the pavement. By subdividing each layer into convenient thickness (Δz_j) and determining the average stress state at each layer increment, the permanent deformation within the jth layer, δ_i^p may be found by summing the (ε_i^p) * (Δz_j) products. This process is done for each layer present in the pavement, and the total permanent deformation is found from:

$$\delta_T^p = \sum_{j=1}^{n} \delta_j^p \tag{59}$$

Obviously, such a summation process is done along a vertical axis (constant horizontal plane coordinates). While different permanent deformation models have been proposed, only four most widely promising models are presented: MEPDG rutting model (*110*), NCHRP 1-40B rutting model (*111*), VESYS rutting model (*112, 113*), and WesTrack-shear-based rutting model (*114*).

- *MEPDG rutting model*

The final MEPDG AC rutting model is presented below:

$$\frac{\varepsilon_p}{\varepsilon_r} = k_1 \times 10^{-3.4488} T^{1.5606} N^{0.479244} \tag{60}$$

where T is temperature (F), N is number of load repetitions, and k_1 is depth adjustment coefficient and defined as follows:

$$k_1 = (C_1 + C_2 \times depth) \times 0.328196^{depth} \quad (61)$$

$$C_1 = -0.1039 h_{ac}^{\ 2} + 2.4868 h_{ac} - 17.342 \quad (62)$$

$$C_2 = 0.0172 h_{ac}^{\ 2} - 1.7331 h_{ac} + 27.428 \quad (63)$$

- *NCHRP 1-40B rutting model*

NCHRP 1-40B rutting model has the same format as the MEPDG rutting model. The enhancement is to adjust permanent deformation constants based on HMA volumetric properties.

$$\frac{\varepsilon_p}{\varepsilon_r} = k_1 \left(10^{k_{r1}} T^{k_{r2}} N^{k_{r3}}\right) \quad (64)$$

where k_1 is depth adjustment function defined in the MEPDG rutting model. k_{r1}, k_{r2}, and k_{r3} are material properties and defined below.

Constant k_{r1} is defined as follows:

$$k_{r1} = \log\left[1.5093 \times 10^{-3} \times K_{r1} \times V_a^{\ 0.5213} \times V_{beff}^{\ 1.0057}\right] - 3.4488 \quad (65)$$

where:

V_{beff}= effective asphalt content in volume (%), and

K_{r1}= intercept coefficient (see Figure 12).

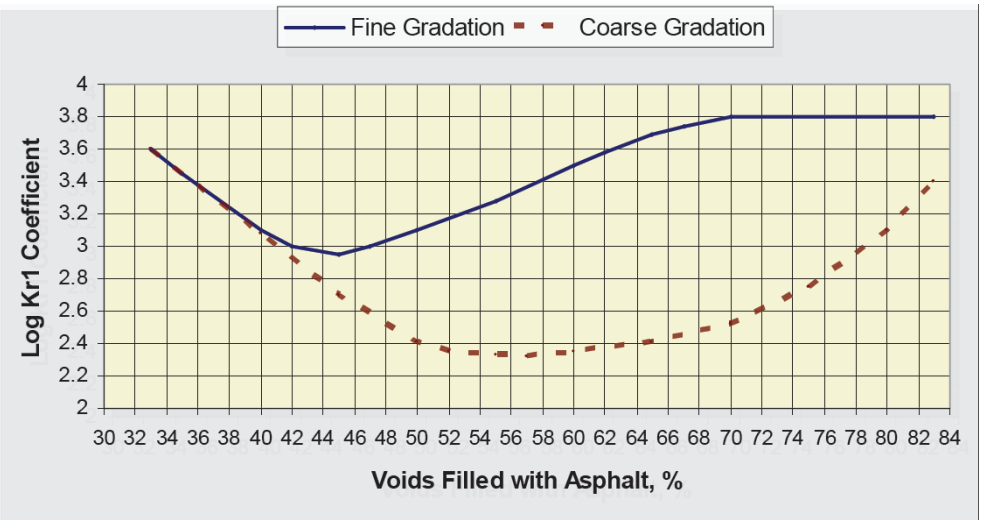

Figure 12. LogKr$_1$ Coefficient vs. Voids Filled with Asphalt (%).

Constant k_{r2} is defined below:

$$k_{r2} = 1.5606 \left(\frac{V_a}{V_{a(design)}}\right)^{0.25} \left(\frac{P_b}{P_{b(opt)}}\right)^{1.25} F_{index} C_{index} \quad (66)$$

where:

$V_{a(design)}$ = design air voids,
P_b = asphalt content by weight,
$P_{b(opt)}$ = design asphalt content by weight,
F_{index} = fine aggregate angularity index (Table 3), and
C_{index} = coarse aggregate angularity index (Table 4).

Table 3. Fine Aggregate Angularity Index Used to Adjust F_{index}.

Gradation – External to Restricted Zone	Fine Aggregate Angularity	
	<45	>45
Dense Grading – External to Restricted Zone	1.00	0.90
Dense Grading – through Restricted Zone	1.05	1.00

Table 4. Coarse Aggregate Angularity Index Used to Adjust C_{index}.

Type of Gradation	Percent Crushed Material with Two Faces				
	0	25	50	75	100
Well Graded	1.1	1.05	1.0	1.0	0.9
Gap Graded	1.2	1.1	1.05	1.0	0.9

Constant k_{r3} is presented below:

$$k_{r3} = 0.4791 \times K_{r3} \times \frac{P_b}{P_{b(opt)}} \tag{67}$$

where:

K_{r3} = slope coefficient:
Fine-graded mixes with GI<20 $K_{r3} = 0.40$;
Coarse-graded mixes with 20<GI<40 $K_{r3} = 0.70$;
with GI>40 $K_{r3} = 0.80$.
GI = Gradation index = $\sum_{i=3/8}^{\#50} \left| P_i - P_{i(0.45)} \right|$

- *VESYS rutting model*

The VESYS rutting model is based on the assumption (or laboratory permanent deformation law) that the permanent strain per loading pulse occurring in a material specimen can be expressed by:

$$\frac{\Delta\varepsilon_p(N)}{\varepsilon} = \mu N^{-\alpha} \tag{68}$$

where:

$\Delta\varepsilon_p(N)$ = vertical permanent strain at load repetition, N;
ε = peak haversine load strain for a load pulse of duration of 0.1 sec measured on the 200th repetition; and
μ , α = material properties depending on stress state, temperature, etc.

The above equation assumes that ε remains relatively constant throughout the test, and thus, the permanent strain increment, $\Delta\varepsilon_p(N)$, at any load cycle is:

$$\Delta\varepsilon_p(N) = \varepsilon - \varepsilon_r(N) \tag{69}$$

where $\varepsilon_r(N)$ is the resilient or rebound strain taking place at cycle N. Then, the rut depth for any single layer after N load cycles can be written as:

$$R_D = H \times \varepsilon_p = H \times \varepsilon \frac{\mu}{1-\alpha} N^{1-\alpha} \tag{70}$$

where H is layer thickness.

The VESYS layer rutting model estimates the permanent deformation in each finite layer as the product of the elastic compression in that layer and the layer material permanent deformation law associated with that layer. The layer rutting model is expressed by:

$$R_D = \int_{N_1}^{N_2} U_s^{+} \frac{e_t}{e_s} \mu_{sub} N^{-\alpha_{sub}} + \sum_{i=1}^{n-1} \int_{N_1}^{N_2} (U_i^{+} - U_i^{-}) \mu_i N^{-\alpha_i} \quad (71)$$

where:

U_s^{+}	= deflection at top the subgrade due to single axle load,
U_i^{+}, U_i^{-}	= deflection at top and bottom of finite layer i due to axle group,
e_t	= strain at top of subgrade due to the axle group,
e_s	= strain at top of subgrade due to a single axle,
μ_{sub}, α_{sub}	= permanent deformation parameters of the subgrade, and
μ_i, α_i	= permanent deformation parameters of layer *i*.

The major feature of the VESYS rutting model is to characterize layer properties rather than global parameters used by MEPDG. For each layer, the VESYS rutting model requires permanent deformation parameters: μ and α_i.

- *WesTrack shearing-strain rutting model*

An alternative to the layer strain approach has been recently proposed to describe the rutting behavior of the WesTrack test sections. In this approach, the pavement is modeled as a multi-layered elastic system, with the asphalt concrete modulus determined from the repeated simple shear test at constant height (RSST-CH) tests. Rutting in AC is assumed to be controlled by shear deformations. Computed elastic shear stress and strain (τ, γ^e) at a depth of 50 mm beneath the edge of the tire are used for rutting estimates. Densification of the asphalt concrete is excluded in the rutting estimates since it has a comparatively small influence on surface rutting.

In simple loading, permanent shear strain in the AC is assumed to accumulate according to the following expression:

$$\gamma^i = a \times \exp(b\tau) \times \gamma^e \times n^c \quad (72)$$

where:

τ	= shear stress determined at this depth using elastic analysis,
γ^e	= corresponding elastic shear strain,
n	= number of axle load repetitions, and
a, b, c	= regression coefficients obtained from field data, RSST-CH laboratory test data and the elastic simulations.

The time-hardening principle is used to estimate the accumulation of inelastic strains in the asphalt concrete under in situ conditions. The resulting equations are as follows:

$$\gamma_j^i = a_j \left[\left(\frac{\gamma_{j-1}^i}{a_j} \right)^{\left(\frac{1}{c}\right)} + \Delta n_j \right]^c \quad (73)$$

where:

j = the j^{th} hour of trafficking,
γ_j^i = the elastic shear strain at the j^{th} hour, and
Δn = the number of axle load repetitions applied during the j hour.

Rutting in AC layer due to the shear deformation is determined from the following:

$$RD_{AC} = K * \gamma_j^i \tag{74}$$

For a 150 mm (6 in.) layer, the value of *K* is 5.5 where the rut depth (RD) is expressed in inches.

3.3.3 Rutting Accumulation Principle

To consider the effects of stresses of different magnitudes on the development of rutting, which result from variations in *traffic loads* and *environmental conditions*, an accumulative damage hypothesis is required, just as for fatigue. A **"***time-hardening***"** procedure appears to provide a reasonable approach (*114, 115*).

For each season *i*, ε_i^p is computed from:

$$\varepsilon_i^p = \varepsilon_i^p(atN=1)\left[\left(N_{eqi} + n_i\right)^S - N_{eqi}^S\right] \tag{75}$$

where:

ε_i^p(at N=1) = permanent strain for *i*, first load repetition computed using the Vermeer model,
n_i = number of load repetitions during season *i*,
N_{eqi} = equivalent total number of load repetitions at beginning of season *i*, and
S = slope of logε^p –logN curve derived from test results.

The N_{eq} is obtained for each element *k* with the time-hardening matching scheme as follows:

Season 1

$$N_{eq} = 0$$
$$\varepsilon_1^p = \varepsilon_1^p(N=1)N_1^{S_1} \tag{76}$$

Season 2

$$N_{eq2} = \left[\frac{\varepsilon_1^p}{\varepsilon_2^p(N=1)}\right]^{\frac{1}{S_2}} \tag{77}$$

$$\varepsilon_2^p = \varepsilon_2^p(N=1)\left[\left(N_{eq2} + n_2\right)^{S_2} - N_{eq2}^{S_2}\right] \tag{78}$$

Season *l*

$$N_{eql} = \left[\frac{\varepsilon_{l-1}^p}{\varepsilon_l^p(N=1)}\right]^{\frac{1}{S_l}} \tag{79}$$

$$\varepsilon_l^p = \varepsilon_l^p\left(N=1\right)\left[\left(N_{eql}+n_l\right)^{S_l} - N_{eql}^{S_l}\right] \quad (80)$$

3.3.4 Comments on Rutting Models

- The layer-strain method is considered a reasonable approach for predicting rut depth, at least for comparative purposes; it provides the added flexibility of allowing use of either linear or nonlinear elastic theory.
- As noted by Brown et al., the development of permanent strain in pavement materials is very difficult to predict from basic material characteristics because of the many variables involved (*116*). This particular mechanical property, even more than dynamic modulus or fatigue cracking resistance, requires a laboratory test to be conducted on the material under consideration. This is because the aggregate structure has a fundamental influence on the result. Consequently, details such as particle surface characteristics, shape, and grading, together with packing and orientation after compaction, are all influential and cannot reliably be predicted using an empirical model.

  For the present, it would be better to rely on good mixture design and testing to limit rutting from the HMA layers and to use allowable stress criteria to deal with the lower layers. Stress criteria could be based on accumulated research knowledge from repeated load triaxial testing, which has identified "Threshold Stress" limits for many materials (*117*).
- Regarding rutting prediction models, both MEPDG and NCHRP 1-40B rutting models have specific parameters and do not need to run laboratory testing. While the NCHRP 1-40B rutting model is an enhanced MEPDG model and considers many more factors (e.g., asphalt binder content, angularity, gradation) influencing rutting, asphalt binder PG grade (a parameter that most affects rutting of HMA pavement based on accelerated load testing) is not directly considered in the NCHRP 1-40B rutting model. It is worth noting that not requiring laboratory testing is both advantageous and disadvantageous for these two models, because while it makes the models simple to implement, not using laboratory characterization of HMA mixes may lead to inaccurate rutting prediction. As noted above by Brown, HMA mixes are very complex, and laboratory characterization of permanent deformation properties is critical to adequately predict field rutting performance.

  WesTrack shearing rutting model requires the RSST-CH to characterize permanent deformation properties of HMA mixes and predict pavement rutting using empirical shift factors. The feature of the WesTrack shearing rutting model is that only the HMA layer located at 2 inches below the pavement surface, regardless of how many HMA layers exist in the pavement structure, is required to be evaluated under the RSST-CH. The disadvantages of the WesTrack shearing rutting model are:

  - high variability of RSST-CH,
  - very limited validation and calibration, and
  - only UC-Berkeley uses this model.

The major feature of the VESYS rutting model is to characterize layer properties rather than global parameters used by MEPDG. For each layer, the VESYS rutting model requires permanent deformation parameters: α_i and μ_i. Its disadvantage also is acquiring these layer properties and running repeated load tests for each layer. However, recognizing the complexity of HMA mixes, it is necessary to characterize each HMA layer's permanent deformation properties in order to make a more accurate prediction.

CHAPTER 4

PERMANENT DEFORMATION MODELS FOR GRANULAR BASE AND SUBGRADES

This chapter reviews permanent deformation models developed from previous research to predict rutting in flexible pavement systems. Rutting generated from permanent deformation of each layer is one of the major distresses associated with increasing roughness and reducing overall serviceability. According to the Project 0-5798 proposal, there is a special concern in dealing with thin flexible pavements. Permanent deformations of thin pavements are primarily generated from the underlying materials. In addition, the proposal mentioned that while calibrated permanent deformation models for the asphalt layer are relatively well-established, models for underlying layers are not as developed. With this in mind, the researchers reviewed existing permanent deformation models for underlying materials, with emphasis on identifying models that are applicable for flexible pavements constructed under thin AC layers.

Based on a review of previous studies, Lekarp et al. identified the following factors that need to be considered for predicting permanent deformation of unbound granular materials (*118*):

- Effect of stress: Permanent deformation is directly related to deviator stress and inversely related to confining pressure.
- Effect of principal stress reorientation: Permanent deformation increases with higher principal stress reorientation.
- Effect of density, fines content, and aggregate type: Higher density generally gives less permanent deformation development. Permanent deformation resistance is reduced as the amount of fines increases. Angular aggregates provide better permanent deformation resistance due to particle interlocking.
- Effect of number of load applications: Permanent deformation gradually accumulates with the number of load applications. The rate of permanent deformation accumulation varies with material properties and stress states as shown in Figure 13. Permanent deformation can become unstable after the flow point.
- Effect of moisture content: Increasing moisture content leads to reduction of effective stress because of excess pore water pressure resulting in loss of cohesion and bearing capacity and generation of permanent deformations.

There are two representative approaches for computing rutting in flexible pavement systems. The first approach is to calculate the permanent strain under the wheel load at different depths along the same vertical line and to sum up the contributions of all layers. The other approach is to compute the rate of rutting for each load application and integrate it over the design life. To use these approaches, the appropriate permanent strains need to be estimated. There are several models that have been proposed for predicting permanent strains. Table 5 summarizes models that can be used to predict permanent strains in materials underlying the

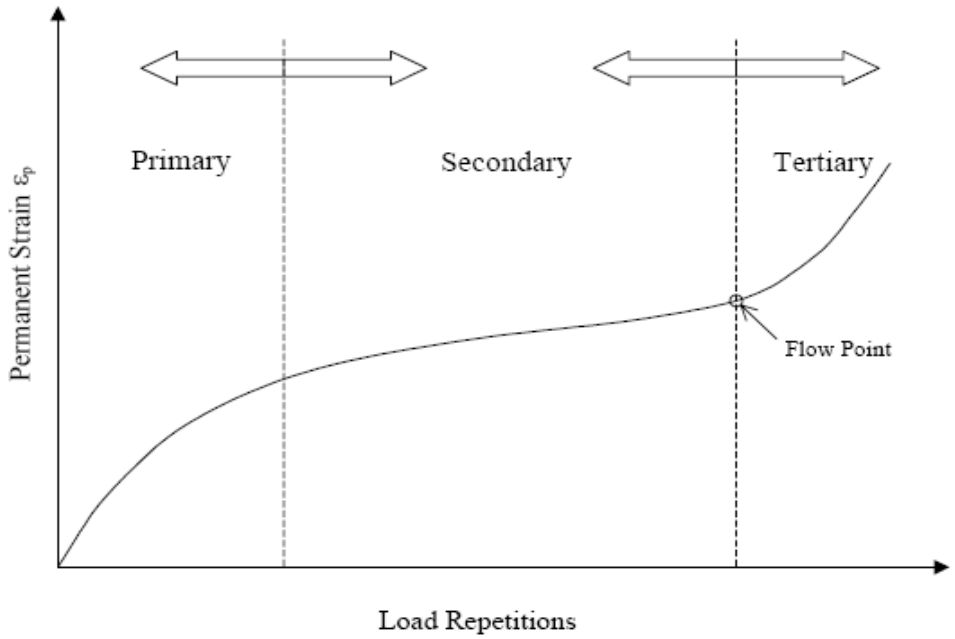

Figure 13. Typical Permanent Deformation Behavior (After MEPDG Supplemental Documentation Appendix GG-1).

pavement surface. From Table 5, it is observed that permanent strains have been related to the stress state, Mohr-Coulomb strength parameters, and the number of load applications, respectively.

Recently, additional studies have been conducted to expand or improve model equations through intensive laboratory and field test data. Ceratti et al. performed full-scale tests, developed in a Brazilian pavement test facility, to investigate rutting of thin pavements (*126*). They built five test sections with 1-inch seal coat over weathered basalt base materials, which had three different thickness levels (6.3, 8.3, and 12.6 inches), two levels of strength index, constructed on a 2-ft layer of clayey subgrade. Trafficking was simulated until 1-inch ruts developed. Test results showed that the contribution of base rutting was most pronounced, and the number of applications (N) for 1-inch rutting was related to axle load (L), pavement thickness (T), and material strength index (IS). They obtained the following equation from the tests:

$$N = 10^{5.25} L^{-3.97} T^{4.12} IS^{1.98} \quad (81)$$

In addition, thicker pavements showed two distinct phases of rutting development: a rapid growth at the beginning of the test, and after that a gradual rate of growth. In thinner pavements, a third phase in which rutting grows exponentially was also identified. This finding indicates that rutting of thin pavements accelerates after some number of applications due to weakened structural capacity.

Table 5. Summary of Permanent Deformation Prediction Models.

Reference	Model
Duncan and Chang (*119*)	$\varepsilon_a = \frac{\sigma_d}{k\sigma_3^n} \Big/ \left[\left(1 - \frac{\sigma_d R_f}{2(C\cos\phi + \sigma_3 \sin\phi)}\right)\frac{1}{(1-\sin\phi)}\right]$ ε_a = permanent axial strain $k\sigma_3^n$ = relationship defining the initial tangent modulus as a function of confining pressure (k and n are constants) R_f = a constant relating compressive strength to an asymptotic stress difference C = cohesion ϕ = angle of internal friction σ_d = deviatoric stress
Barksdale (*120*)	$\varepsilon_p = a + b \log N$ ε_p = total permanent axial strain N = number of load cycles a and b = constants
Monismith et al. (*121*)	$\varepsilon_p = IN^S$ ε_p = total permanent axial strain N = number of load cycles I and S = experimentally derived parameters
Kenis (*122*)	$\frac{\varepsilon_p(N)}{\varepsilon_r} = \mu N^{-\alpha}$ $\varepsilon_p(N)$ = permanent strain due to single or Nth load application ε_r = resilient strain at the 200th repetition N = number of load cycles μ and α = VESYS parameters
Lentz and Baladi (*123*)	$\varepsilon_p = \varepsilon_{0.95\,S_d} \cdot Ln\left(1 - \frac{\sigma_d}{S_d}\right)^{-0.15} + Ln(N)\left(\frac{\sigma_d}{S_d}\right)n \Big/ \left(1 - m\left(\frac{\sigma_d}{S_d}\right)\right)$ S_d = static shear strength $\varepsilon_{0.95Sd}$ = static strain at 95 percent of static strength n = $(0.809399+0.003769\sigma_3)*10^{-4}$ m = $0.856355+0.049650 Ln\sigma_3$
Tseng and Lytton (*124*)	$\varepsilon_a = \varepsilon_0 \exp\left(-\frac{\rho}{N}\right)^{\beta}$ ε_0, β, and ρ = three parameter model constants
Ullidtz (*125*)	$\varepsilon_p = \alpha\left(\frac{\sigma_d}{P_a}\right)^{\beta} \cdot N^{\gamma}$ P_a = atmospheric pressure α, β, and γ = constants

Park conducted permanent deformation testing with different base materials and clayey subgrade in order to correlate material properties with the coefficients of the VESYS and three parameter permanent deformation models (*127*). Consequently, he established equations to estimate these parameters as functions of water content, dry density, confining and deviatoric pressures, resilient modulus, first stress invariant, and total suction. He predicted rutting based on an accelerated rutting model proposed by Lytton that considered moisture ingress into thin low-volume pavements. Using liquefaction criteria and soil-water characteristic curves expressed by Gardner's equation, the VESYS α value was adjusted for saturated and unsaturated conditions.

$$\text{For saturated conditions, } \alpha = 1 - \frac{\theta\left(\partial h / \partial\theta\right) N e^{-k\left(\partial h / \partial\theta\right) t_v \delta}}{K(1 - n + \theta)} \tag{82}$$

$$\text{For unsaturated conditions, } \alpha = 1 - \frac{f\theta^2\left(\partial h / \partial\theta\right) N e^{-k\left(\partial h / \partial\theta\right) t_v \delta}}{K(1 - n + \theta)} \tag{83}$$

$$\partial h / \partial\theta = \frac{1}{0.4343} \frac{S\gamma_w}{\gamma_d} h \tag{84}$$

where:

S = degree of saturation,
γ_w = unit weight of water,
γ_d = dry unit of weight of soils,
h = soil suction (cm),
θ = volumetric water content,
N = number of load repetitions,
k = Gardner's unsaturated permeability,
t_v = time between vehicles,
δ = a factor depending on the range of soil size ($1/D_{10}^2$),
K = bulk stress of soils, and
f = unsaturated shear strength function ($1/\theta$).

Generated rutting curves showed a rapid rut rate after around 100,000 load repetitions due to the effect of moisture on the change of modulus.

The MEPDG uses a different set of equations to predict the parameters of the permanent deformation model proposed by Tseng and Lytton (*124*). In their original work, the three parameters were originally correlated with water content (W_c), deviatoric and bulk stresses, and resilient modulus. Through calibrations of the model, NCHRP 1-37A (*128*) came up with a revised set of equations, which eliminated the stress terms as given below. The guide recommends that further calibrations be conducted for local practice.

$$\frac{\varepsilon_p}{\varepsilon_r} = \left(\frac{\varepsilon_0}{\varepsilon_r}\right) e^{-\left(\frac{\rho}{N}\right)^{\beta}}$$
$$\left(\frac{\varepsilon_0}{\varepsilon_r}\right) = \frac{\left(0.15e^{\rho^{\beta}}\right) + \left(20e^{(\rho/10^9)^{\beta}}\right)}{2}, \quad (85)$$
$$\rho = 10^9 \left(\frac{-4.89285}{1-\left(10^9\right)^{\beta}}\right)^{\frac{1}{\beta}}, \text{ and } \log\beta = -0.61119 - 0.017638W_c$$

VESYS is a well-developed probabilistic and mechanistic flexible pavement analysis computer program (http://www.volpe.dot.gov/sbir/sol03/docs/vesys-intro.doc). Two types of rutting models are incorporated into the VESYS program, which are called the "layer rutting" and "system rutting" models. The layer rutting model estimates the permanent deformation in each finite layer as the product of the elastic compression in that layer and the layer material permanent deformation law associated with the layer. The layer rutting model is expressed by:

$$R_D = \int_{N_1}^{N_2} U_s^{+} \frac{e_t}{e_s} \mu_{sub} N^{-\alpha_{sub}} + \sum_{i=1}^{n-1} \int_{N_1}^{N_2} (U_i^{+} - U_i^{-}) \mu_i N^{-\alpha_i} \quad (86)$$

where:

U_s^{+}	= deflection at top of the subgrade due to a single axle load,
U_i^{+} and U_i^{-}	= deflection at top of and bottom of the finite layer *i* due to axle group,
e_t	= strain at top of subgrade due to the axle group,
e_s	= strain at top of subgrade due to a single axle load,
α_{sub}, μ_{sub}	= permanent deformation parameters of the subgrade, and
α_i, μ_i	= permanent deformation parameters of layer *i*.

The system rutting formulation treats the pavement system as a whole and first calculates an equivalent set of pavement system permanent deformation parameters, μ_{sys} and α_{sys}, which are determined as functions of load repetitions by least square regression analysis. Pavement surface rut depth is estimated according to the equation:

$$R_D = \int_{N_1}^{N_2} U \mu_{sys} N^{-\alpha_{sys}} dN \quad (87)$$

where U is pavement surface deflection. Zhou and Scullion calibrated the VESYS rutting model using the TxMLS data on US 281 (*129*). Rutting parameters (μ and α) were backcalculated and used to calibrate the rutting parameters determined from laboratory tests conducted using the protocol developed at TTI.

Uzan expanded the universal soil model to express the ratio of the accumulated permanent strain to the resilient strain as a function of the bulk and octahedral shear stress for granular materials as follows (*130*).

$$\log\frac{\varepsilon_p}{\varepsilon_r}=\left[a_0+a_1\left(\frac{\theta+k_6}{p_a}\right)+a_2\left(\frac{\tau_{oct}}{p_a}\right)\right]+\left[b_0+b_1\left(\frac{\theta+k_6}{p_a}\right)+b_2\left(\frac{\tau_{oct}}{p_a}\right)\right]\log N \quad (88)$$

where $a_0 = -0.01891$, $a_1 = -0.2514$, $a_2 = 0.358983$, $b_0 = 0.310932$, $b_1 = -0.072703$, $b_2 = 0.098332$, and $k_6 = 0.055$ MPa.

He also proposed the equation below to predict the ratio of the accumulated permanent strain to the resilient strain for clayey subgrades.

$$\log\frac{\varepsilon_p}{\varepsilon_r}=-1.38164+0.324655LogN \quad (89)$$

Zhou recently expanded Uzan's model based on the HVS data from the cold regions research lab including the water content term for A-2-4 and A-4 soils, respectively.

$$\log\frac{\varepsilon_p}{\varepsilon_r}=0.000851-0.246165\left(\frac{\theta}{p_a}\right)+3.418417\left(\frac{\tau_{oct}}{p_a}+1\right)+2.895124\log W_c+0.16627\log N \quad (90)$$

$$\log\frac{\varepsilon_p}{\varepsilon_r}=0.0112462-0.7195857\left(\frac{\theta}{p_a}\right)+3.8593287\left(\frac{\tau_{oct}}{p_a}+1\right)+0.6191976\log W_c+0.2659706\log N \quad (91)$$

Henning et al. presented LTPP studies in New Zealand (*131*). Since establishing 63 LTPP sites during 2000, they updated the database each year and currently manage 82 sites. Using the LTPP and the Canterbury Accelerated Pavement Testing Indoor Facility (CAPTIF) data, they tried to model pavement deterioration with respect to cracking and rutting. The CAPTIF data was required since the LTPP data was limited in the number of sections that have failed. From the developed rutting progression model data, the following findings were drawn:

- Three phases of rutting were identified: 1) initial densification; 2) rutting progression; 3) initiation of accelerated rut progression. For strong pavements, only two phases, initial densification and progression, were detected.
- There is no appropriate model to predict rutting progression at the current time.
- A linear logistic model was developed to predict the initiation of accelerated rut rate.

From analyses of the test data, researchers found that the initial densification (in mm) is related to the structural number, SNP, according to the equation:

$$\mathrm{Rut}_{\mathrm{initial}}=3.5+\mathrm{e}^{(2.44-0.55\mathrm{SNP})} \quad (92)$$

where SNP is the structural number derived from the falling weight deflectometer (FWD). Researchers also found the rut progression in thin pavements (total layer thickness less than 6 inches) to be about 0.02 inches per year, and 0.01 inch per year for thick pavements. With respect to modeling the initiation of accelerated rut progression, researchers came up with the following equation:

$$\text{Rut}_{\text{accel}} = \frac{1}{1+e^{(-7.568*10^{-6}*\text{ESA}+2.434*\text{SNP}-[(4.426,0.4744)\text{for thickness}=(0,1)]}} \quad (93)$$

where ESA is equivalent standard axles. In the above, the thickness code is 0 for base layer thickness less than 6 inches and 1 for thickness greater than 6 inches.

In thinner pavements, pavement maintenance in the form of surface overlays is commonly performed to prevent further rutting from water intrusion. Mishalani and Kumar studied the impact of overlays on pavement rutting with respect to design level and material quality (*132*). They modified the rutting models proposed by Archilla and Madanat to take into account the overlay effect on rutting development (*133*). The cumulative rut depth at a point in time t is given by the summation of the incremental changes in each period s up to t as follows:

$$RD_t = \beta_{14} + \sum_{s=1}^{t} a_s \exp(\beta_9 N_s)\Delta N_s + \sum_{s=1}^{t} m_s \exp(\beta_{13} N_s')\Delta N_s' + \mu + \varepsilon_t \quad (94)$$

$$a_s = \beta_4 \exp[-(\beta_1 T_1 + \beta_2 T_2 + \beta_3 T_3)]\exp[\beta_8 (TI_s/1000)] \quad (95)$$

$$m_s = (\gamma_1 + \gamma_2 \cdot GI) + (\gamma_3 + \gamma_4 \cdot GI)\left(\frac{VFA}{100}\right)^{(\gamma_5+\gamma_6/GI)} \cdot TempDum_s + \gamma_8 AV \exp(\gamma_9 N_s') \quad (96)$$

where:

β_{14}	=	parameter that captures the initial rut depth immediately after pavement construction,
β_9, β_{13}	=	parameters capturing the hardening of the underlying and the AC layers, respectively,
N_s	=	cumulative loading up to period s for rutting originating in the underlying layers,
ΔN_s	=	load applications during period s for rutting originating in the underlying layers,
N_s'	=	cumulative loading up to period s for rutting originating in the AC layers,
ΔN_s'	=	load applications during period s for rutting originating in the AC layers,
T_1	=	thickness of the AC layer,
T_2	=	thickness of the granular base layer,
T_3	=	thickness of the subbase layer,
TI_s	=	thawing index during period s,
βi	=	model parameters (i = 1, 2, 3, 4, 8),
GI	=	gradation index of the AC mix,
VFA	=	voids filled with asphalt,
AV	=	in-place air voids,
$TempDum_s$	=	1 if the mean maximum temperature during period s is greater than 28.6 °C, 0 otherwise,
γi	=	model parameters (i = 1, 2, 3, 4, 5, 6, 8, 9),

μ	=	time invariant random distance with zero mean and constant variance reflecting unobserved heterogeneity across the pavement sections, and
ε_t	=	error term with zero mean and constant variance reflecting measurement errors and unobserved explanatory variables.

Overall rutting versus time was predicted using Equation 94 with three levels (low, medium, and high) of design and material quality based on experimental design. Design levels varied with thicknesses of each layer. The researchers selected three levels of GI, VFA, and AV and noted the following findings:

- The rut predictions over the time varied with design level when overlays are applied but eventually the rut depth converged to a constant value.
- The rut predictions over the time varied with material quality when overlays are applied and the rut depth converged to different levels.
- The sensitivity in terms of absolute values of rutting to design levels decreased as maintenance frequency increased.
- The sensitivity in terms of absolute values of rutting to material quality levels increased as maintenance frequency increased, implying that for reaping the most value from using a high material quality, a high maintenance frequency should be adopted.
- The model needs to be further verified with field test data.

CHAPTER 5
FATIGUE CRACKING MODELS FOR CHEMICALLY STABILIZED MATERIALS

This chapter reviews fatigue cracking models developed mainly from a PCA research project (*134*) to predict fatigue cracking of chemically stabilized layers in flexible pavement systems. In this chapter, the chemically stabilized materials are defined first before discussing two fatigue models including the MEPDG and PCA-CTB (cement treated base) models. Finally, the model input requirements and associated laboratory tests are also discussed.

5.1 DEFINITION OF CHEMICALLY STABILIZED MATERIALS

In both the MEPDG and the PCA-CTB programs, chemically stabilized layers are high quality base materials that are treated with cement. These programs are intended for use with "engineered" bases or sub-bases. An engineered base requires a formal laboratory design procedure where both strength and durability criteria are achieved. Where a small amount of chemical stabilizer is added to granular base materials to improve their strength, lower the plasticity index, or decrease moisture susceptibility, this will not be considered an "engineered" material unless a strength/durability test is performed. Without the use of strength and durability criteria in the design process, the resulting bases should be considered unbound materials.

On the other hand, if these layers are engineered to provide structural support, then they can be treated as chemically stabilized structural layers. To ensure durability and long-term adequate performance of chemically stabilized materials, the MEPDG recommends the 7-day UCS criteria shown in Table 6.

Table 6. Minimum Values of 7 Days Unconfined Compressive Strength, for Chemically Stabilized Materials in the MEPDG.

	Rigid pavements	Flexible pavements
Base	500 psi	750 psi
Subbase, select material, and subgrade	200 psi	250 psi

The numbers proposed in Table 6 are thought to be high, many DOT's have recently moved to designing stabilized bases with lower strength requirements. A common 7-day strength requirement is 300 psi. In some DOT's, 7-day strengths of between 200 and 250 psi have been used with success. For the purpose of the PCA-CTB program, 7-day strength of lower than 250 psi may be used if the base also meets a moisture susceptibility requirement.

5.2 FATIGUE CRACKING MODELS FOR CHEMICALLY STABILIZED MATERIALS

Both the MEPDG and PCA-CTB models are presented as follows.

MEPDG Fatigue Cracking Models for Chemically Stabilized Materials

The fatigue relationship used in the MEPDG is a function of the stress ratio:

$$\log N_f = \frac{(0.972\beta_{c1} - (\frac{\sigma_t}{M_r})}{0.0825 * \beta_{c2}} \quad (97)$$

where

N_f = number of repetitions to fatigue cracking of the stabilized layer;
σ_t = maximum traffic induced tensile stress at the bottom of the stabilized layer (psi);
M_r = 28-day modulus of rupture (Flexural Strength) (psi); and
β_{c1}, β_{c2} = field calibration factors.

PCA-CTB Fatigue Cracking Models for Chemically Stabilized Materials

The PCA already have a fatigue relationship which they have used for many years to design pavements containing cement treated bases. This relationship, which is also included in the PCA-CTB program is also a function of the stress ratio but in an exponential form and is shown below:

$$N_f = \left(\frac{\beta_{c4}}{\sigma_t / M_r} \right)^{\beta_{c3} \cdot 20} \quad (98)$$

where

β_{c3}, β_{c4} = field calibration factor.

In a recently completed PCA study (134) Dr. Jacob Uzan calibrated these two models using the accelerated pavement test data from PCA. He developed factors for two materials types: cement treated base and fine graded soil cement. The fine graded soil cement would be equivalent to a treated sub-base or subgrade layer. The final calibration factors for two types of cement treated materials are presented below:

- For cement treated base:

  β_{c1}=1.0645, β_{c2}=0.9003, β_{c3}=1.0259, and β_{c4}=1.1368

- For fine-grained soil cement:

  β_{c1}=1.8985, β_{c2}=2.5580, β_{c3}=0.6052, and β_{c4}=2.1154

The PCA has evaluated these models and compared them with existing procedures. Both models have been incorporated into simple design programs. The current plan is to incorporate both of these design models into new PCA software to be released in mid 2008. The TTI research team from study 5798 will review these models and other models developed for other stabilizers, and consider them for incorporation into TexME.

5.3 MODEL INPUT REQUIREMENTS AND ASSOCIATED LABORATORY TESTING

The two major inputs required by the models are resilient modulus and modulus of rupture of the chemically stabilized materials. Significant efforts have been made to evaluate how to generate these two input parameters by Scullion under the PCA research project (*134*). The final recommendation is presented as follows:

- Level 1 resilient modulus input: The standard resilient modulus test is not recommended for routine use. The test is very difficult to run on cement treated materials. The strain levels are very low, requiring accurate instrumentation. The biggest problem was that even with careful sample preparation, problems are still encountered with the end conditions - unlike other materials where a few seating loads will ensure good contact. Seating loads do not ensure uniform contact with cement treated materials, where even small unevenness of the surface causes major differences in strains measured on either side of the test sample.

  For the limited test program conducted by Scullion et al. (*134*), it appears that the seismic modulus device is a better, more repeatable test for estimating the resilient modulus of stabilized materials. However, samples for this test should have a minimum length to diameter ratio of 1.5 to 1. The seismic modulus equipment used in the PCA study is widely available within TxDOT; it was found in this study that the resilient modulus can be estimated to be 75% of the measured seismic modulus.

  Measuring Modulus of Rupture in the laboratory was performed in the PCA study however this is also difficult particularly if the cement treated base has a relatively low cement content. Level 1 testing was found to be very difficult with these materials.

- Level 2 resilient modulus input: The most attractive level for most users will be Level 2 where the design values are related to the standard 7-day UCS value. The recommended relationships are given below:

  <u>For cement treated bases</u>

  $$\text{28 day Modulus of Rupture (ksi)} = 7.30^* \sqrt{UCS} \quad (99)$$

  $$\text{Resilient Modulus (ksi)} = 36.5^* \sqrt{UCS} \quad (100)$$

  <u>For fine-grained soil cement</u>

  $$\text{28 day Modulus of Rupture (ksi)} = 6.32^* \sqrt{UCS} \quad (101)$$

  $$\text{Resilient Modulus (ksi)} = 31.6^* \sqrt{UCS} \quad (102)$$

- Level 3 resilient modulus input: The default values are given below.

  <u>For cement treated bases</u>

  Resilient Modulus 1000 ksi, Modulus of Rupture 200 psi, Poisson's Ratio 0.15

  <u>For fine-grained soil cement</u>

  Resilient Modulus 500 ksi, Modulus of Rupture 100 psi, Poisson's Ratio 0.25

Note that the relationships and values proposed will be further reviewed in this study. The level 2 approach seems reasonable. Necessary lab test will be conducted to evaluate these UCS relationships for other chemical stabilizers. Additionally, the PCA software will also be reviewed for consideration for use in Texas.

CHAPTER 6

REVIEW OF LABORATORY TESTING PROCEDURES

One critical part of any pavement design procedure is how to measure the material properties that must be used as inputs to the design models. Many sophisticated models have been developed, but few (or none) have been implemented for routine pavement design. One difficulty is the high cost of obtaining the required rutting and cracking material properties for each layer. DOTs run many tests to select the optimal asphalt content and gradation for HMA layers, but these tests do not traditionally provide inputs to structural design models. In Texas, the performance/acceptance test from HMA is the Hamburg wheel tracking test; more recently the cracking potential of HMA layers is being assessed with an overlay tester. For granular base materials, the different classes of base are routinely characterized by their triaxial strength, both confined and unconfined after capillary soak. Up until now, the results of these tests have not been used to provide inputs to thickness design programs.

In recent years, it has been proposed that multiple levels of material inputs may be required for any new ME empirical design program. The research team believes that this approach is reasonable for the future development of the Texas ME. Such an approach is described below.

- Level 3 will be default values in look up tables for each specification item.
- Level 2 will be material properties inferred from TxDOT current design and acceptance tests (Hamburg/Overlay tester), triaxial strength (Tex Method 117E or 143E), and unconfined compressive strengths (Tex Method 121E). These will typically be regression equations.
- Level 1 properties will be obtained from running advanced tests such as repeated load triaxial, beam fatigue, etc.

In the remainder of this section, a description will be given of the different laboratory tests available for characterizing the rutting and cracking potential of pavement layers. This will be followed by recommendations on which tests to include in Year 2 of this project. These tests will be run on materials obtained from test pavements being monitored to evaluate either pavement response or pavement performance. The test pavements include the NCAT test track, the recently completed HVS test track in California, the instrumented site being installed on SH 6 north of Calvert, and the thin instrumented site being constructed at Texas A&M's Riverside Campus.

6.1 ASPHALT RUTTING TESTING

HMA mixtures need to be designed to resist rutting (accumulation of permanent deformation) under high tire contact pressures and from a large number of load repetitions. Rutting is caused by a combination of densification (decrease in volume and AV) and shear deformation (equal volume movement and increase in AV). For well-compacted HMA concrete pavements, past research has indicated that shear deformation rather than densification was the primary rutting mechanism. Resistance to permanent deformation or shearing stress has been

defined as a stability-related phenomenon. It is obvious that HMA mixtures must be designed with adequate stability to ensure adequate performance. That is why stability is considered the core aspect of HMA mixture design with respect to rutting.

Stability is affected by type/grade and amount of asphalt binder, aggregate properties (such as absorption, texture, shape of particle), gradation, compaction level, and temperature. Higher stability is promoted by using hard aggregates with rough surface textures, dense gradations, comparatively low asphalt binder contents, harder (stiffer) asphalts, and well-compacted mixtures as long as the air voids do not fall below a certain level.

In the past, at least three laboratory tests – Hubbard-Field (*135*), Marshall (*136*), and Hveem tests (*136*) – have been used to characterize the stability of HMA mixtures. Necessary minimum values for the measured stability have been established in different HMA mixture design methods (*135, 136*) to ensure adequate pavement stability. The minimum value established will, of course, depend on the type of stability test, weight and volume of traffic, and other factors such as climatic condition, type of underlying structure, and thickness of surfacing. *Because of the uncertainties of these factors and doubts about how to measure true pavement stability, there is, quite often, a tendency to design for maximum stability. Sometimes, this is done at the detriment of other very important design factors, such as cracking resistance and durability.*

With the renewed interest in HMA mixture design generated by the SHRP, several new laboratory tests have recently been developed to characterize the permanent deformation properties of HMA mixtures. Sousa et al. made an excellent review of available permanent deformation tests for HMA mixture, which is shown in Table 7 (*137*). During the SHRP, the series of performance-based tests listed in Table 8 were also developed (*138*). Christensen et al. summarized the latest development after the SHRP which is described in Table 9 (*139*).

In summary, permanent deformation tests have evolved from purely empirical tests (Hubbard-Field, Marshall, and Hveem tests) through simulation tests (such as Hamburg Wheel Track Test [HWTT], Asphalt Pavement Analyzer, French wheel tracking test) to more fundamental tests, such as the repeated load test (*140*). Furthermore, the HMA rutting model recommended in Chapter 3 also requires the repeated load test to determine model parameters. Therefore, it is highly recommended to use repeated load test to characterize permanent deformation properties of HMA mixes and then make rutting prediction using VESYS rutting model shown below:

$$\frac{\Delta\varepsilon_p(N)}{\varepsilon} = \mu N^{-\alpha} \tag{103}$$

where:

$\Delta\varepsilon_p(N)$ = vertical permanent strain at load repetition, N;
ε = peak haversine load strain for a load pulse duration of 0.1 sec measured on the 200th repetition; and
μ, α = material properties depending on stress state, temperature, etc.

However, it should be noted that the repeated load test is currently not a routine test like the HWTT. Therefore, the researchers recommended a three-level HMA characterization of permanent deformation:

- Level 1: the repeated load test,
- Level 2: the HWTT, and
- Level 3: default values recommended based on catalogued values from previous lab testing.

The repeated load test procedure for HMA materials is provided in Appendix B of this report, and the HWTT procedure is well documented in the Tex-242-F. The key issue here is to establish the relationship between the repeated load test and the HWTT test, and to develop a methodology for extracting the rutting parameter (μ, α) from the HWTT test. Chapter 7 presents more discussion and a detailed lab test plan.

Table 7. Comparison of Various Test Methods for Permanent Deformation Evaluation (*137*).

Test Method	Sample Shape	Measured Characteristics	Advantages and Limitations	Field Simulation	Simplicity	Overall Ranking
Diametral Static (creep)	4 in diameter 2.5 in high	Creep modulus vs. time Permanent deformation vs. time	Easy to implement Field cores can be easily obtained Shear stress field not uniform State of stress is predominantly tension Equipment is relatively simple in static test For repeated and dynamic tests, the complexity of the equipment is similar to that of triaxial repeated and dynamic equipment.	3	1	2
Diametral Repeated		Resilient modulus Permanent deformation vs. cycles				
Diametral Dynamic		Dynamic modulus Damping ratio Permanent deformation vs. cycles				
Hollow Cylindrical	1 in wall thickness 18 in high 9 in external diameter	Dynamic axial modulus Dynamic shear modulus Axial damping ratio Shear damping ratio Axial permanent deformation vs. cycles Shear permanent deformation vs. cycles	Almost all states of stress can be duplicated. Capability of determining damping as a function of frequency for different temperatures for shear as well as axial Sample preparation is tedious. Expensive equipment Cores cannot be obtained from pavement.	1	3	Not suitable for routine use
Simple Shear Static (Creep)	4 in diameter 2.5 in high	Shear creep modulus vs. time Shear permanent deformation vs. time	Shear stress can be directly applied to the specimen. Cores can be easily obtained from existing pavement.	2	2	1
Simple Shear Repeated		Shear resilient modulus Shear permanent deformation vs. cycles	Better expresses traffic conditions			
Simple Shear Dynamic		Shear dynamic modulus Damping ratio Shear permanent deformation vs. cycles	Capability of determining the damping as a function of frequency for different temperatures Equipment not generally available			

Table 8. Performance Test Included in the Superpave Mixture Analysis System (*138*).

Distress	Test	Device
Permanent Deformation	Frequency sweep at constant height	Superpave Shear Tester
	Repeated shear at constant stress ratio	
	Simpler shear	
	Uniaxial strain	
	Volumetric	
Fatigue Cracking	Frequency sweep at constant height	Superpave Shear Tester
	Tensile strength	Indirect Tensile Tester
Low-temperature Cracking	Creep compliance	Indirect Tensile Tester
	Tensile strength	

Table 9. Summary of Post SHRP Permanent Deformation Testing Research (*139*).

Test	Device	Demonstrated Correlation with Measured Rutting	Criteria	Advantages	Disadvantages
Dynamic Shear Modulus	Superpave shear tester	High	Preliminary based on sensitivity analysis	Applicable to field cores and lab specimens	Specimen preparation Equipment cost and complexity
Repeated Shear Constant Height	Superpave shear tester	High	Preliminary based on sensitivity analysis	Applicable to field cores and lab specimens Stimulates traffic loading Large deformation test	Specimen preparation Equipment cost and complexity Available permanent deformation model not widely accepted
Dynamic Modulus	Simple performance test system	High	MEPDG	Compatible with the AASHTO MEPDG rutting model Active equipment development	Specimen preparation Cannot test field cores
Flow Number	Simple performance test system	High	None	Simulates traffic loading Wide range of stress states possible Large deformation test Active equipment development	Specimen preparation Cannot test field cores
Flow Time	Simple performance test system	High	None	Very simple test Wide range of stress states possible Large deformation test Active equipment development	Specimen preparation Cannot test field cores
High Temperature Indirect Tensile Strength plus Compaction Slope	Superpave Gyratory Compactor plus AASHO T283 indirect tension test	Potentially high based on correlation with repeated shear constant height test	Preliminary repeated shear constant height criteria	Uses existing equipment Applicable to quality control testing	Requires field verification
Gyratory Shear Resistance	Superpave Gyratory compactor with shear force capability	Fair	To identify unstable mixtures	Results available after compaction	Requires shear force measurement capability Can only identify mixture instability
Rapid Performance	Superpave Gyratory Compactor with indenter	Potentially high based on correlation with repeated load test	Preliminary based on sensitivity analysis	Uses existing equipment and low-cost indenter Applicable to quality control testing	Requires field verification
Wheel Tracking	Asphalt pavement analyzer	High	Location, facility, and mix specific	Intuitive test	Equipment cost Extensive calibration to establish local criteria
	Hamburg wheel tracking test	High	Yes	Very simple test and applicable to field cores and lab specimens	Equipment cost Extensive calibration to establish local criteria

6.2 ASPHALT CRACKING TESTING

Since the late 1950s, many efforts have been made to evaluate the fatigue cracking resistance of HMA mixes. Table 10 presents the most often used laboratory tests to characterize fatigue properties of HMA mixes (*141*). During the SHRP, UC-Berkeley chose the flexural beam fatigue test for characterizing the fatigue properties of HMA mixes after a comprehensive comparison among the flexural beam test, flexural cantilever test, and repeated diametral test. Later, the flexural beam fatigue test was adopted by AASHTO (AASHTO T321) as a performance test for evaluating fatigue cracking resistance of HMA mixes. Even today, the flexural beam fatigue test still is the most widely used test for fatigue characterization of HMA mixes.

In addition to the flexural beam fatigue test, alternative methods were developed for evaluating fatigue cracking resistance. NCHRP 9-19 evaluated the dynamic modulus test and IDT creep compliance test for characterizing fatigue resistance of HMA mixes (*142*). However, there are not enough data published to support the conclusion that fatigue cracking is related to dynamic modulus or creep compliance. Another significant effort was to use continuum damage theory to analyze fatigue test results. With the leading research conducted at Texas A&M University (*143*) and North Carolina State University (*144*), the continuum damage theory was applied to the fatigue analysis of HMA mixes. Laboratory test protocols have been proposed. However, sophisticated data analysis prohibits this approach from being used routinely for characterizing fatigue resistance of HMA mixes. Further simplification is absolutely necessary to this advanced approach of evaluating fatigue properties.

The latest development for fatigue cracking evaluation was the overlay tester-based fatigue cracking characterization approach proposed by Zhou et al. (*145*). The overlay tester-based fatigue cracking characterization and prediction approach was developed based on fracture mechanics. The fundamental HMA fracture properties (A and n) determined from the overlay tester were used to estimate fatigue life of asphalt pavements. However, not only is the fatigue crack propagation considered, but the crack initiation (the number of load repetitions required to form a macro-crack from micro-cracks) is also included in this approach. Therefore, the overlay tester-based approach is different from traditional fatigue crack approaches (such as the flexural beam fatigue-based models used in the MEPDG) in which the fatigue crack propagation stage is not directly considered; it is also different from the traditional fracture mechanics approaches in which the fatigue crack initiation stage is often ignored. This overlay tester-based approach is not only a more fundamental test-based approach, but it can also be easily implemented in DOTs. Furthermore, the approach has been validated through analyzing the FHWA-ALF fatigue tests (*145*).

The overlay tester-based approach has the advantage over other crack tests-based approaches such as the flexural beam fatigue test because it allows for evaluation of either laboratory-molded gyratory samples or field cores. Furthermore, the overlay test takes less than 1 hour to run for traditional mixes. However, beam tests have been around for many years and have been restricted to research institutions, and they have never been implemented as routine design tests in DOTs. Additionally, beam tests use long samples that are difficult to fabricate or extract from the field. The beam test itself can take many hours to run, and the test equipment is

very expensive. Therefore, the overlay tester is recommended for fatigue cracking characterization.

The overlay tester procedure is described in Tex Method 248-F. A step-by-step procedure for determining fracture properties (A and n) has been presented in Appendix A. Additionally, Chapter 2 presents the overlay tester-based fatigue cracking prediction approach. To provide input for the design equations, it will be necessary to run tests at three temperatures: 77°F, 59°F, and 41°F. HMA fracture properties at other temperatures can be interpolated based on those at the three temperatures. A more detailed testing plan for the overlay tester is presented in Chapter 7.

Table 10. Comparison of Test Methods for Cracking (*141*).

Method	Application of Test Results	Advantages	Disadvantages and Limitations	Simulation of Field Conditions	Simplicity	Overall Ranking
Repeated Flexure Test	Yes σ_b or ε_b ,S_{mix}	Well known, widespread Basic technique can be used for different concepts Results can be used directly in design Options of controlled stress or strain.	Costly, time consuming Specialized equipment needed	2	4	I
Direct Tension Test	Yes (through correction) σ_b or ε_b ,S_{mix}	Need for conducting fatigue tests is eliminated Correlations exist with fatigue test results	In the LCPC methodology: The correlations based on one million repetitions Temperature only at 10ºC. Use of thickness of bituminous layer for 1 million repetitions only.	7	1	I
Diametral Repeated Load Test	Yes $4\sigma_b$ and S_{mix}	Simple in nature Same equipment can be used for other tests Tool to predict cracking	Biaxial stress state Underestimates fatigue life	4	2	II
Dissipated Energy Method	Φ, ψ, S_{mix} and σ_b or ε_b	Based on a physical phenomenon Unique relation between dissipated energy and N	Accurate prediction requires extensive fatigue test data Simplified procedures provide only a general indication of the magnitude of the fatigue life.	3	5	III
Fracture Mechanics Tests	Yes K_I, S_{mix} curve (a/h - N); calibration function (also K_{II})	Strong theory for low temperature In principle the need for conducting fatigue tests eliminated.	At high temp., K_I is not a material constant. Large amount of experimental data needed Only stable crack propagation is accounted for.	5	7	IV
Repeated Tension or Tension and Compression Test	Yes σ_b or ε_b ,S_{mix}	Need for flexural fatigue tests eliminated	Compared to direct tension test, this is time consuming, costly, and special equipment is required.	6	3	V
Traxial Repeated Tension and Compression Test	Yes σ_d, σ_c, S_{mix}	Relatively better simulation of field conditions	Costly and special equipment is required Imposition of shear strains is required	1	6	VI

Note: the lower number, the better ranking.

6.3 BASE AND SUBGRADE TESTING

Based on the review of permanent deformation models, researchers propose to investigate the application of the layer-strain approach to model the permanent deformation behavior of thin pavements. This mechanistic-empirical approach provides a general method for predicting rutting and will enable researchers to develop a unified framework for predicting permanent deformation in flexible pavements (both hot-mix and thin-surface pavements). The same approach is used in the MEPDG program developed from NCHRP Project 1-37A and in the Texas VESYS program.

For the purpose of this investigation, thin pavements are considered to cover the pavement structures shown in Figure 14, where the primary load bearing layer is the flexible base. Using the layer-strain approach to predict the development of rutting in these pavements will require characterizing the permanent deformation behavior of the flexible base and subgrade materials comprising these pavements. This behavior is generally characterized using the two-parameter VESYS model or the three-parameter model illustrated in Figure 15, where the model parameters are determined using data from repeated load tests conducted on material samples. The MEPDG program uses the three-parameter model for predicting permanent deformation in flexible pavements. This same model was used in a recent project to verify the load-thickness design curves in TxDOT Test Method Tex-117E. In that project, TTI researchers used the three-parameter model to evaluate relationships between permanent deformation and applied load based on plate bearing test data collected on field test sections. In these tests, researchers monitored the displacements during the loading and unloading stages of the step loads applied to the pavement sections. The three-parameter model was found to provide a good fit to the unrecovered deformation data from plate bearing tests conducted under the different step loads. Thus, researchers plan to evaluate this model, as well as the two-parameter model used in the Texas VESYS program to investigate the permanent deformation behavior of thin pavements. The results of this work will be useful in developing design guidelines for thin pavements that supplement the existing triaxial design check with criteria based on the development of permanent deformation under repeated loading. For this development, researchers propose to conduct laboratory tests on selected base and subgrade materials commonly found on thin pavements in Texas.

Figure 16 illustrates the laboratory test program for evaluating relationships and test methods to predict rutting under repeated loading. This test program has the following major elements:

- characterization of Mohr-Coulomb strength parameters based on the triaxial test method proposed in the provisional TxDOT Test Method Tex-143E,
- characterization of permanent deformation behavior based on triaxial tests of material samples under repeated loading, and
- evaluation of an alternate method of triaxial testing to investigate if a simpler test procedure can be identified for characterizing strength properties and permanent deformation behavior.

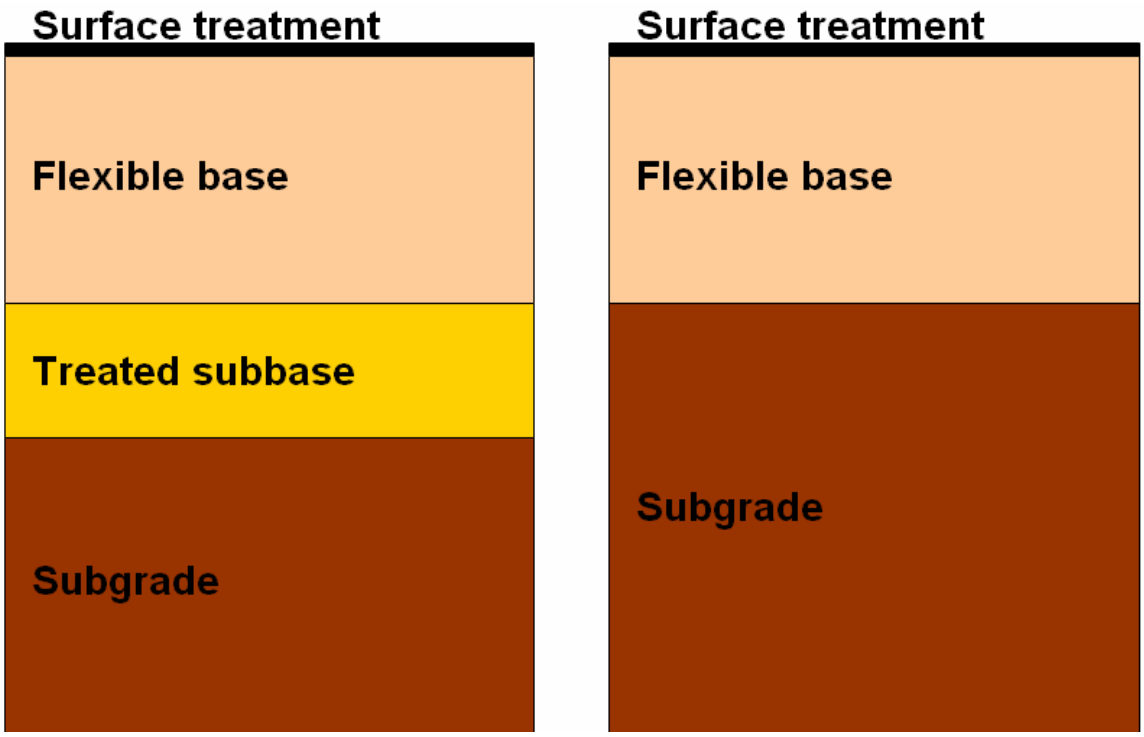

Figure 14. Thin Pavement Structures Considered in Test Plan.

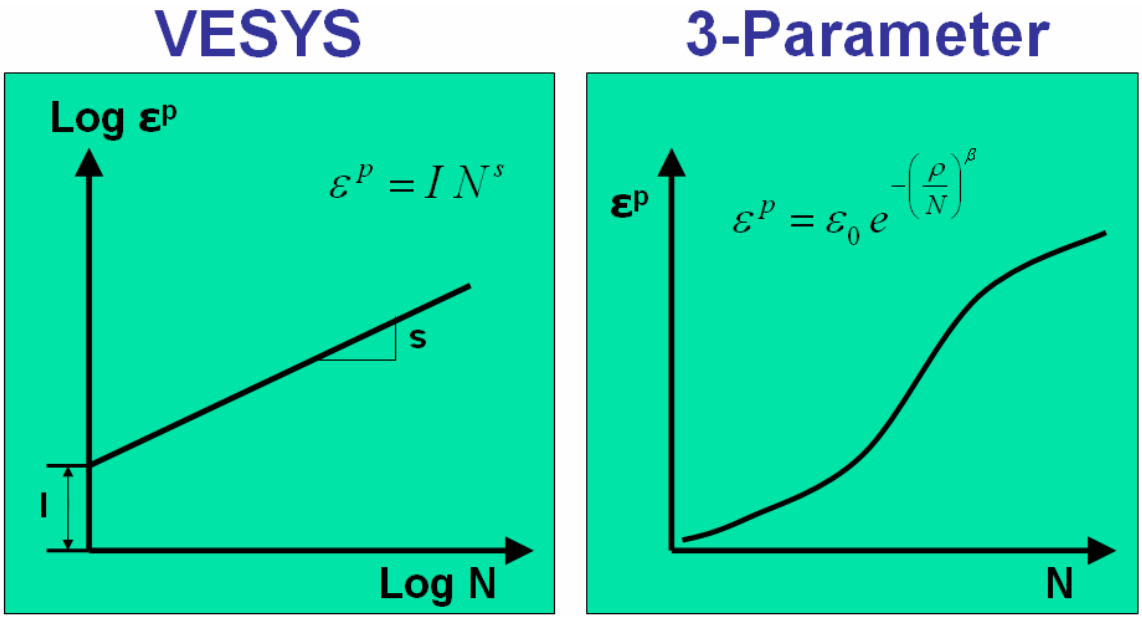

Figure 15. Permanent Strain Development under Repeated Loading.

The test program recognizes that a simpler alternative to the repeated load permanent deformation test would facilitate the implementation of design guidelines for thin pavements that are based on the mechanism of rut development under repeated loading. It also recognizes that the triaxial design check will likely continue to be used within TxDOT for flexible pavement design. Thus, the proposed laboratory test program includes work to investigate an alternate triaxial test, which is like the conventional geotechnical triaxial test except that the specimen is subjected to a load and recovery cycle at the start of the test as illustrated in Figure 16. Researchers plan to analyze the creep and recovery data from the load and recovery cycle to investigate resilient and permanent deformation properties of the materials tested. These same properties will then be compared against corresponding properties determined from repeated load permanent deformation tests to assess the applicability of the alternate triaxial test for characterizing properties needed to predict rutting on thin pavements. In particular, the load and recovery cycle will provide data for evaluating the slope of the creep compliance curve, which has been related (from theoretical considerations) to the parameter *s* of the VESYS model (see Figure 15). In addition, the recovery data will provide an estimate of the amount of deformation that remains after the specimen is unloaded, which may prove useful to evaluate relationships for determining the intercept *I* of the VESYS model. Note that this parameter physically corresponds to the permanent deformation at the first load cycle (N=1) and might prove useful in a material specification for thin pavements to assess material durability on the basis of its propensity to rut.

As Figure 16 indicates, researchers also plan on comparing the cohesion and friction angles determined from alternate triaxial tests with corresponding parameters from tests based on Tex-143E. By comparing test results with data from existing test procedures, an assessment will be made of the applicability of using the alternate triaxial test to characterize material properties for designing thin pavements on the basis of triaxial design and repeated load permanent deformation criteria. Table 11 summarizes the proposed laboratory test program, which covers tests on two flexible bases and two subgrade materials commonly found on thin pavements built in Texas. These materials will be taken from the construction on SH 6 north of Calvert, which has a Class 1 base on a sandy subgrade and from the experimental pavement constructed at the TTI Riverside Campus, which has a clay subgrade and Grade 2 base material. The proposed program includes tests to characterize resilient modulus. Researchers plan to run these tests on the same specimens prepared for permanent deformation testing with the specimens first tested for resilient modulus and then for permanent deformation behavior.

In terms of developing design guidelines for thin pavements, this project will also need field test data to verify and calibrate rutting models, such as those used in the MEPDG and Texas VESYS programs. For this purpose, researchers plan on reviewing and assembling relevant data from accelerated pavement tests, from in-service surface-treated pavements, and from instrumented field sections built and tested in this project. In this regard, researchers have built a number of surface-treated and hot-mix asphalt pavement sections at the Riverside Campus, as well as instrumented sections of ongoing construction projects to investigate the response of flexible pavements under repeated loading. Researchers note that these field tests are not intended to verify predictions of pavement service life as this verification is not realistic within the time frame of this project. Rather, researchers plan to use the test data from instrumented

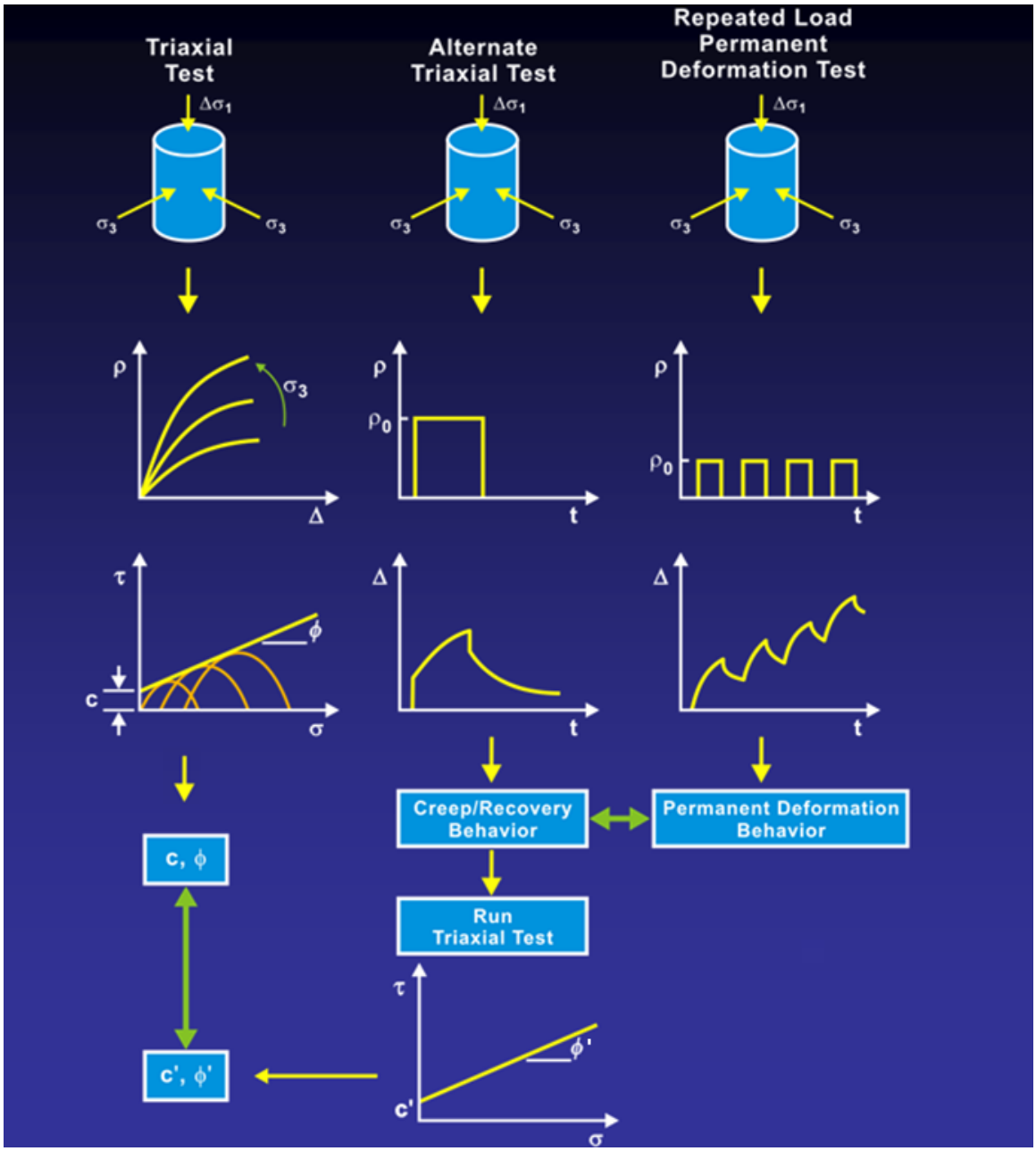

Figure 16. Proposed Laboratory Test Program for Thin Pavements.

field sections to verify predictions of pavement response, assess the relative contributions of the different layers to the total pavement deformation, and rank the test sections with respect to rutting potential. Thus, pavement response and rutting models for thin pavements will be verified based on these factors.

With respect to verifying predictions of pavement life and calibrating the permanent deformation model, researchers plan to use available data from accelerated pavement tests and in-service pavements identified from ongoing TxDOT database development projects. The extent to which this task can be accomplished will depend on the availability of good performance data on thin pavements that have gone through or are close to the end of their life cycles.

Table 11. Proposed Laboratory Test Program for Thin Pavements.

Material	Triaxial Test		Permanent Deformation	Resilient Modulus	Moisture-density Curve	Atterberg Limits	Soil Suction	Dielectric Test
	Standard	Alternate						
Grade 1 Crushed Limestone	T	T	T	T	T	T	T	T
Grade 2 Crushed Limestone	T	T	T	T	T	T	T	T
Clay	T	T	T	T	T	T	T	T
Sand	T	T	T	T	T	T	T	T

CHAPTER 7

PROPOSED TESTING PROGRAM FOR YEAR 2 OF PROJECT 0-5798

Chapters 2, 3, 4, and 5 presented an overview of the performance models that are available for consideration for inclusion in the Tex-ME. However, as described, many of the models, particularly the advanced cracking models, are many years away from practical implementation. Given the scope of this project, the research team recognized the importance of obtaining material properties from existing TxDOT laboratory tests. After a realistic appreciation of the complexity of merging test procedures used with pavement design as compared with those required for thickness design, the research team strongly believes that the most appropriate model for predicting the rutting in flexible pavement systems is a VESYS-type model in which the repeated load test is required to determine HMA permanent deformation properties. For HMA layers, the HWTT will be explored as an alternative test for evaluating HMA permanent deformation properties. Meanwhile, the most practical fatigue cracking model is the Overlay Tester-based fatigue model in which the Overlay Tester is used to determine HMA fracture properties. This chapter provides the proposed laboratory testing program to determine materials input parameters including modulus, permanent deformation, and fatigue (or fracture) properties.

7.1 LABORATORY TEST PROGRAM FOR HMA MIXES

7.1.1 The Dynamic Modulus Test

Dynamic Modulus (DM) testing is an AASHTO standardized test method for characterizing the viscoelastic properties of asphalt mixtures, measured in terms of the complex modulus |E*|. A typical DM test is often performed over five different temperatures of 14, 40, 70, 100, and 130°F and six loading frequencies of 25, 10, 5, 1, 0.5, and 0.1 Hz for each test temperature, respectively. DM is a stress-controlled test involving application of a repetitive sinusoidal dynamic compressive-axial load (stress) to an unconfined specimen. Figure 17 shows TTI's Universal Testing Machine (UTM-25) setup that was used for conducting the DM test and includes the loading configuration and test specimens.

The standard DM test specimen is cylindrically shaped with dimensions of 4 in. diameter (ϕ) by 6 in. height (h). However, for most of the field cores with thinner layers (< 6 in.), prismatic specimens as shown in Figure 17 were used. These prismatic specimens were cut consistent with the procedure suggested by Dr. Jacob Uzan under the Report 0-4822-1 (*146*). The minimum specimen dimensions were 2 in. breadth by 2 in. width by 5 in. in length to ensure at least a minimum 1.5 aspect ratio and coverage of the nominal aggregate size. The stress level for conducting the DM test was chosen to maintain the measured resilient strain (recoverable) within 50 to 150 microstrain consistent with the AASHTO TP 62-03 test protocol (*147*). The order for conducting each test sequence was from the lowest to the highest temperature and the highest to the lowest loading frequency at each temperature to minimize specimen damage. For each test sequence, the test terminates automatically when a preset number of load cycles have been reached. During DM testing, the measurable parameters include the applied load (stress), loading frequency, temperature, vertical axial deformations, phase angle, and the dynamic modulus.

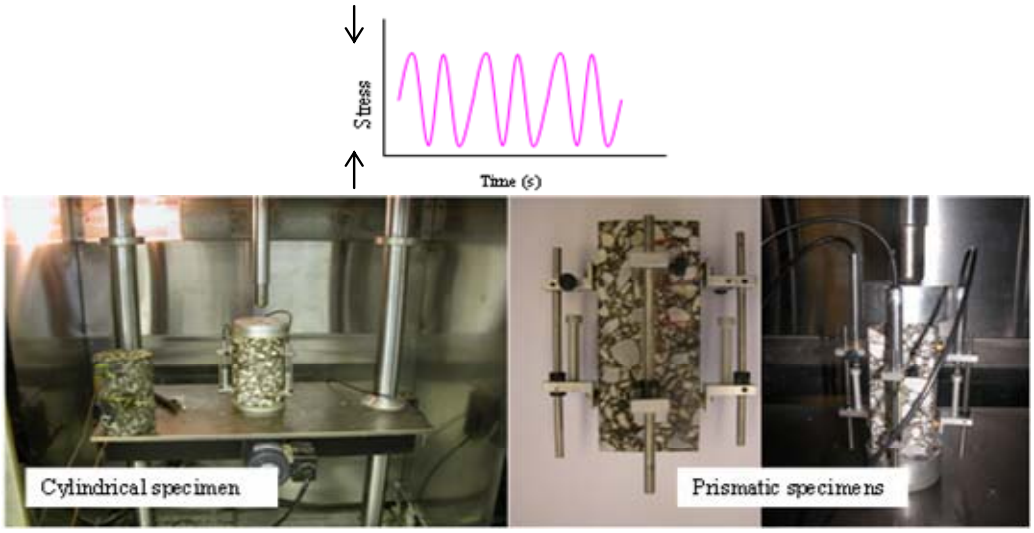

Figure 17. DM Test Setup and Test Specimens (Cylindrical and Prismatic).

7.1.2 The Repeated Load Permanent Deformation Test

The Repeated Load Permanent Deformation (RLPD) test is often used to characterize the permanent deformation properties of HMA mixtures under repeated compressive haversine loading. The detailed test procedure is presented in Appendix B.

RLPD is a stress-controlled test involving repetitive application of a haversine-shaped compressive-axial load (stress) to an unconfined specimen, at a frequency of 1 Hz with 0.1 s loading time and 0.9 s rest period, respectively, for up to 5000 load cycles. The RLPD tests are often conducted at three test temperatures (77, 104, and 122°F). As with the DM test, TTI's UTM-25 setup was used for conducting the RLPD testing, and the loading configuration is shown in Figure 18. During RLPD testing, the measurable parameters include the applied load (stress), test temperature, time, number of load cycles, axial permanent deformation, and strains.

From a plot of the accumulative axial permanent microstrain versus load repetitions on a log-log scale, permanent deformation parameters ε_r, a, b, alpha (α), and gnu (μ) were determined consistent with the procedure described by Zhou and Scullion (*129*). These parameters constitute the VESYS5 rutting input parameters (μ and α) for asphalt mixtures and are defined as follows:

- ε_r = axial resilient microstrain measured at the 100th load cycle,
- a and b = intercept and slope of the linear portion of the permanent microstrain curve (log-log scale),
- alpha (α) = rutting parameter computed as $\alpha = 1 - b$, and
- gnu (μ) = rutting parameter computed as $\mu = ab/\varepsilon_r$.

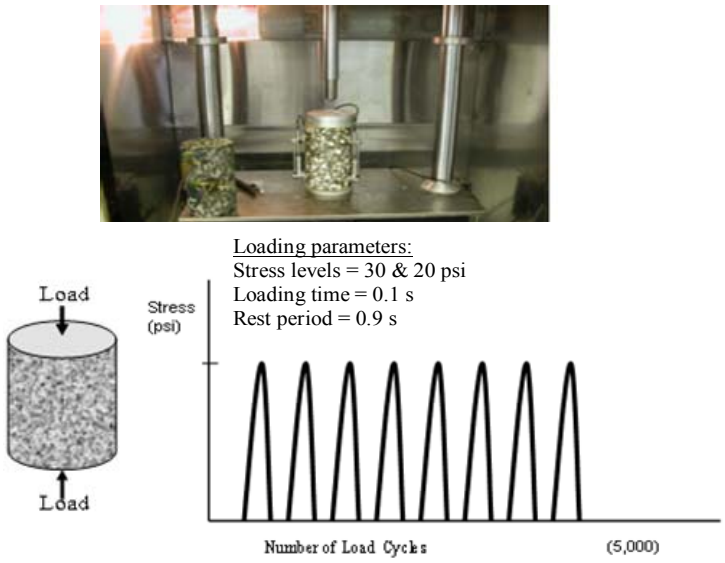

Figure 18. RLPD Loading Configuration.

7.1.3 The Hamburg Wheel Tracking Test

The HWTT is a test device used for characterizing the rutting resistance of asphalt mixtures in the laboratory including a stripping susceptibility assessment (moisture damage potential). The loading configuration consists of a repetitive passing load of 158 lb-force (705 N) at a wheel speed of 52 passes per minute and a test temperature of 122°F in a controlled water bath. The HWTT test specimens are 2.5 in. thick by 6 in. diameter, with one trimmed edge. Figure 19 shows the Hamburg test device with a specimen setup. During HWTT testing, the measurable parameters include the applied load, temperature, number of load passes, and vertical permanent deformation (rutting). The research team will evaluate the potential relationship between the RLPD test and the Hamburg test through extensive laboratory testing.

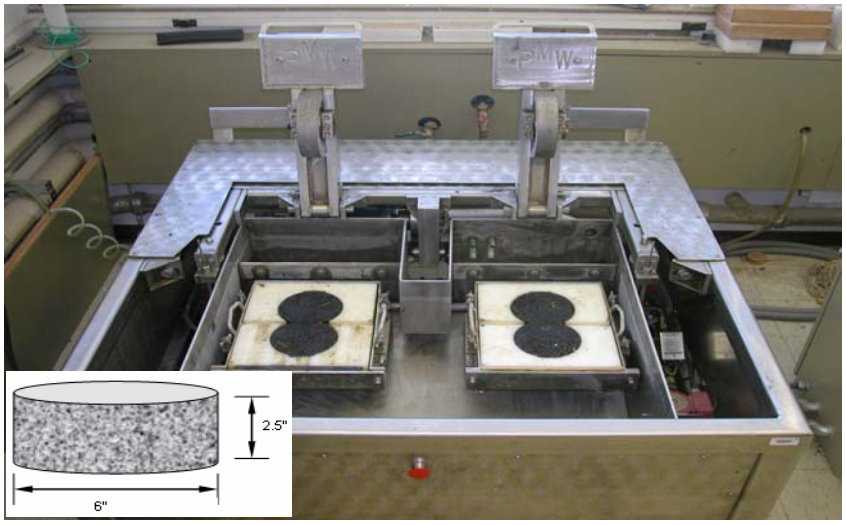

Figure 19. The Hamburg Test Device and Test Specimen.

7.1.4 The Overlay Tester

The overlay tester is a simple performance test for characterizing HMA cracking resistance. The test loading configuration consists of a cyclic triangular displacement-controlled waveform at a maximum horizontal displacement of 0.025 in. and a loading rate of 10 s per cycle (5 s loading and 5 s unloading). Typical overlay test specimens are 6 in. total length, 3 in. wide, and 1.5 in. thick that can be conveniently cut by trimming a lab-molded Superpave gyratory compactor (SGC) specimen or a 6 in. diameter highway core. Figure 20 shows the overlay test setup and a test specimen. During the overlay testing, the measurable parameters include the applied load, opening displacement, time, number of load cycles, and the test temperature. Details of the overlay test for HMA fracture properties (A and n) are presented in Appendix A. Generally, the overlay test is conducted at 77ºF. However, in this project researchers proposed to run the overlay test at the following three temperatures: 77, 59, and 41ºF.

Figure 20. The Overlay Tester and Specimen Setup.

Proposed Laboratory Testing Program for HMA Mixes

The proposed laboratory testing program for HMA mixes is shown in Table 11. The objectives of the laboratory testing are four-fold:

- Finalize the laboratory testing protocols proposed previously.
- Develop the default values for HMA engineering properties including modulus, permanent deformation, and fracture properties.
- Establish the relationships between Level 1 and Level 2 inputs.
- Provide input parameters for calibrating models developed in this project.

In addition, the research team is working with NCAT and University of California at Davis to test cores from their APT sites for performance model calibration. It is envisioned that the same tests as listed in Table 12 will be conducted on those cores from both APT sites.

Table 12. Proposed Laboratory Testing Program for HMA Mixes.

Mix Type	Locations	Aggregate Type	Binder Type	E* 5 temp. 6 freq	Cracking	Rutting	
					OT 3 temp.	RLPD 3 temp.	Hamburg 1 temp.
SMA-C	SH 114	Limestone	PG 70-28	T	T	T	T
SMA-C	IH 35	Traprock + gravel	PG76-22	T	T	T	T
Superpave A	SH 114	Limestone	PG 70-22	T	T	T	T
	IH 35-Laredo	Traprock/gravel	PG 76-22	T	T	T	T
			PG 64-22	T	T	T	T
Type B	SH 114	Limestone	PG 64-22	T	T	T	T
	IH 35-Waco	Limestone	PG 64-22	T	T	T	T
Superpave B	SH 114	Limestone	PG 76-22	T	T	T	T
	IH 35-Laredo	Traprock/gravel	PG 76-22	T	T	T	T
			PG 70-22	T	T	T	T
Type C	SH 114	Limestone	PG 70-22	T	T	T	T
			PG 64-22	T	T	T	T
	SH 6	Gravel	PG 64-22	T	T	T	T
Superpave C	IH 35-Laredo	Gravel	PG 70-22	T	T	T	T
	IH 35-San Antonio	Limestone	PG 64-22	T	T	T	T
Type D	Riverside	Limestone	PG 76-22	T	T	T	T
	SH 12	Granite	PG 76-22	T	T	T	T

7.2 LABORATORY TESTING PROGRAM FOR BASE/SUBGRADE MATERIALS

The proposed method for characterizing the permanent deformation behavior of granular materials and subgrades is provided in Appendix C. However, the research team feels that it is critical to evaluate this procedure to ensure that representative samples are being tested and that realistic permanent deformation properties are being obtained. There has been much discussion on several issues, namely:

- the size of the sample–6 by 8 in. as opposed to 6 by 12 in.,
- the method of compacting samples–drop hammer or vibratory compactor,
- method of mounting sensors on sample to avoid slippage,
- the range of stress combinations needed for resilient modulus testing,
- integration of resilient modulus and permanent deformation testing,
- sample conditioning prior to testing (moisture and load conditioning), and
- problems associated with laboratory testing of low fines bases.

Substantial work has already been performed in each of these areas. For example, Project 0-4358 measured resilient modulus at different sample sizes, and Project 0-3512 examined the differences between drop hammer versus vibratory compaction for base and subgrade materials. The research team is well aware that TxDOT procedures for acceptance have been in place for many years, and they will not be changed in the foreseeable future. The research team is also aware that this level of testing on granular materials requires complex equipment so that it is not anticipated that non-TxDOT standard test methods will be run for

routine pavement design purposes. For these materials, a correlation will be needed between the routine test results and the required model inputs.

Prior to executing the test plan for thin pavements presented in Section 6.3, researchers propose to conduct a comparative evaluation of permanent deformation test procedures to establish the most appropriate methods for compacting the specimens and mounting the LVDTs for the proposed permanent deformation tests in Section 6.3. Table 13 shows the test matrix for this comparative evaluation. Sebesta, Harris, and Liu conducted permanent deformation tests on granular base specimens prepared by impact hammer and vibratory compaction methods (*148*). They found that permanent deformation curves of base materials varied significantly, as illustrated in Figures 21 and 22, with vibratory-compacted specimens developing less permanent deformation under repeated loading as compared to specimens of the same materials compacted using the conventional impact hammer method. Other researchers have also reported problems with slippage and rotation of LVDT holders pressed onto the specimen using clamps (*149*). In view of these findings from reported research studies, the first phase of permanent deformation tests in Year 2 of this project will cover the comparative tests presented in Table 13 to identify the best approach for compacting and instrumenting the specimens. As proposed, two methods of compaction, vibratory and impact hammer, will be compared, as well as two methods of mounting the LVDTs—studs versus the traditional method of using rubber bands to press the LVDT holders onto the specimen for testing. For these tests, researchers will prepare specimens using samples of the base materials placed at the Annex test site and on the SH 6 project north of Calvert in the Bryan District. Consistent with current TxDOT practice, researchers propose to mold 6-inch diameter by 8-inch high specimens for testing, with specimens compacted at optimum moisture contents. For these tests, researchers plan on using the permanent deformation test protocols reported by Zhou and Scullion as a guide for running the comparative laboratory tests proposed herein (*129*). Appendix C of this report presents these test protocols.

Table 13. Test Matrix for Comparative Evaluation of Permanent Deformation Setups.

Base Material	Compaction Method	Method of Mounting LVDTs	
		LVDT Holders Pressed onto Specimen with Rubber Bands	LVDT Holders Anchored to Specimen with Studs
Annex	Impact hammer	T	T
	Vibratory	T	T
SH 6	Impact hammer	T	T
	Vibratory	T	T

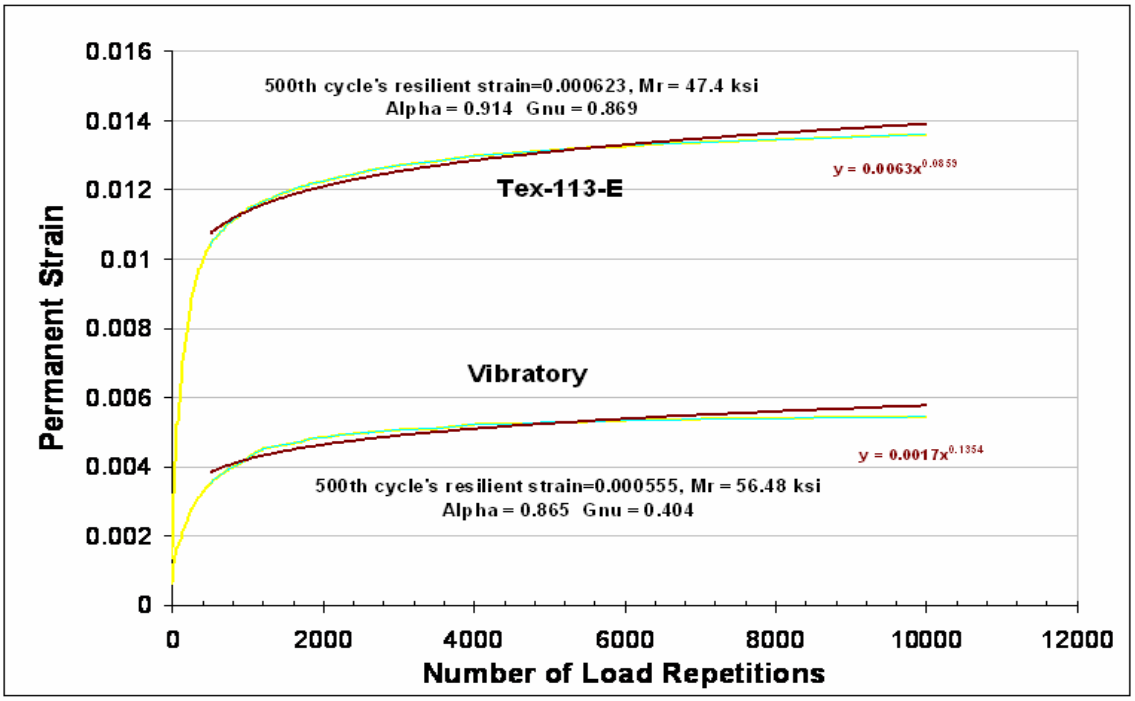

Figure 21. Permanent Deformation Curves from Tests on Grade 1 Spicewood Base Specimens (*148*).

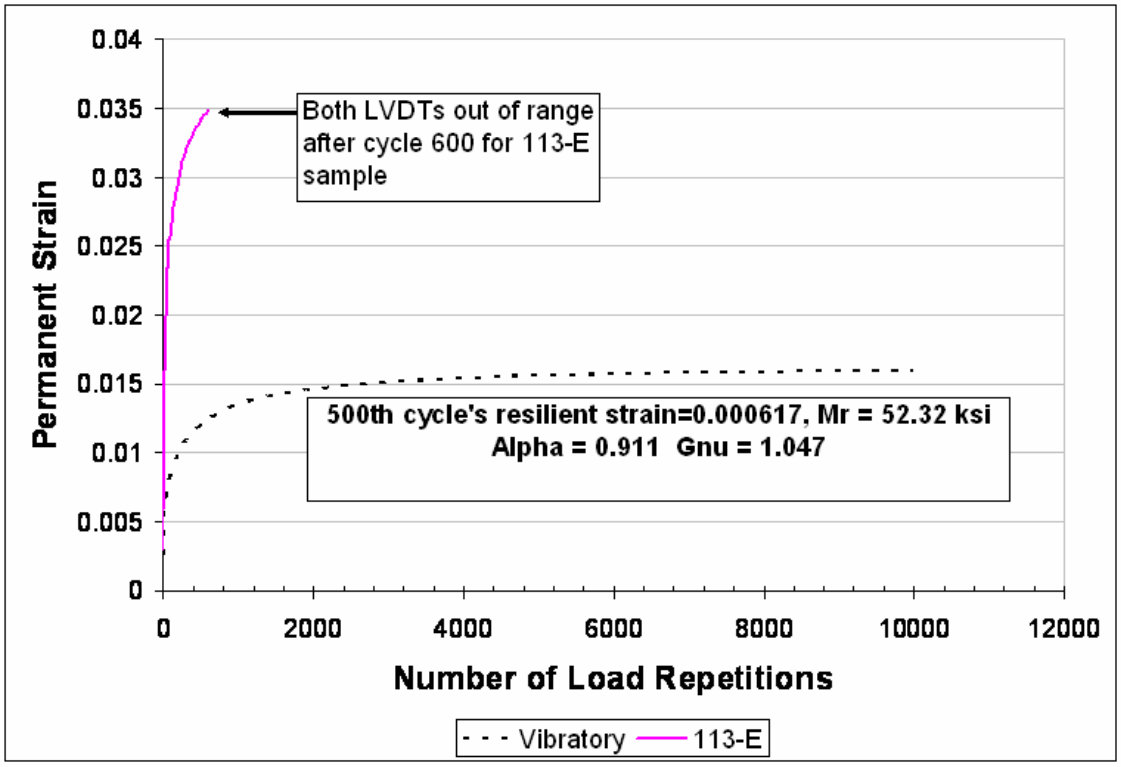

Figure 22. Permanent Deformation Curves from Tests on Grade 2 Groesbeck Base Specimens (*148*).

Permanent deformation properties will be determined from the test data, and differences in permanent deformation behavior will be examined to establish the test setup that provides the

most reasonable results. Researchers plan on examining the permanent deformation traces to check for evidence of slippage. If slippage occurs, the specimen deformation will not be fully transmitted to the LVDT resulting in lower resilient strains measured from the LVDT and higher values of the permanent deformation parameter μ of the VESYS model. Changes in the orientation of the LVDT holders will also be monitored to establish the effectiveness of studs at minimizing the rotation of the LVDTs during testing. In addition, researchers propose to perform Computed Tomography (CT) scans on the specimens to check for uniformity of compaction, particularly at the vicinities of studs on specimens where these anchors for the LVDT holders are used, and to compare these with corresponding scans obtained from specimens tested where the LVDTs are mounted in the conventional manner. By examining and comparing the test results from the different setups considered in the test matrix (Table 13), a determination will be made as to the most appropriate test setup for running the permanent deformation tests proposed in Section 6.3.

REFERENCES

1. Suresh, S., (1991). *Fatigue of Materials.* Cambridge University Press, Cambridge, UK, 1991.
2. Lytton, R.L., et al., (1993). "Development and Validation of Performance Prediction Model and Specifications for Asphalt Binders and Paving Mixes." The Strategic Highway Research Program Project Report SHRP-A-357, Washington D.C.
3. Hveem, F.N., "Pavement Deflections and Fatigue Failures." *Bulletin 114 HRB*, National Research Council, Washington, D.C, pp. 43-87, 1955.
4. Bonnaure, F., Gravois, A., and Udron, J., A New Method of Predicting the Fatigue Life of Bituminous Mixes. *Journal of the Association of Asphalt Paving Technologists*, Vol. 49, pp. 499-529.
5. Asphalt Institute. *Thickness Design Manual (MS-1)*, 9th ed. The Asphalt Institute, College Park, MD, 1981.
6. Tayebali, A.A., Deacon, J.A., Coplantz, J.S., Harvey, J.T., and Monismith, C.L., *Fatigue Response of Asphalt Aggregate Mixes*. SHRP-A-404, Strategic Highway Research Program, National Research Council, Washington, D.C., 1994.
7. NCHRP, Guide for Mechanistic-Empirical Design of New and Rehabilitation Pavement Structures, Transportation Research Board of the National Academics, Washington, D.C., 2004.
8. Finn, F.N., Sraf, C., Kulkarni, R., Nair, K., Smith, W., and Abdullad, A., (1977). "The Use of Prediction Subsystems for the Design of Pavement Structures." *Proceedings of Fourth International Conference on Structural Design of Asphalt Pavements*, University of Michigan, Ann Arbor, MI, pp. 3-38.
9. Harvey, J.T., Deacon, J., Tsai, B., and Monismith, C.L., *Fatigue Performance of Asphalt Concrete Mixes and Its Relationship to Asphalt Concrete Pavement Performance in California.* RTA-65W485-2, Asphalt Research Program, CAL/APT Program, Institute of Transportation Studies, University of California at Berkeley, Berkeley, CA, 1996.
10. M., El-Basyouny, and Witczak, M., Calibration of Alligator Fatigue Cracking Model for 2002 Design Guide. *Journal of Transportation Research Board* 1919, Washington D.C., 2005, pp. 77-86.
11. Van Dijk, W. (1975). "Practical Fatigue Characterization of Bituminous Mixes." *Proceedings of the Association of Asphalt Paving Technologists (AAPT)*, Vol. 44, p. 38.
12. Rowe, G.M., (1993). "Performance of Asphalt Mixtures in the Trapezoidal Fatigue Test." *Proceedings of Associations of Asphalt Paving Technologists*, Vol. 62, pp. 344-384.
13. Baburamani, P.S., and Porter, D.W., (1996). "Dissipated Energy Approach to Fatigue Characterisation of Asphalt Mixes." *Proceedings of Combined 18th ARRB TR Conference Transit New Zealand Symposium*, Part 2, pp. 327-347.
14. Ghuzlan, K., (2001). "Fatigue Damage Analysis in Asphalt Concrete Mixtures Based Upon Dissipated Energy Concepts." Ph.D. Thesis, University of Illinois at Urbana-Champaign, Urbana, IL.
15. Shen, S., and Carpenter, S.H., (2005). "Application of Dissipated Energy Concept in Fatigue Endurance Limit Testing." *Journal of Transportation Research Record: Transportation Research Board*, No. 1929, pp. 165-173.
16. Van Dijk, W., and Visser, W., (1977). "The Energy Approach to Fatigue for Pavement Design." *Proceedings of Annual Meeting of the Association of Asphalt Paving Technologists (AAPT)*, Vol. 46, pp.1-40.

17. Pronk, A.C., and Hopman, P.C., (1991). "Energy Dissipation: The Leading Factor of Fatigue." *Proceedings of the Conference of the United States Strategic Highway Research Program*, pp. 255-267.
18. Tayebali, A.A., Rowe, G.M., and Sousa, J.B., (1992). "Fatigue Response of Asphalt Aggregate Mixtures." *Proceedings of Asphalt Paving Technologists*, Vol. 62, pp. 385-421.
19. Fakhri, M., (1997). "Characterisation of Asphalt Pavement Materials," Ph.D. Thesis, The University of New South Wales, Sydney, Australia.
20. Carpenter, S.H., and Jansen, M., (1997). "Fatigue Behavior Under New Aircraft Loading Conditions." *Proceedings of Aircraft Pavement Technology in the Midst of Change*, pp. 259-271.
21. Ghuzlan, K., and Carpenter, S.H., (2000). "An Energy-Derived/Damage-Based Failure Criteria for Fatigue Testing." *Transportation Research Record (TRR)*, No. 1723, pp. 131-141.
22. Carpenter, S.H., Ghuzlan., K.A., and Shen, S., (2003). "A Fatigue Endurance Limit for Highway and Airport Pavement." *Journal of Transportation Research Record (TRR)*, No. 1832, pp. 131-138.
23. Shen, S., Ph.D. Thesis, University of Illinois at Urbana-Champaign, Urbana, IL, 2007.
24. Daniel, J. S., Bisirri, W. M., et al., (2004). "Fatigue Evaluation of Asphalt Mixtures Using Dissipated Energy and Viscoelastic Continuum Damage Approach." *Journal of the Association of Asphalt Paving Technologists (AAPT)*, Baton Rouge, LA, Vol. 73, pp. 557-583.
25. Daniel, J.S., and Bisirri, W.M., (2005). Characterizing Fatigue in Pavement Materials Using a Dissipated Energy Parameter. *Proceedings of the Geo-Frontiers 2005 Congress*, Austin, TX.
26. Schapery, R.A., A Theory of Mechanical Behavior of Elastic Media with Growing Damage and Other Changes in Structure. *Journal of Mechanics and Physics of Solids*, Vol. 38, 1990, pp. 215-253.
27. Schapery, R.A., On Viscoelastic Deformation and Failure Behavior of Composite Materials with Distributed Flaws. *Advances in Aerospace Structures and Materials*, AD-01, ASME, New York, NY, 1981, pp. 5-20.
28. Schapery, R.A., "Correspondence Principles and a Generalized J-Integral for Large Deformation and Fracture Analysis of Viscoelastic Media." *International Journal of Fracture*, Vol. 25, 1984, pp. 195-223.
29. Little, D.N., Lytton, R.L., Williams, D., Chen, C.W., and Kim, Y.R., "Fundamental Properties of Asphalts and Modified Asphalts—Task K: Microdamage Healing in Asphalt and Asphalt Concrete." FHWA Final Report, Vol. 1, Report No. DTFH61-92-C-00170, Springfield, VA: National Technical Information Service, 1997.
30. Lee, H.J., *Uniaxial Constitutive Modeling of Asphalt Concrete Using Viscoelasticity and Continuum Damage Theory*, Ph.D. Dissertation, North Carolina State University, Raleigh, NC, 1996.
31. Kim, Y.R., Lee, H.J., and Little, D.N., "Fatigue Characterization of Asphalt Concrete Using Viscoelasticity and Continuum Damage Theory," *Journal of the Association of Asphalt Paving Technologists*, Vol. 66, 1997, pp. 520-569.
32. Lee, H.J., and Kim, Y.R., "A Uniaxial Viscoelastic Constitutive Model for Asphalt Concrete Under Cyclic Loading," *ASCE Journal of Engineering Mechanics*, Vol. 124, 1998, No. 11, pp. 1224-1232.

33. Kim, Y.R., Little, D.N., and Lytton, R.R., "Use of Dynamic Mechanical Analysis (DMA) to Evaluate the Fatigue and Healing Potential of Asphalt Binders in Sand Asphalt Mixtures," *Journal of the Association of Asphalt Paving Technologists*, Vol. 71, 2002, pp. 176-199.
34. Daniel, J.S., and Kim, Y.R., "Development of a Simplified Fatigue Test and Analysis Procedure Using a Viscoelastic, Continuum Damage Model," *Journal of the Association of Asphalt Paving Technologists*, Vol. 71, 2002, pp. 619-645.
35. Lee, H.J., Kim, Y.R., and Lee, S.W., Prediction of Asphalt Mix Fatigue Life with Viscoelastic Material Properties, *Journal of the Transportation Research Board*, No. 1832, 2003, pp.139-147.
36. Christensen, Jr., D., and Bonaquist, R., Practical Application of Continuum Damage Theory to Fatigue/Phenomena in Asphalt Concrete Mixtures, *Journal of the Association of Asphalt Paving Technologists*, Vol. 74, 2005, pp. 963-1001.
37. Tsai, B.W., Harvey, J.T., and Monismith, C.L. "Application of Weibull Theory in Prediction of Asphalt Concrete Fatigue Performance." *Transportation Research Record No. 1832.* Transportation Research Board, National Research Council, Washington, D.C., 2003, pp. 121-130.
38. Ullidtz, P., Harvey, J.T., Tsai, B.-W., and Monismith, C.L., April 2006. *Calibration of Incremental-Recursive Flexible Damage Models in CalME Using HVS Experiments.* Report prepared for the California Department of Transportation (Caltrans) Division of Research and Innovation by the University of California Pavement Research Center, Davis and Berkeley. UCPRC-RR-2005-06.
39. Majidzadeh, K., Kaufmann, E.M., and Ramsamooj, D.V., Application of Fracture Mechanics in the Analysis of Pavement Fatigue, *Proceedings of Association of Asphalt Pavement Technologists*, Vol. 40, 1970, pp. 227-246.
40. Monismith, C.L., "Reflection Cracking, Analyses, Laboratory Studies, and Design Considerations," Proceedings AAPT, Volume 49, pp. 268-313, 1980.
41. Paris, P.C., and Erdogan E., A Critical Analysis of Crack Propagation Laws, *Journal of Basic Engineering,* Transaction of the American Society of Mechanical Engieering, Series D., Vol. 85, pp. 528-883, 1963.
42. Schapery, R.A., *A Theory of Crack Growth in Visco-Elastic Media*, Report MM 2764-73-1, Mechanics and Materials Research Center, Texas A&M University, College Station, TX, 1973.
43. Schapery, R.A., A Theory of Crack Initiation and Growth in Visco-Elastic Media; I: Theoretical Development; II: Approximate Methods of Analysis; III: Analysis of Continuous Growth; *International Journal of Fracture*, Sijthoff and Noordhoff International Publisher; Vol. 11, No. 1, pp. 141-159; Vol. 11, No. 3, pp. 369-388; and Vol. 11, No. 4, pp. 549-562, 1975.
44. Schapery, R.A., A Method for Predicting Crack Growth in Nonhomogeneous Visco-Elastic Media, *International Journal of Fracture*, Sijthoff and Noordhoff International Publishers, Vol.14, No. 3, pp. 293-309, 1978.
45. Chang, H.S., Lytton, R.L., and Carpenter, S.H., *Prediction of Thermal Reflection Cracking in West Texas,* Texas Transportation Institute. Research Report 18-3, Study 2-8-73-18, College Station, TX, March 1976.
46. Jayawickrama, P.W., and Lytton, R.L., Methodology for Predicting Asphalt Concrete Overlay Life Against Reflection Cracking, *Proceedings 6th International Conference on Structural Design of Asphalt Pavements*, Volume I, pp. 912-924, 1987.

47. Zhou, F., Hu, S., Scullion, T., Chen, D., Qi, X., and Claros, G., Development and Verification of an Overlay Tester Based Fatigue Crack Prediction Approach, *Journal of Association of Asphalt Paving Technologist,* March 2007, San Antonio, TX.
48. Barsoum, R.S., On the Use of Isoparametric Elements in Linear Fracture Mechanics, *International Journal Numerical Methods in Engineering*, Vol. 10, p. 25, 1976.
49. Ingraffea, A.R., and Manu, C., Stress-Intensity Factor Computation in Three Dimensions with Quarter-Point Crack Tip Elements, *International Journal Numerical Methods in Engineering*, Vol. 12, p. 235, 1978.
50. Salam, Y.M., and Monismith, C.L., Fracture Characteristics of Asphalt Concrete, *Proceedings of Association of Asphalt Paving Technologists*, Vol. 41, pp. 215-256, 1972.
51. Majidzadeh, K., Dat, M., and Makdisi-Ilyas, F., *Application of Fracture Mechanics for Improved Design of Bituminous Concrete, Vol. 2 Evaluation of Improved Mixture Formulations, and the Effect of Temperature Conditions on Fatigue Models*, Report No. FHWA-RD-76-92, Final Report, June 1976.
52. Elmitiny, M.R.N., *Material Characterization for Studying Flexible Pavement Behavior in Fatigue and Permanent Deformation*, Ph.D. Dissertation, The Ohio State University, 1980.
53. Molenaar, A.A.A., *Structural Performance and Design of Flexible Road Constructions and Asphalt Concrete Overlays*, Ph.D. Dissertation, Delft University of Technology, The Netherlands, 1983.
54. Molenaar, A.A.A., Fatigue and Reflection Cracking due to Traffic Loads, *Proceedings of the Association of Asphalt Paving Technologists*, Vol. 53, pp. 440-474, 1984.
55. Jacobs, M.M.J., *Crack Growth in Asphaltic Mixes,* Ph.D. Dissertation, Delft University of Technology, the Netherlands, 1995.
56. Jacobs, M.M.J., Hopman, P.C., and Molenaar, A.A.A., Application of Fracture Mechanics in Principles to Analyze Cracking in Asphalt Concrete, *Journal of the Association of Asphalt Paving Technologists*, Vol. 65, pp 1-39, 1996.
57. Erkens, S., Moraal, J., Molenaar, A.A.A., Groenendijk, J., and Jacobs, M., Using Paris' Law to Determine Fatigue Characteristics – A Discussion, *Proceedings of the 8th International Conference on Asphalt Pavements*, Seattle, WA, pp. 1123-1142, August 10-14, 1997.
58. Medani, T.O. and Molenaar, A.A.A., Estimation of Fatigue Characteristics of Asphaltic Mixes Using Simple Tests, Herron, TNO Building and Construction Research and The Netherlands School for Advanced Studies in Construction, Vol. 45, No. 3, pp. 155-165, 2000.
59. Uzan, J., and Levenberg, E., Strain Measurements in Asphalt Concrete Specimens towards the Development of a Fracture Model, *International Journal of Pavement Engineering*, Vol. 2, No. 4, pp. 243-258, 2001.
60. Jenq, Y.S., Liaw, C.J., and Liu, P., Analysis of Crack Resistance of Asphalt Concrete Overlays − A Fracture Mechanics Approach, *Transportation Research Record*, No. 1388, pp. 160-166, 1993.
61. Dugdale, D. S., Yielding in Steel Sheets Containing Slits, *Journal of the Mechanics and Physics of Solids*, Vol. 8, pp. 100-108, 1960.
62. Barenblatt, G.I., The Mathematical Theory of Equilibrium Cracks in Brittle Fracture, *Advances in Applied Mechanics*, Academic Press, Vol. VII, pp. 55-129, 1962.
63. Hillerborg, A., Modeer, M., and Peterson, P.E., Analysis of Crack Formation and Crack Growth in Concrete by Means of Fracture Mechanics and Finite Elements, *Cement and Concrete Research*, Vol. 6, pp. 773-782, 1985.
64. Bazant, Z.P. and Planas, J., *Fracture and Size Effect in Concrete and other Quasibrittle*

Materials, CRC Press, Boca Raton, FL, p. 616, 1998.
65. Petersson, P.E., (1981). "Crack Growth and Development of Fracture Process Zone in Plain Concrete and Similar Materials," Report No. TVBM-1006, Lund Institute of Technology, Lund, Sweden.
66. Jenq, Y.S. and Perng, J.D., (1991). "Analysis of Crack Propagation in Asphalt Concrete Using a Cohesive Crack Model," *Transportation Research Record*, TRB, 1317, pp. 90-99.
67. Superpave model team (1999). "Advanced AC Mixture Material Characterization Models Framework and Laboratory Test Plan Final Report," NCHRP 9-19, *Superpave Support and Performance Models Management,* Tempe, AZ.
68. Seo, Y., Kim, Y.R., Schapery, R.A., Witczak, M.W., and Bonaquist, R., A Study of Crack-Tip Deformation and Crack Growth in Asphalt Concrete Using Fracture Mechanics, *Journal of Association of Asphalt Paving Technologists*, Vol. 74, 2004, pp. 790-795.
69. Soares, J.B., de Freitas, F.A.C., and Allen, D.H., Considering Material Heterogeneity in Crack Modeling of Asphaltic Mixtures, Transportation Research Record, No. 1832, pp. 113-120, 2003.
70. Paulino, G.H., Song, S.H., and Buttlar, W.G., Cohesive Zone Modeling of Fracture in Asphalt Concrete, *Proceedings of the 5th International Conference on Cracking in Pavements*, May 5-7, Lemoges, France, pp. 63-70, 2004.
71. Kim, H., and Buttlar, W.G., Micromechanical Fracture Modeling of Hot-Mix Asphalt Concrete Based on a Disk-shaped Compact Tension Test, *Journal of Association of Asphalt Paving Technologists*, Vol. 75E, 2005.
72. Wagoner, M.P., Buttlar, W.G., and Paulino, G.H., Disk-shaped Compact Tension Test for Asphalt Concrete Fracture, *Journal of Society for Experimental Mechanics*, Vol. 45, No. 3, pp. 270-277, 2005.
73. Wagoner, M.P., Buttlar, W.G., and Paulino, G.H., Development of a Single-Edge Notched Beam Test for Asphalt Concrete Mixtures, *ASTM Journal of Testing and Evaluation*, Vol. 33, No. 6, pp. 1-9, 2005.
74. Wu, R., Harvey, J.T.,and Monismith, C.L., Towards a Mechanistic Model for Reflective Cracking in Asphalt Concrete Overlays, *Journal of the Association of Asphalt Paving Technologists*, Vol. 75, pp. 491-534, March 2006.
75. Chaboche, J.L., Continuum Damage Mechanics: Part I - General Concepts. *ASME Journal of Applied Mechanics*, Vol. 55, No. 1, pp. 59–64, March 1988.
76. Chaboche, J.L., Continuum Damage Mechanics: Part II - Damage Growth, Crack Initiation, and Crack Growth. *ASME Journal of Applied Mechanics*, 55(1):65–72, March 1988.
77. Lee, H.J., and Kim, Y.R., Viscoelastic Constitutive Model for Asphalt Concrete under Cyclic Loading. *Journal of Engineering Mechanics-ASCE*, 124(1):32–40, 1998.
78. Lee, H.J., and Kim, Y.R., Viscoelastic Continuum Damage Model of Asphalt Concrete with Healing. *Journal of Engineering Mechanics-ASCE*, 124(11):1224–1232, 1998.
79. Bazant, Z.P., and Jirasek, M., Nonlocal Integral Formulations of Plasticity and Damage: Survey of Progress. *Journal of Engineering Mechanics*, Vol. 128, No. 11, pp. 1119–1149, 2002.
80. Mazars, J., and Pijaudier-Cabot, G., Continuum Damage Theory–Application to Concrete, *Journal of Engineering Mechanics-ASCE*, Vol. 115, No. 2, pp. 345–365, 1989.

81. Peerlings, R.H.J., Brekelmans, W.A.M., de Borst, R., and Geers, M.G.D., Gradient-Enhanced Damage Modelling of High-Cycle Fatigue, *International Journal for Numerical Methods in Engineering*, Vol. 49, No. 12, pp. 1547–1569, 2000.
82. Lemaitre, J., *A Course on Damage Mechanics*. Springer, Berlin, 2nd edition, 1996.
83. Peerlings, R.H.J., de Borst, R., Brekelmans, W.A.M, and deVree, J.H.P., Gradient Enhanced Damage for Quasi-Brittle Materials, *International Journal for Numerical Methods in Engineering*, Vol. 39, No. 19, pp. 3391–3403, 1996.
84. Walubita, L.F., Epps-Martin, A., Glover, C.J., Jung, S.H., Cleveland, G.S., Lytton, R.L., and Park, E.S., Application of the Calibrated Mechanistic Approach with Surface Energy (CMSE) Measurements for Fatigue Characterization of Asphalt Mixtures, *Journal of the Association of Asphalt Paving Technologists*, Vol. 75, 2006.
85. Sousa, J.B., Pais, J.C., Prates, M., Barros, R., Langlois, P., and Leclerc, A-M, Effect of Aggregate Gradation on Fatigue Life of Asphalt Concrete Mixes, *Transportation Research Record*, No. 1630, 1998, pp. 62-68.
86. Tsai, B.W., *High Temperature Fatigue and Fatigue Damage Process of Aggregate-Asphalt Mixes*, Ph.D. Dissertation, University of California at Berkeley, June 2001.
87. Ghuzlan, K.A., and Carpenter, S. H., Traditional Fatigue Analysis of Asphalt Concrete Mixtures, Transportation Research Board, CD-ROM, Washington, D.C., 2003.
88. Tsai, B.W., and Monismith, C.L., Influence of Asphalt Binder Properties on the Fatigue Performance of Asphalt Concrete Pavements, *Journal of the Association of Asphalt Paving Technologists*, Vol. 74, 2005.
89. Zhou, F., Hu, S., and Scullion, T., *Development and Verification of the Overlay Tester Based Fatigue Cracking Prediction Approach*, FHWA/TX-07/9-1502-01-8, Texas Transportation Institute, College Station, TX, January 2007.
90. Highway Research Board, The AASHO Road Test, Special Report 73, Publication No. 1012, Washington, D.C., p. 117, 1962.
91. Hofstra, A., and Klomp, A.J.G., Permanent Deformation of Flexible Pavements Under Simulated Road Traffic Conditions, Proceedings of the 3rd International Conference on the Structural Design of Asphalt Pavements, Vol. I, London, England, 1972, pp. 613-621.
92. Uge, P., and van de Loo, P.J., Permanent Deformation of Asphalt Mixes, Koninklijke/Shell Laboratorium, Amsterdam, The Netherlands, November 1974.
93. Eisenmann, J., and Hilmer, A., Influence of Wheel Load and Inflation Pressure on the Rutting Effect at Asphalt-Pavements-Experiments and Theoretical Investigations, Proceedings of the 6th International Conference on the Structural Design of Asphalt Pavements, Vol. I, Ann Arbor, MI, 1987, pp. 392-403.
94. Brown, E.R., and Cross, S., A Study of In-Place Rutting of Asphalt Pavements. Proceedings, Association of Asphalt Paving Technologists, Volume 58, 1989.
95. Harvey, J.T., and Popescu, L., *Rutting of Caltrans Asphalt Concrete and Asphalt-Rubber Hot Mix Under Different Wheels, Tires, and Temperatures–Accelerated Pavement Testing Evaluation*, Draft report prepared for California Department of Transportation Pavement Research Center, CAL/APT Program, Institute of Transportation Studies, University of California, Berkeley, CA. UCPRC-RR-2000-0, January 2000.
96. Stuart, K.D., Mogawer, W.S., and Romero, P., (1999). "Validation of the Superpave Asphalt Binder and Mixture Tests that Measure Rutting Susceptibility Using an Accelerated Loading Facility." *Rep. No. FHWA-RD-99-204*, Federal Highway Administration, McLean, VA.

97. Chen, D., Bilyeu, J., Scullion, T., Lin, D., and Zhou, F., "Forensic Evaluation of Premature Failures of Texas Specific Pavement Study-1 Sections." *Journal of Performance and Construction Facility*, Vol. 17, pp. 67-74, Nov. 2 2003.
98. Brown, E.R., Prowell, B., Cooley, A., Zhang, J., and Powell, R.B., "Evaluation of Rutting Performance on the 2000 NCAT Test Track," Preprints, *Journal of the Association of Asphalt Paving Technologists*, March 2004.
99. David, T., West, R., Priest, A., Powell, B., Selvaraj, I., Zhang, J., and Brown, R., Phase II NCAT Test Track Results, NCAT Report 06-05, National Center for Asphalt Technology, December 2006.
100. Gokhale, S., Choubane, B., Byron, T., and Tia, M., Rut Initiation Mechanisms in Asphalt Mixtures as Generated Under Accelerated Pavement Testing, Transportation Research Record 1940, 2005, pp. 136-145.
101. Claessen, A.I.M., Edwards, J.M., Sommer, P., and Uge, P., Asphalt Pavement Design, The Shell Method, Proceedings of the 4rd International Conference on the Structural Design of Asphalt Pavements, Vol. I, Ann Arbor, MI, 1977, pp. 39-74.
102. Brown, S.F., and Brunton, J.M., Improvements to Pavement Subgrade Strain Criterion, ASCE. *Journal of Transportation Engineering,* 110(6), 1984.
103. Brown, S.F., Achievements and Challenges in Asphalt Pavement Engineering, the ISAP Distinguished Lecture series, delivered in Seattle, WA, August 1997.
104. Huekelom, W., and Klomp, A.J.G., Consideration of Calculated Strains at Various Depths in Connection with the Stability of Asphalt Pavements, Proceedings of the 2nd International Conference on the Structural Design of Asphalt Pavements, Vol. I, Ann Arbor, MI, 1967.
105. Monismith, C.L., Permanent Deformation Studies of Pavements, FCP Research Progress Review Report, San Francisco, CA, 1973.
106. McLean, D.B., Permanent Deformation Characteristics of Asphalt Concrete, Ph.D. Dissertation, University of California, Berkeley, CA, 1973.
107. Romain, J.E., Rut Depth Prediction in Asphalt Pavements, Research Report No. 150, Centre de Recherches Routieres, Brasseks, Belgium, 1969.
108. Barksdale, R.D., Laboratory Evaluation of Rutting in Base Course Materials, Proceedings of the 3rd International Conference on the Structural Design of Asphalt Pavements, Vol. I, London, England, 1972.
109. Morris, J., and Haas, R.C.G., Designing for Rutting in Asphalt Pavements, Canadian Technical Asphalt Association Annual Meeting, 1972.
110. *Guide for Mechanistic–Empirical Design of New and Rehabilitated Pavement Structures.* Final Report, NCHRP Project 1-37A. Transportation Research Board, National Research Council, Washington, D.C., March 2004. http://trb.org/mepdg/guide.htm.
111. Charles Schwartz, Improving Mechanistic-Empirical Models for Predicting HMA Rutting, Presented at 2006 Symposium on Models Used to Predict Pavement Performance, Laramie, WY. http://www.petersenasphaltconference.org/download/Schwartz%20Improving%20Mechanistic-Empirical%20Models%20for%20Predicting%20HMA%20Rutting.pdf
112. Kenis, W.J., *Predictive Design Procedure, VESYS User's Manual: An Interim Design Method for Flexible Pavement Using the VESYS Structural Subsystem*. Final Report No. FHWA-RD-77-154, FHWA, Washington D.C., 1978.

113. Kenis, W.J., and Wang, W., (1997) "Calibrating Mechanistic Flexible Pavement Rutting Models From Full Scale Accelerated Tests, Proceedings of the Eighth International Conference on Asphalt Pavements, Vol. I, pp. 663-672, Seattle, WA.
114. Epps, J.A., Hand, A., Seeds, S., Scholz, T., Alavi, S., Ashmore, C., Monismith, C.L., Deacon, J.A., Harvey, J.T., and Leahy, R.B., "Recommended Performance-Related Specifications for Hot-Mix Asphalt Construction." *NCHRP Report 455,* National Cooperative Highway Research Program, Transportation Research Board, National Research Council, Washington, D.C., 2002, 496 pp.
115. Lytton, R. L., et al. (1993). "Development and Validation of Performance Prediction Model and Specifications for Asphalt Binders and Paving Mixes." The Strategic Highway Research Program Project Report SHRP-A-357.
116. Brown, S.F., et al., Independent Review of the Mechanistic-Empirical Pavement Design Guide and Software, Research Results Digest 307, Transportation Research Board, September 2006.
117. Brown, S.F., Design Considerations for Pavement and Rail Track Foundations, Ed. Correia and Loizos, Geotechnics in Pavement and Railway Design and Construction, Athens, GA, pp. 61-72, 2003.
118. Lekarp, F., Isacsson, U., and Dawson, A., State of the Art. II: Permanent Strain Response of Unbound Aggregates. *Journal of Transportation Engineering*, ASCE, Vol. 126, No. 1, pp. 76-83, 2000.
119. Duncan, J.M., and Chang, C.Y., Nonlinear Analysis of Stress and Strain in Soils. J*ournal of the Soil Mechanics and Foundations Division*, ASCE, 96(SM5), pp. 1629-1653, 1970.
120. Barksdale, R.D., *Laboratory Evaluation of Rutting in Base Course Materials*. Proc. 3rd International Conference on the Structural Design of Asphalt Pavements, Vol. 1, Ann Arbor, MI, pp. 161-174. 1972.
121. Monismith, C.L., Ogawa, L., and Freeme, C.R., *Permanent Deformation Characteristics of Subgrade Soils due to Repeated Loading*. Transportation Research Record, No. 537, Transportation Research Board, National Research Council, Washington D.C., pp. 1-17, 1975.
122. Kenis, W.J., *Predictive Design Procedure, VESYS User's Manual: An Interim Design Method for Flexible Pavement Using the VESYS Structural Subsystem*. Final Report No. FHWA-RD-77-154, FHWA, Washington D.C., 1978.
123. Lentz, R.W., and Baladi, G.Y., *Constitutive Equation for Permanent Strain of Sand Subjected to Cyclic Loading*. Transportation Research Record, No. 810, Transportation Research Board, National Research Council, Washington D.C., pp. 50-53, 1981.
124. Tseng, K-H., and Lytton, R.L., *Prediction of Permanent Deformation in Flexible Pavement Materials*. Implication of Aggregates in the Design, Construction, and Performance of Flexible Pavements, ASTM STP 1016, ASTM, Philadelphia, PA, pp. 154-172, 1989.
125. Ullidtz, P., *Modeling of Granular Materials Using the Discrete Element Method*. Proceedings of the Eight International Conference on Asphalt Pavements, Seattle, WA, pp. 757-769, 1997.
126. Ceratti, J.A., Washington, P.N., Wai, Y.Y.G., and Jose, A., *Rutting of Thin Pavements: Full-Scale Study*. Transportation Research Record, No. 1716, Transportation Research Board, National Research Council, Washington D.C., pp. 82-88, 2000.

127. Park, S.W., *Evaluation of Accelerated Rut Development in Unbound Pavement Foundations and Load Limits on Load-Zoned Pavements*. Ph.D. Dissertation, Texas A&M University, College Station, TX, 2000.
128. Applied Research Associates. *Guide for Mechanistic-Empirical Design of New and Rehabilitated Pavement Structures*. Final Report, NCHRP 1-37A, Champaign, IL, 2004.
129. Zhou, F., and Scullion, T., *VESYS5 Rutting Model Calibrations with Local Accelerated Pavement Test Data and Associated Implementation*. Report No. FHWA/TX-03/9-1502-01-2, Texas Transportation Institute, College Station, TX, 2002.
130. Uzan, J., *Permanent Deformation in Flexible Pavements*. Journal of Transportation Engineering, ASCE, Vol. 130, No. 1, pp. 6-13, 2004.
131. Henning, T.F.P., Dunn, R.C. M., Parkman, C.C., and Brass, J., *Long-Term Pavement Performance (LTPP) Studies in New Zealand – A Progress Update*. NZIHT & Transit NZ 8th Annual Conference, pp. 1-19, 2006.
132. Mishalani, R.G., and Kumar, A., *Impact of Overlays on Pavement Rutting and Their Interactions with Design and Material Quality*. Transportation Research Record, No. 1869, Transportation Research Board, National Research Council, Washington D.C., pp. 97-105, 2004.
133. Archilla, A.R., and Madanat. S., *Estimation of Rutting Models by Combining Data from Different Sources*. Journal of Transportation Engineering, ASCE, Vol. 127, No. 5, pp. 379-389, 2001.
134. Scullion, T., Uzan, J., Hilbrich, S., and Chen, P., Thickness Design Systems for Pavements Containing Soil Cement Bases, PCA R&D Serial No. 2863, Portland Cement Association, Skokie, Ill, 2007.
135. Goetz, W.H., and Wood, L.E., *Highway Engineering Handbook*, 1st Ed., K.B. Woods, Ed., McGraw-Hill, New York, NY, 1960, pp. 18-52 to 18-92.
136. The Asphalt Institute, *Mix Design Methods for Asphalt Concrete (MS-2)*, 6th Ed., Lexington, KY, 1997.
137. Sousa, J., Craus, J., and Monismith, C.L., Summary Report on Permanent Deformation in Asphalt Concrete, SHRP A/IR/91-104, Strategic Highway Research Program, National Research Council, Washington, D.C., 1991.
138. Cominsky, R.J., Huber, G.A., Kennedy, T.W., and Anderson, M., *The Superpave Mix Design Manual for New Construction and Overlays*, SHRP-A-407, Strategic Highway Research Program, National Research Council, Washington, D.C., 1994.
139. Christensen, D.W., Bonaquist, R., and Cooley, A., A Mix Design Manual for Hot-Mix Asphalt, NCHRP 9-33, Draft Interim Report, May 2005.
140. Witczak, M.W., Kaloush, K., Pellinen, T., El-Basyouny, M., and Von Quintus, H., Simple Performance Test for Superpave Mix Design, NCHRP Report 465, National Cooperative Highway Research Program, Washington, D.C., 2002.
141. Tangella, S., Rao, C.S., Craus, J., Deacon, J.A., and Monismith, C.L., Summary Report on Fatigue Response of Asphalt Mixtures, TM-UCB-A-003A-89-3, Prepared for Strategic Highway Research Program, Project A-003-A, University of California, Berkeley, CA, February 1990.
142. Witczak, M.W., Kaloush, K., Pellinen, T., El-Basyouny, M., and Von Quintus, H., *Simple Performance Test for Superpave Mix Design*, NCHRP Report 465, National Cooperation Highway Research Program, Washington, D.C., 2002.

143. Walubita, L.F., Epps-Martin, A., Jung, S.H., Glover, C.J., Park, E.S., Chowdhury, A., and Lytton, R. L., *Comparison of Fatigue Analysis Approaches for Two Hot Mix Asphalt Concrete (HMAC) Mixtures*, Draft TxDOT Technical Research Report FHWA/TX-05/0-4468-2, October 2005.
144. Kim, Y.R., Lee, H.J., and Little, D.N., Fatigue Characterization of Asphalt Concrete Using Viscoelasticity and Continuum Damage Theory, *Journal of the Association of Asphalt Paving Technologists*, Vol. 66, 1997, pp. 520-569.
145. Zhou, F., Hu, S., Scullion, T., Qi, X., Chen, D., and Claros, G., Development and Verification of Overlay Tester Based Fatigue Cracking Prediction Approach, *Journal of Association of Asphalt Paving Technologists*, San Antonio, TX, March 12-14, 2007.
146. Scullion, T., "Perpetual Pavements in Texas: The State of the Practice," Report FHWA/TX-05/0-4822-1, Texas Transportation Institute, College Station, TX, 2006.
147. AASHTO. *AASHTO Designation: TP 62-03, Standard Method of Test for Determining Dynamic Modulus of Hot Mix Asphalt Concrete Mixtures*, *AASHTO Standards,* Washington D.C., 2001.
148. Sebesta, S., Harris, P., and Liu, W., "Improving Lab Compaction Methods for Roadway Base Materials," Research Report 0-5135-2, Texas Transportation Institute, Texas A&M University, College Station, TX, 2006.
149. Andrei, D., "Development of a Predictive Model for the Resilient Modulus of Unbound Materials," Ph.D. Dissertation, Department of Civil and Environmental Engineering, Arizona State University, Tempe, AZ, May 2003.

APPENDIX A

OT FOR FRACTURE PROPERTIES OF HMA MIXES

It is well known that HMA mixtures are complex materials. However, for simplicity and practical applications, HMA mixtures are often assumed to be quasi-elastic materials represented by dynamic modulus and Poisson's ratio. With this assumption, the well-known Paris' law shown in Equation 1 can be used to describe crack propagation of HMA mixtures (*1*).

$$\frac{dc}{dN} = A(\Delta K)^n \tag{1}$$

where:

c = crack length,
N = number of load repetitions,
dc/dN = crack speed or rate of crack growth,
ΔK = change of stress intensity factor (SIF), and
A, n = fracture properties of material.

In view of Equation 1, it can be seen that the information required for determining fracture properties (A and n) includes 1) the SIF corresponding to any specific crack length (c) and 2) crack length (c) corresponding to a specific number of load repetitions (N). The proposed approach for determining the SIF and crack length (c) is discussed as follows:

- Determination of SIF

A two dimensional (2D) finite element (FE) program named *2D-CrackPro* was developed to analyze the SIF under the OT testing. In the *2D-CrackPro* program, the desired $1/\sqrt{r}$ stress singularity in the crack tip region was met by placing the mid-side nodes of two adjacent sides of an 8-node isoparametric element at the one-fourth distance mark from the common corner node (*2*). The accuracy of this program has been verified by comparing the computed SIFs of an infinite slab with a center crack with those given in "*the stress analysis of cracks handbook*" (*3*).

Figure A1 shows the 2D FE mesh plus the singularity elements used. Since Poisson's ratio has minor influence on SIF, a constant Poisson's ratio (υ=0.35) was used for all the analyses. With the above quasi-elastic assumption, it has been found that the SIF is proportional to dynamic modulus (E) of the overlay tester (OT) specimen and the specified maximum opening displacement (MOD). Therefore, the SIFs corresponding to variable crack length (c) were calculated at an assumed condition: 1) dynamic modulus of the OT specimen: E =1 MPa, and 2) MOD = 1 mm. The results are presented in Figure A2. To facilitate implementation, a regression equation shown in Figure A2 was developed for the SIF versus crack length at the condition of E=1 MPa and MOD = 1 mm.

For any other *E* and *MOD* combination, the corresponding SIF can be determined by the following equation:

$$SIF = 0.2911 * E * MOD * c^{-0.4590} \quad (2)$$

where:

SIF = stress intensity factor, MPa*mm$^{0.5}$,
E = dynamic modulus, MPa,
MOD = maximum opening displacement, mm, and
c = crack length, mm.

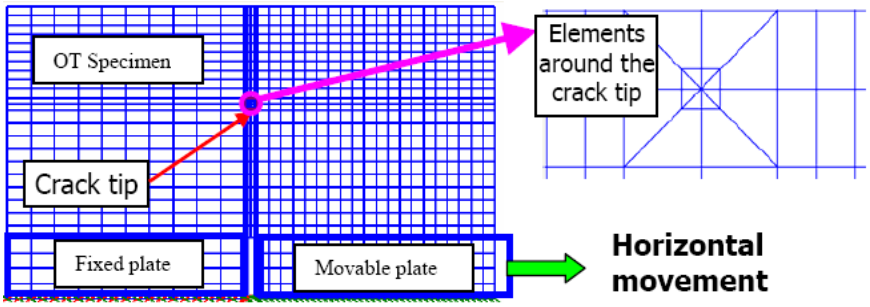

Figure A1. A 2-D FE Mesh of the OT System.

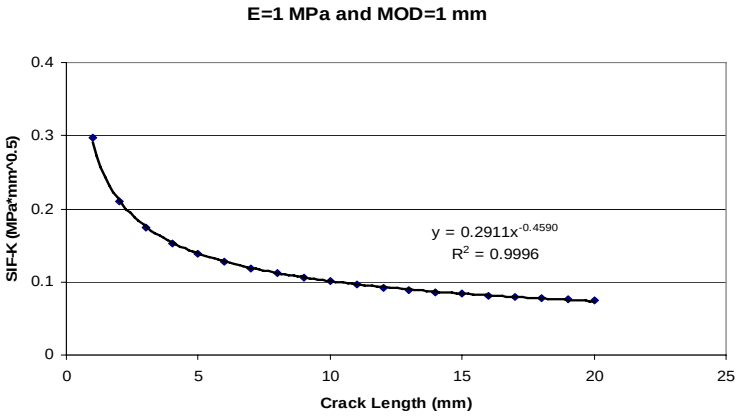

Figure A2. Calculated SIF vs. Crack Length.

Additionally, it can be seen that the SIF shown in Figure A2 decreases rapidly at the beginning, and its decreasing rate becomes smaller and smaller with crack length growth. This observation indicates that the initial crack propagation stage is very important to determine reasonable fracture properties of HMA mixtures, which means that the required fracture properties can be determined from the initial stage of the OT testing (perhaps within 15 minutes). This feature separates the OT from other types of fracture tests (such as, direct tension test [*4, 5, 6*], indirect tension test [*7*]), because the other tests often focused on the late crack propagation stage where the SIF increased rapidly so that these tests generally take a very long time (say hours).

- Determination of crack length (c)

To monitor crack length growth, researchers have used several different techniques such as crack foil (*5*). Recently, Seo et al. applied a Digital Image Correlation (DIC) technique to monitor crack propagation and crack length (*6*). The DIC is a non-contact, full-field displacement (or strain) measurement system that analyzes the displacement (or strain) by comparing digital images of a deformed specimen with that of an initial undeformed specimen. Compared with other techniques, the DIC is one of most advanced techniques for monitoring crack propagation. However, using the DIC system will definitely increase the difficulty and cost of running the OT. Fortunately, there is an alternative method used for estimating crack length, namely the backcalculation approach, which has been successfully used by Jacobs (*5*) and Roque et al. (*7*) to backcalculate the crack length from the recorded load or displacements. However, this backcalculation approach needs to be calibrated.

Three assumptions listed below were made for establishing the theoretical relationship between an equivalent crack length and the maximum load required to reach a specified MOD.

1) An equivalent (or ideal) crack starts from the bottom at the center of the OT specimen and propagates vertically to the top surface of the specimen.
2) The reduction of maximum load from the first cycle is attributed to crack growth.
3) As assumed previously, HMA mixtures are quasi-elastic and are represented by a dynamic modulus and Poisson's ratio (υ=0.35).

With the above three assumptions, the maximum load required to reach a MOD is proportional to the dynamic modulus of the OT specimen and decreases with crack length growth, provided that the MOD is constant. To exclude the influence of the dynamic modulus and the MOD, the maximum load corresponding to any crack length was normalized to the maximum load corresponding to "zero" crack length which is determined through extrapolation. Figure A3 shows the relationship between the normalized maximum load (*y-axis*) and crack length (*x-axis*). A corresponding regression equation is also presented in Figure A3.

Since the maximum load at each cycle is automatically recorded during the OT testing, it is easy to develop the relationship between the normalized maximum load at each cycle and the number of cycles. Finally, combining with Figure A3, crack growth rate (dc/dN) can be calculated.

- Determination of fracture properties: A and n

With known SIF (K) and crack growth rate (dc/dN), the fracture properties (A and n) can be readily determined. Figure A4 shows the five steps of determining fracture properties (A and n) of HMA mixtures. Currently, a Microsoft Excel® macro named *TTI-OT* is under development to automatically analyze the OT test results and determine fracture properties (A and n).

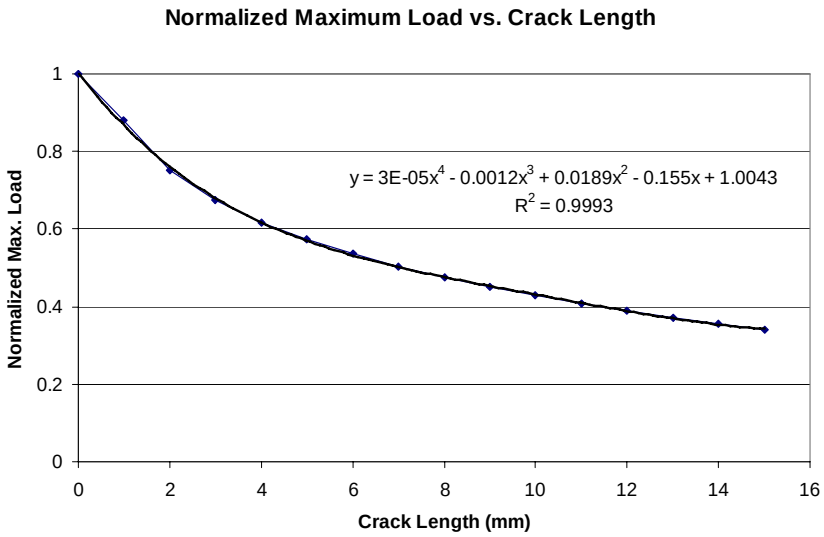

Figure A3. Normalized Maximum Load vs. Crack Length.

In summary, this section focused on developing the methodology of determining fracture properties (*A* and *n*) using the OT. As listed below, this OT based methodology for fracture properties has several desirable features:

1. Specimen size (150 mm long by 75 mm wide by 38 mm high): This size of specimen can be easily cut from samples compacted by the SGC or from field cores.
2. Specimen preparation: Neither a hole in the center nor a notch at the bottom of the specimen is required, since a crack is always initiated in the first cycle due to large opening displacement.
3. Testing time: In contrast to other fracture types of tests (i.e., IDT or repeated direct tension test), which generally take long testing time, the OT for fracture properties (*A* and *n*) can generally be done within 15 minutes.

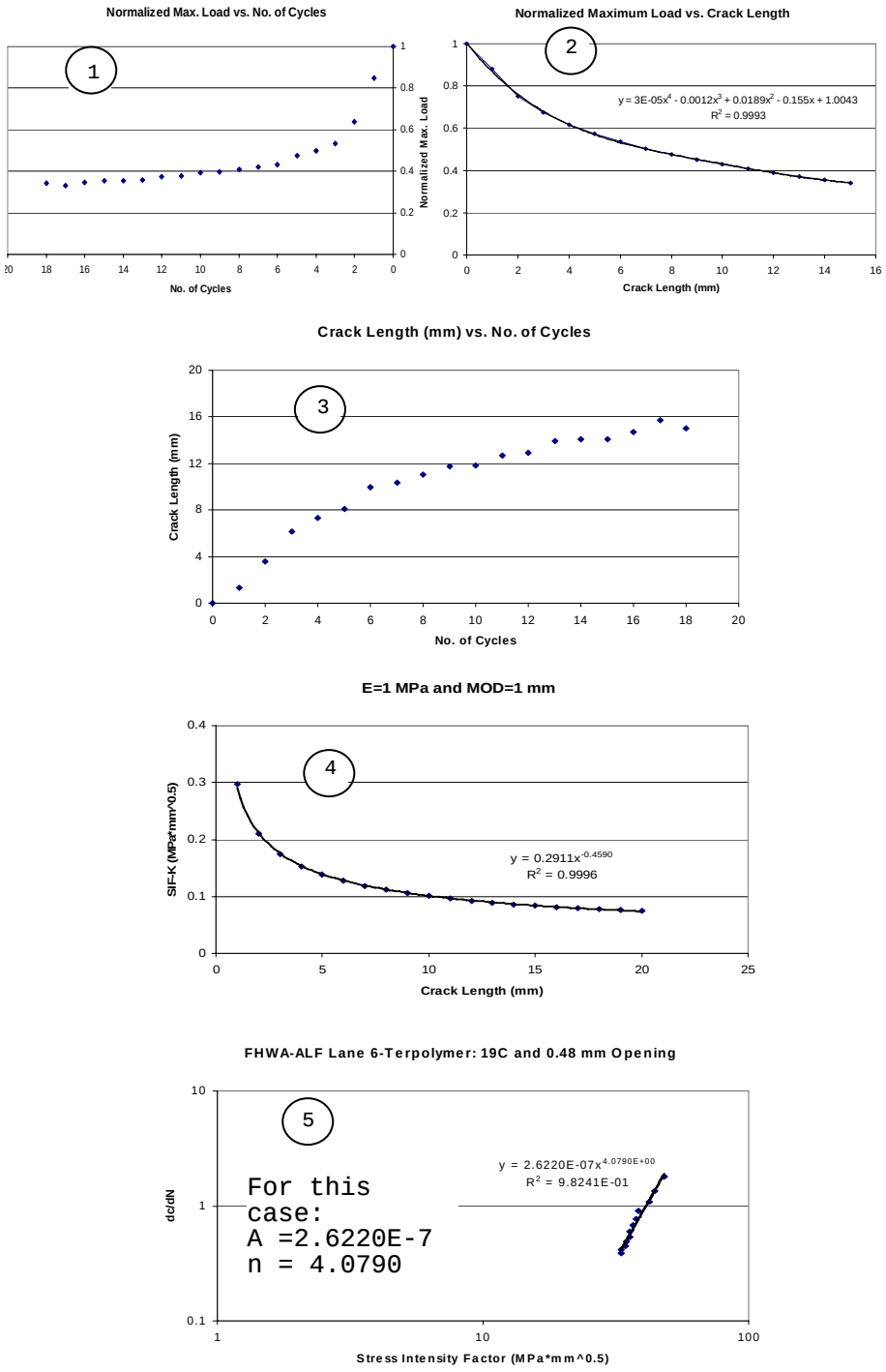

Figure A4. Determination of Fracture Properties: *A* and *n*.

APPENDIX A REFERENCES

1. Paris, P.C., and Erdogan, F., A Critical Analysis of Crack Propagation Laws, *Transactions of the ASME, Journal of Basic Engineering*, Series D, 85, No. 3, 1963.
2. Barsoum, R.S., On the Use of Isoparametric Elements in Linear Fracture Mechanics, *International Journal of Numerical Methods in Engineering*, Vol. 10, pp. 25, 1976.
3. Tada, H., Paris, P.C., and Irwin, G.R., *The Stress Analysis of Cracks Handbook*, 3rd Ed., New York, ASME Press, 2000.
4. Molenaar, A.A.A., "Structural Performance and Design of Flexible Road Constructions and Asphalt Concrete Overlays," Ph.D. Dissertation, *Delft University of Technology,* 1983.
5. Jacobs, M.M. J., *Crack Growth in Asphaltic Mixes*, Ph.D. Dissertation, Delft University of Technology, Road Railraod Research Laboratory, The Netherlands, 1995.
6. Seo, Y., Kim, Y.R., Schapery, R.A., Witczak, M.W., and Bonaquist, R., A Study of Crack-Tip Deformation and Crack Growth in Asphalt Concrete Using Fracture Mechanics, *Journal of the Association of Asphalt Paving Technologists,* Vol. 73, 2004, pp. 200-228.
7. Roque, R., Zhang, Z., and B. Sankar, B., Determination of Crack Growth Rate Parameters of Asphalt Mixtures Using the Superpave IDT, *Journal of the Association of Asphalt Paving Technologists,* Vol. 68, 1999, pp. 404-433.

APPENDIX B

VESYS TEST PROTOCOL FOR ASPHALT MIXES

1. Test Samples

1.1 Size

Testing shall be performed on 100 mm (4 inch) diameter by 150 mm (6 inch) high or more test samples from laboratory or cores from field.

1.2 Aging

For laboratory compacted samples, mixture shall be aged in accordance with the short-term oven aging procedure in AASHTO PP2.

1.3 Gyratory Specimens

For laboratory compacted samples, prepare 150 mm (6 inch) high samples to the required air void content in accordance with AASHTO TP-4. The gyratory compactor is shown in Figure B1.

1.4 End Preparation

The ends of all test samples shall be smooth and perpendicular to the axis of the specimen. Prepare the ends of the samples by milling with a single- or double-bladed saw. To ensure that the sawed samples have parallel ends, the sample ends shall have a cut surface waviness height within a tolerance of ±0.05 mm across any diameter.

1.5 Air Void Content

Determine the air void content of the final test sample in accordance with AASHTO T269. Reject samples with air voids that differ by more than 0.5 percent from the target air voids.

1.6 Replicates

The number of test samples required depends on the number of axial strain measurements made per sample and the desired accuracy of the average permanent deformation. Normally, two replicates are acceptable for each sample with two LVDTs.

2. Test Sample Instrumentation

2.1 Attach mounting studs for the axial LVDTs to both sides of the sample with 180 degree intervals (in plan view) using epoxy cement (shown in Figure B2). Make sure the studs are aligned.

Figure B1. Superpave Gyratory Compactor.

Figure B2. Samples with Studs.

2.2 The gauge length for measuring axial deformations shall be 100 mm ± 1 mm (4 inch ± 0.04 inch). The gauge length is normally measured between the stud centers.

3. Test Procedures

3.1 The recommended test protocol for Alpha and Mu used in the VESYS program consists of testing the asphalt mix at two temperatures with specified stress level. Table B1 shows the recommended test temperatures and associated stress level.

Table B1. Recommended Test Temperatures and Associated Stress Level.

Test Temperature (°F [°C])	Test Stress Level (psi [kPa])
77 (25)	30 (207)
104 (40)	20 (138)

3.2 Place the test sample in the environmental chamber and allow it to equilibrate to the specified testing temperature. A dummy specimen with a temperature sensor mounted at the center can be monitored to determine when the specimen reaches the specified test temperature. In the absence of the dummy specimen, Table B2 provides a recommended temperature equilibrium time for samples starting from room temperature (77°F).

Table B2. Recommended Equilibrium Times.

Test Temperature (°F [°C])	Time (min.)
77 (25)	10
104 (40)	30

3.3 After temperature equilibrium is reached, place one of the friction-reducing end treatments on top of the platen at the bottom of the loading frame. Place the sample on top of the lower end treatment, and mount the axial LVDTs to the studs glued to the sample. Adjust the LVDT to near the end of its linear range to allow the full range to be available for the accumulation of compressive permanent deformation.

3.4 Place the upper friction-reducing end treatment and platen on top of the sample. Center the specimen with the load actuator visually in order to avoid eccentric loading.

3.5 Apply a contact load equal to 5 percent of the total load level that will be applied to the specimen, while monitoring the proper response of the LVDTs (i.e., check for proper direction sensing for all LVDTs).

3.6 Close the environmental chamber and allow sufficient time (normally 10 to 15 minutes) for the temperature to stabilize within the specimen and the chamber.

3.7 After the time required for the sample to reach the testing temperature, apply the haversine load that yields the desired stress on the specimen. The procedure uses a loading cycle of 1.0 Hz frequency and consists of applying 0.1 second haversine load followed by a 0.9 second rest period. The maximum applied load (P_{max}) is the maximum

total load applied to the sample, including the contact and cyclic load: $P_{max} = P_{contact} + P_{cyclic}$.

3.8 The contact load ($P_{contact}$) is the vertical load placed on the sample to maintain a positive contact between loading strip and the sample: $P_{contact} = 0.05 \times P_{max}$.

3.9 The cyclic load (P_{cyclic}) is the load applied to the test sample that is used to calculate the permanent deformation parameters: $P_{cyclic} = P_{max} - P_{contact}$.

3.10 Apply the haversine load (P_{cyclic}) and continue until 5000 cycles or until the sample fails and results in excessive tertiary deformation, whichever comes first.

3.11 During the load applications, record the load applied and the axial deflection measured from all LVDTs through the data acquisition system. All data should be collected in real time and collected so as to minimize phase errors due to sequential channel sampling. It is recommended to use the data acquisition of the cycles shown in Table B3.

Table B3. Suggested Data Collection for VESYS Rutting Test.

Data Collected during Cycles	Data Collected during Cycles	Data Collected during Cycles
1 through 10	598 through 600	2723 through 2725
18 through 20	698 through 700	2998 through 3000
28 through 30	798 through 800	3248 through 3250
48 through 50	898 through 900	3498 through 3500
78 through 80	998 through 1000	3723 through 3725
98 through 100	1248 through 1250	3998 through 4000
148 through 150	1498 through 1500	4248 through 4250
198 through 200	1723 through 1725	4498 through 4500
298 through 300	1998 through 2000	4723 through 4725
398 through 400	2248 through 2250	4998 through 5000
498 through 500	2498 through 2500	

4. Calculations

4.1 Calculate the average axial deformation for each specimen by averaging the readings from the two axial LVDTs. Convert the average deformation values to total axial strain by dividing by the gauge length (100 mm [4 inch]).

4.2 Compute the cumulative axial permanent strain and resilient strain (ε_r) at the 100^{th} load repetition.

4.3 Plot the cumulative axial permanent strain versus number of loading cycles in log-log space (Figure B3). Determine the permanent deformation parameters, intercept (a), and slope (b) from the linear portion of the permanent strain curve.

4.4 Compute the rutting parameters: Alpha, Mu:

$$\mu = \frac{ab}{\varepsilon_r}$$

$$\alpha = 1 - b$$

5. Report

Report all sample information including mix identification, dates of manufacturing (or cored) and testing, sample diameter and length, volumetric properties, stress levels used, and axial permanent deformation parameters: α, μ (or ε_r, a, b).

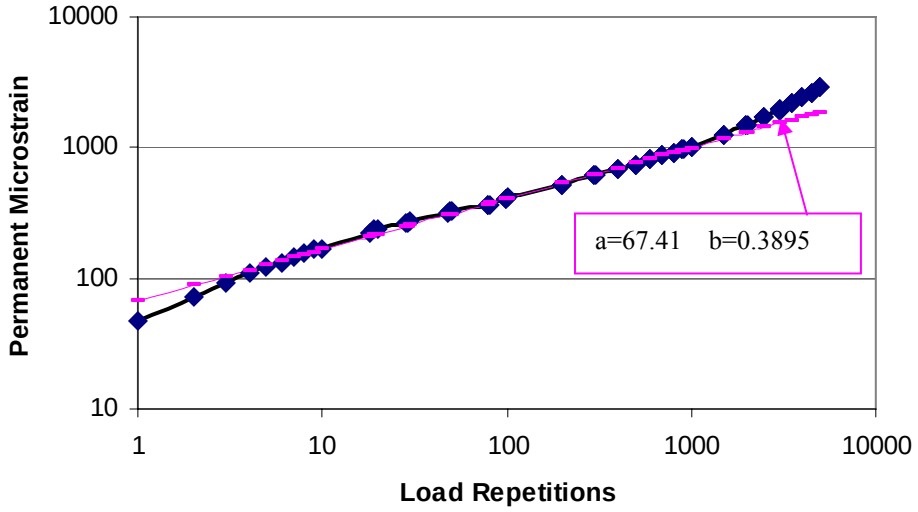

Figure B3. Plot of Regression Constants "a" and "b" from Log Permanent Strain – Log Number of Loading Cycles.

Example: Alpha and Mu Calculation

ε_r = 88.1250

A = 67.4100

b = 0.3895

μ = a x b/ε_r =67.41 x 0.3895/88.125 = 0.2979

α = 1 – b = 1 – 0.3895 = 0.6105

APPENDIX C

RECOMMENDED PERMANENT DEFORMATION AND RESILIENT MODULUS LABORATORY TEST PROTOCOLS FOR UNBOUND GRANULAR BASE/SUBBASE MATERIALS AND SUBGRADE SOILS

1. Scope

1.1. This test method describes the laboratory preparation and testing procedures for the determination of permanent deformation and resilient modulus (M_r) of unbound granular base/subbase materials and subgrade soils for pavement performance prediction. The stress conditions used in the test represent the ranges of stress states likely to be developed beneath flexible pavements subjected to moving wheel loads. This test procedure has been adapted from the standard test methods given in the VESYS user manual, National Cooperative Highway Research Program (NCHRP) 1-28A Draft Report (unpublished), and AASHTO designation: T294-92, TP46, and T292-91.

1.2. The methods described herein are applicable to laboratory-molded samples of unbound granular base/subbase materials and subgrade soils.

1.3. In this test procedure, stress states used for permanent deformation and resilient modulus testing are based upon whether the specimen is located in the base/subbase or the subgrade. Specimen size for testing depends upon the maximum particle size of the material.

1.4. The values of permanent deformation and resilient modulus determined from these procedures are the measures of permanent deformation properties and the elastic modulus of unbound granular base/subbase materials and subgrade soils with the consideration of their stress-dependency.

1.5. Resilient modulus values can be used with structural response analysis models to calculate the pavement structural response to wheel loads, and with the combination of permanent deformation properties and pavement design procedures to predict rutting performance.

1.6. This standard may involve hazardous materials, operations, and equipment. This standard does not purport to address all of the safety concerns associated with its use. It is the responsibility of the user of this standard to consult and establish appropriate safety and health practices and determine the applicability of regulatory limitations prior to use.

2. Referenced Documents

2.1. AASHTO Standards:

T88 Particle Size Analysis of Soils

T89 Determining the Liquid Limit of Soils

T90 Determining the Plastic Limit and the Plasticity Index of Soils

T100 Specific Gravity of Soils

T180 Moisture-Density Relations of Soils using a 454 kg (10 lb) Rammer and 457 mm (18 inch) Drop

T233 Density of Soil-in-Place by Block, Chunk, or Core Sampling

T292-91 Resilient Modulus of Subgrade Soils and Untreated Base/Subbase Materials

T296 Strength Parameters of Soils by Triaxial Compression

T265 Laboratory Determination of Moisture Content of Soils

3. Terminology

3.1. Unbound Granular Base and Subbase Materials – These include soil-aggregate mixtures and naturally occurring materials. No binding or stabilizing agent is used to prepare unbound granular base or subbase layers. These materials are classified as Type 1 and Type 2, as subsequently defined in 3.3 and 3.4.

3.2. Subgrade – Subgrade soils may be naturally occurring or prepared and compacted before the placement of subbase and/or base layers. These materials are classified as Type 1, Type 2, and Type 3, as subsequently defined in 3.3, 3.4, and 3.5.

3.3. Material Type 1 – Includes all unbound granular base and subbase materials and all untreated subgrade soils with maximum particle sizes greater than 9.5 mm (3/8 inch). All material greater than 25.4 mm (1.0 inch) shall be scalped off prior to testing.

Materials classified as Type 1 shall be molded in either a 152 mm (6 inch) diameter mold or a 102 mm (4 inch) diameter mold. Materials classified as Type 1 shall be compacted by impact or vibratory compaction.

3.4. Material Type 2 – Includes all unbound granular base and subbase materials and all untreated subgrade soils that have a maximum particle size less than 9.5 mm (3/8 inch) and that meet the criteria of less than 10 percent passing the 75 μm (No. 200) sieve. Materials classified as Type 2 shall be molded in a 102 mm (4 inch) diameter mold and compacted by vibratory compaction.

3.5. Material Type 3 – Includes all untreated subgrade soils that have a maximum particle size less than 9.5 mm (3/8 inch) and that meet the criteria of more than 10 percent passing the 75 mm (No. 200) sieve. Materials classified as Type 3 shall be molded in a 102 mm (4 inch) diameter mold and compacted by impact compaction.

3.6. Permanent Deformation – Permanent deformation is determined by repeated load compression tests on specimens of the unbound materials. Permanent deformation is the unrecovered deformation during the testing.

3.7. Resilient Modulus – The resilient modulus is determined by repeated load compression tests on test specimens of the unbound materials. Resilient modulus (M_r) is the ratio of the peak axial repeated deviator stress to the peak recoverable axial strain of the specimen.

3.8. Loading Wave Form – Test specimens are loaded using a haversine load pulse with 0.1-second loading and 0.9-second rest period.

3.9. Maximum Applied Axial Load (P_{max}) – The load applied to the sample consisting of the contact load and cyclic load (confining pressure is not included):

$$P_{max} = P_{contact} + P_{cyclic}$$

3.10. Contact Load ($P_{contact}$) – Vertical load placed on the specimen to maintain a positive contact between the loading ram and the specimen top cap. The contact load includes the weight of the top cap and the static load applied by the ram of the loading system.

3.11. Cyclic Axial Load – Repetitive load applied to a test specimen:

$$P_{cyclic} = P_{max} - P_{contact}$$

3.12. Maximum Applied Axial Stress (S_{max}) – The axial stress applied to the sample consisting of the contact stress and the cyclic stress (the confining stress is not included):

$$S_{max} = P_{max}/A$$

where: A = cross sectional area of the sample.

3.13. Cyclic Axial Stress – Cyclic (resilient) applied axial stress:

$$S_{cyclic} = P_{cyclic}/A$$

3.14. Contact Stress ($S_{contact}$) – Axial stress applied to a test specimen to maintain a positive contact between the specimen cap and the specimen:

$$S_{contact} = P_{contact}/A$$

The contact stress shall be maintained so as to apply a constant anisotropic confining stress ratio:

$$(S_{contact} + S_3)/S_3 = 1.2$$

where: S_3 = confining pressure.

3.15. S_3 is the applied confining pressure in the triaxial chamber (i.e., the minor principal stress σ_3).

3.16. e_r is the resilient (recoverable) axial deformation due to S_{cyclic}.

3.17. ε_r is the resilient (recoverable) axial strain due to S_{cyclic}:

$$\varepsilon_r = e_r/L$$

where: L = distance between measurement points for resilient axial deformation, e_r.

3.18. e_p is the permanent (unrecoverable) axial deformation due to S_{cyclic}.

3.19. ε_p is the permanent (unrecoverable) axial strain due to S_{cyclic}:

$$\varepsilon_p = e_p/L$$

where: L = distance between measurement points for permanent axial deformation, e_p.

3.20. Resilient Modulus (M_r) is defined as:

$$M_r = S_{cyclic}/\varepsilon_r$$

3.21. Load duration is the time interval the specimen is subjected to a cyclic stress pulse.

3.22. Cycle duration is the time interval between the successive applications of a cyclic stress (usually 1.0 second).

4. Summary of Method

4.1. A repeated axial stress of fixed magnitude, load duration, and cycle duration is applied to a cylindrical test specimen. The test is performed in a triaxial cell, and the specimen is subjected to a repeated (cyclic) stress and a constant confining stress provided by means of cell air pressure. Both total resilient (recoverable) and permanent axial deformation responses of the specimen are recorded and used to calculate the permanent deformation properties and the resilient modulus.

5. Significance and Use

5.1. The resilient modulus test results provide a basic constitutive relationship between stiffness and stress state of pavement materials for use in the structural analysis of layered pavement systems. Furthermore, permanent deformation properties of pavement materials also can be determined from the first 10,000 cycles of the repeated load test. The information is critical for pavement rutting performance prediction. The permanent deformation and resilient modulus tests simulate the conditions in a pavement with the application of moving wheel loadings.

6. Permanent Deformation and Resilient Modulus Test Apparatus

6.1. Triaxial Pressure Chamber – The pressure chamber is used to contain the test specimen and the confining fluid during the test. A typical triaxial chamber suitable for use in resilient modulus testing of soils is shown in Figure C1. The axial deformation is measured internally, directly on the specimen, using normal gauges with rubber bands (shown in Figure C2), an optical extensometer, non-contact sensors, or clamps. For soft and very soft subgrade specimens (i.e., $S_u < 36$ kPa or 750 psf, where S_u is the undrained shear strength of the soil), rubber bands or clamps should not be used since they may damage the specimen. However, a pair of LVDTs extending between the top and bottom platens can be used to measure axial deformation of these weak soils.

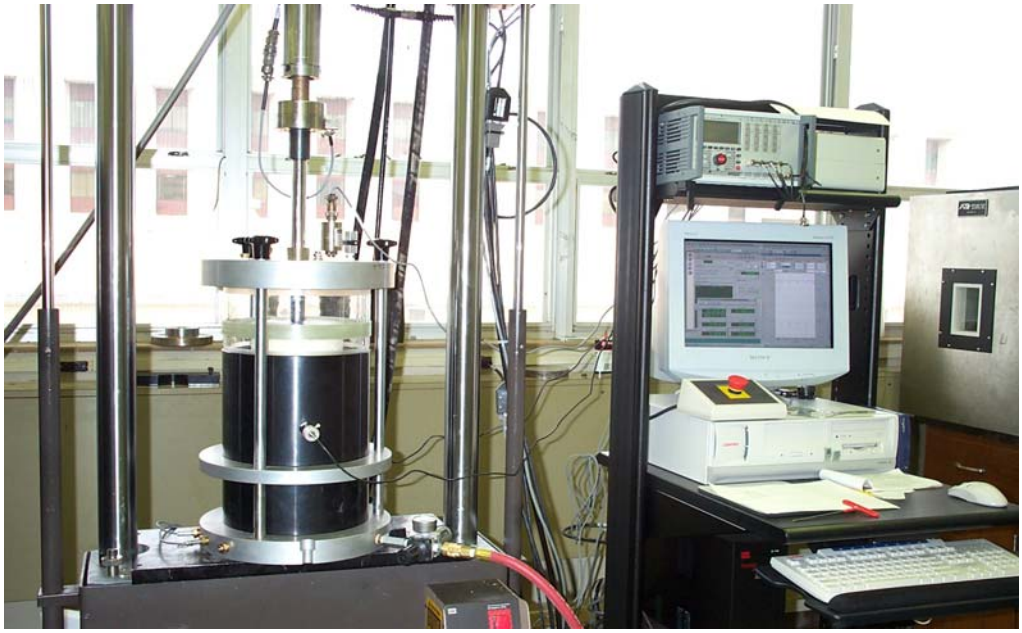

Figure C1. Triaxial Cell and Test System.

Figure C2. Sample with Instruments.

6.1.1. Air shall be used in the triaxial chamber as the confining fluid for all testing.

6.1.2. The chamber shall be made of suitable transparent material (such as polycarbonate).

6.2. Loading Device – The loading device shall be a top-loading, closed-loop electro-hydraulic testing machine with a function generator that is capable of applying repeated cycles of a haversine-shaped load pulse. Each pulse shall have a 0.1 second duration followed by a rest period of 0.9 second duration for base/subbase materials and 0.2 second duration followed by a rest period of 0.8 second duration for subgrade materials. For non-plastic granular material, it is permissible, if desired, to reduce the rest period to 0.4 second to shorten testing time; the loading time may be increased to 0.15 second if required.

6.2.1. All conditioning and testing shall be conducted using a haversine-shaped load pulse. The electro-hydraulic system generated haversine waveform and the response waveform shall be displayed to allow the operator to adjust the gains to ensure they coincide during conditioning and testing.

6.3. Load and Specimen Response Measuring Equipment:

6.3.1. The axial load measuring device should be an electronic load cell, which is preferred to be located inside the triaxial cell. The load cell should have the capacities presented in Table C1.

Table C1. Load Cell Capacity.

Sample Diameter mm (in)	Max. Load Capacity kN (lb)	Required Accuracy N (lb)
102 (4.0)	8.9 (2000)	±17.8 (±4)
152 (6.0)	22.24 (5000)	±22.24 (±5)

Note 1 – During periods of permanent deformation and resilient modulus testing, the load cell shall be monitored and checked once every two weeks or after every 50 permanent deformation and resilient modulus tests with a calibrated proving ring to assure that the load cell is operating properly. An alternative to using a proving ring is to inset an additional calibrated load cell and independently measure the load applied by the original cell. Additionally, the load cell shall be checked at any time there is a suspicion of a load cell problem. The testing shall not be conducted if the testing system is found to be out of calibration.

6.3.2. The chamber pressures shall be monitored with conventional pressure gauges, manometers, or pressure transducers accurate to 0.69 kPa (0.1 psi).

6.3.3. Axial Deformation: Axial deformation is to be measured with displacement transducers referenced to gauge points contacting the specimen with rubber bands as shown in Figure C2. Deformation shall be measured over approximately the middle half of the specimen. Axial deformations shall be measured at a minimum of two locations 180 degrees apart (in a plain view), and a pair of spring-loaded LVDTs are placed on the specimen at quarter points. Spring-loaded LVDTs shall be used to maintain a positive contact between the LVDTs and the surface on which the tips of the transducers rest.

Note 2 – Table C2 summarizes the specifications for spring-loaded LVDTs.

Table C2. Specifications for Axial LVDTs.

Material/specimen Diameter (inch)		Min. Range (inch)	Approximate Resilient Specimen Displacement (inch)
Aggregate Base	6	±0.25	0.001
	4	±0.10	0.00065
Subgrade Soil (sand and cohesive)	4	±0.25	0.0014

Note: For soft subgrade soil, permanent and resilient displacement shall be measured over entire specimen height.

Note 3 – Misalignment or dirt on the shaft of the transducer can cause the shafts of the LVDTs to stick. The laboratory technician shall depress and release each LVDT back and forth a number of times prior to each test to assure that they move freely and are not sticking. A cleaner/lubricant specified by the manufacturer shall be applied to the transducer shafts on a regular basis.

6.3.4. Data Acquisition: An analog-to-digital (A/D) data acquisition system is required. The overall system should include automatic data reduction to minimize production. Suitable signal excitation, conditioning, and recording equipment is required for simultaneous recording of axial load and deformations. The system should meet or exceed the following additional requirements: (1) 25 μs A/D conversion time; (2) 12-bit resolution; (3) single-

or multiple-channel throughput (gain = 1), 30 kHz; (4) software selectable gains; (5) measurement accuracy of full scale (gain = 1) of ±0.02 percent; and (6) non-linearity of ±0.5 percent. The signal shall be clean and free of noise. Filtering the output signal during or after data acquisition is discouraged. If a filter is used, it should have a frequency higher than 10 to 20 Hz. A supplemental study should be made to ensure correct peak readings are obtained from filtered data compared to unfiltered data. A minimum of 200 data points from each LVDT shall be recorded per load cycle.

6.4. Specimen Preparation Equipment–A variety of equipment is required to prepare compacted specimens that are representative of field conditions. Use of different materials and different methods of compaction in the field requires the use of varying compaction techniques in the laboratory.

6.5. Miscellaneous Apparatus–This includes calipers, micrometer gauge, steel rule (calibrated to 0.5 mm [0.02 inch]), rubber membranes from 0.25 to 0.79 mm (0.02 to 0.031 inch) thickness, rubber O-rings, vacuum source with bubble chamber and regulator, membrane expander, porous stones (subgrade), 6.4 mm (0.25 inch) thick porous stones or bronze discs (base/subbase), scales, moisture content cans, and data sheets.

6.6. Periodic System Calibration–The entire system (transducers, signal conditioning, and recording devices) shall be calibrated every two weeks or after every 50 tests. Daily and other periodic checks of the system may also be performed as necessary. No permanent deformation and resilient modulus testing will be conducted unless the entire system meets the established calibration requirements.

7. Preparation of Test Specimens

7.1. The following guidelines, based on the sieve analysis test results, shall be used to determine the test specimen size:

7.1.1. Use 152 mm (6.0 inch) diameter and 305 mm (12 inch) high specimens for all materials with maximum particle sizes greater than 19 mm (0.75 inch). All

material of particle size greater than 25.4 mm (1.0 inch) shall be scalped off prior to testing.

7.1.2. Use 102 mm (4.0 inch) diameter and 204 mm (8.0 inch) high specimens for all materials with maximum particle sizes less than 19 mm (0.75 inch).

7.2. Laboratory Compacted Specimens–Reconstituted test specimens of all types shall be prepared to the specified or in situ dry density (γ_d) and moisture content (w). Laboratory compacted specimens shall be prepared for all unbound granular base and subbase material and for all subgrade soils.

7.2.1. Moisture Content–For in situ materials, the moisture content of the laboratory compacted specimen shall be the in situ moisture content for that layer obtained in the field using T238. If data are not available on in situ moisture content, refer to Section 7.2.3.

7.2.1.1. The moisture content of the laboratory compacted specimen should not vary from the required value by more than ±0.5 percent for all materials.

7.2.2. Compacted Density–The density of a compacted specimen shall be the in-place dry density obtained in the field for that layer using T239 or other suitable methods. If these data are not available on in situ density, then refer to Section 7.2.3.

7.2.2.1. The dry density of a laboratory compacted specimen should not vary more than ±1.0 percent from the target dry density for that layer.

7.2.3. If either the in situ moisture content or the in-place dry density is not available, then use the optimum moisture content and 95 percent of the maximum dry density by using T180 for the base/subbase and 95 percent of T99 for the subgrade.

7.2.3.1. The moisture content of the laboratory compacted specimen should not vary from the required value by more than ±0.5 percent for all materials. The dry density of a laboratory compacted specimen

should not vary more than ±1.0 percent from the target dry density for that layer.

7.2.4. Sample Reconstitution – Reconstitute the specimen for all materials. The target moisture content and density to be used in determining needed material qualities are given in Section 7.2. After this step is completed, specimen compaction can begin.

7.3. Compaction Methods and Equipment for Reconstituting Specimens:

7.3.1. Specimens of Type 1 materials shall be compacted by vibratory or impact compaction. The general method of vibratory compaction is given in T292-91. The general method of impact compaction is given in T292.

7.3.2. Specimens of Type 2 materials shall be compacted by vibratory compaction. The general method of vibratory compaction is presented in T292-92.

7.3.3. Specimens of Type 3 materials shall be compacted by impact compaction. The general method of impact compaction is given in T292-91.

8. Test Procedure

Following this test procedure, a permanent deformation and resilient modulus test is performed on all materials using a triaxial cell (confined).

8.1. Base/Subbase Materials

The procedure described in this section applies to all unbound granular base and subbase materials.

Apparatus and Sample Preparation

8.1.1. Assembly of the triaxial cell: If not already in place, place the specimen with end platens into position on the pedestal of the triaxial cell. Proper positioning of the specimen is extremely critical in applying a concentric load to the specimen. Couple the loading device to the specimen using a smooth steel ball. To center the specimen, slowly rotate the ball as the clearance between the load piston ball decreases and a small amount of load is applied to the specimen. Be sure the ball is concentric with the piston that applies the

load (watch the gap around the ball). Shift the specimen laterally to achieve a concentric loading.

8.1.2. Check and adjust the axial displacement measurement system, load cell, and data acquisition system, and make sure they are working properly.

8.1.3. If not already connected, connect the confining air pressure supply line to the triaxial chamber.

8.1.4. Open all valves on drainage lines leading to the inside of the specimen. This is necessary to develop confining pressure on the specimen.

8.1.5. Apply the specified conditioning confining pressure of 103.5 kPa (15.0 psi) to the test specimen. A contact stress equal to 20 percent of the confining pressure shall be applied to the specimen so that the load piston stays in contact with the top platen at all times.

8.1.6. Preconditioning: Apply 100 repetitions of a load equivalent to a maximum axial stress of 41.4 kPa (6 psi) and a corresponding cyclic stress of 20.7 kPa (3 psi) using a haversine-shaped, 0.1 second load pulse followed by 0.9 second rest period.

Permanent Deformation Test

8.1.7. Apply the haversine loading (P_{cyclic}) equivalent to a maximum axial stress of 227.7 kPa (33 psi) and a corresponding cyclic stress of 207 kPa (30 psi) using a haversine-shaped, 0.1 second load pulse followed by 0.9 second rest period, and continue until 10,000 cycles (2.8 hours) or until the specimen fails and the vertical permanent strain reaches 5 percent during the testing, whichever comes first. The total number of cycles or the testing time will depend on the stress levels applied.

8.1.8. During the load applications, record the load applied and the axial deformation measured from two LVDTs through the data acquisition system. Signal-to-noise ratio should be at least 10. All data should be collected in real time and collected/processed so as to minimize phase errors due to sequential channel sampling. In order to save storage space during data acquisition for

10,000 cycles, researchers recommend using the data acquisition of the cycles shown in Table C3.

Table C3. Suggested Data Collection for Triaxial Repeated Load Permanent Deformation Test for Granular Base and Subbase.

Data Collection During Cycles	Data Collection During Cycles	Data Collection During Cycles	Data Collection During Cycles
1-15	450	1300	4000
20	500	1400	4500
30	550	1500	5000
40	600	1600	5500
60	650	1700	6000
80	700	1800	6500
100	750	1900	7000
130	800	2000	7500
160	850	2200	8000
200	900	2400	8500
250	950	2600	9000
300	1000	2800	9500
350	1100	3000	10000
400	1200	3500	

Resilient Modulus Test

Specimen Testing–If the vertical permanent strain has neither reached 5 percent nor failed during permanent deformation test, use the same specimen to perform the resilient modulus test following the load sequence shown in Table C4. Begin by decreasing the maximum axial stress to 14.5 kPa (2.1 psi) (Sequence No. 1 Table C4), and set the confining pressure to 20.7 kPa (3 psi).

If the vertical permanent strain has reached 5 percent or failed during permanent deformation test, mold a new specimen, and then go back to section 8.1.1. In addition, reduce the load repetitions from 10,000 to 5000

during the repeated load permanent deformation test. If the sample again reaches 5 percent total vertical permanent strain during repeated load test, then the test shall be terminated. No further testing of this material is necessary. If not, perform the resilient modulus test following the load sequence shown in Table C4. Begin by decreasing the maximum axial stress to 14.5 kPa (2.1 psi) (Sequence No. 1 Table C4) and set the confining pressure to 20.7 kPa (3 psi).

8.1.10. Apply 100 repetitions of the corresponding cyclic axial stress using a haversine-shaped load pulse consisting of a 0.1 second load followed by a 0.9 second rest period. Record the average recovered deformations from each LVDT separately for the last five cycles.

8.1.11. Increase the maximum axial stress to 30 kPa (4.2 psi) and the confining pressure to 41.4 kPa (6 psi) (Sequence No. 2 Table C4), and repeat the previous step at this new stress level.

8.1.12. Continue the test for the remaining stress sequences in Table C4 (3 to 30) recording the vertical recovered deformation. If at any time the total permanent strain of the sample exceeds 5 percent, stop the test and report the result on the appropriate worksheet.

Table C4. Permanent Deformation and Resilient Modulus Test Sequence for Granular Base and Subbase.

Sequence	Confining Pressure		Contact Stress		Cyclic Stress		Maximum Stress		$N_{rep.}$
	kPa	psi	kPa	psi	kPa	psi	kPa	psi	
Preconditioning	103.5	15.0	20.7	3.0	20.7	3.0	41.4	6.0	100
Permanent Deformation	103.5	15.0	20.7	3.0	207.0	30.0	227.7	33.0	10000
1	20.7	3.0	4.1	0.6	10.4	1.5	14.5	2.1	100
2	41.4	6.0	8.3	1.2	20.7	3.0	29.0	4.2	100
3	69.0	10.0	13.8	2.0	34.5	5.0	48.3	7.0	100
4	103.5	15.0	20.7	3.0	51.8	7.5	72.5	10.5	100
5	138.0	20.0	27.6	4.0	69.0	10.0	96.6	14.0	100
6	20.7	3.0	4.1	0.6	20.7	3.0	24.8	3.6	100
7	41.4	6.0	8.3	1.2	41.4	6.0	49.7	7.2	100
8	69.0	10.0	13.8	2.0	69.0	10.0	82.8	12.0	100
9	103.5	15.0	20.7	3.0	103.5	15.0	124.2	18.0	100
10	138.0	20.0	27.6	4.0	138.0	20.0	165.6	24.0	100
11	20.7	3.0	4.1	0.6	41.4	6.0	45.5	6.6	100
12	41.4	6.0	8.3	1.2	82.8	12.0	91.1	13.2	100
13	69.0	10.0	13.8	2.0	138.0	20.0	151.8	22.0	100
14	103.5	15.0	20.7	3.0	207.0	30.0	227.7	33.0	100
15	138.0	20.0	27.6	4.0	276.0	40.0	303.6	44.0	100
16	20.7	3.0	4.1	0.6	62.1	9.0	66.2	9.6	100
17	41.4	6.0	8.3	1.2	124.2	18.0	132.5	19.2	100
18	69.0	10.0	13.8	2.0	207.0	30.0	220.8	32.0	100
19	103.5	15.0	20.7	3.0	310.5	45.0	331.2	48.0	100
20	138.0	20.0	27.6	4.0	414.0	60.0	441.6	64.0	100
21	20.7	3.0	4.1	0.6	103.5	15.0	107.6	15.6	100
22	41.4	6.0	8.3	1.2	207.0	30.0	215.3	31.2	100
23	69.0	10.0	13.8	2.0	345.0	50.0	358.8	52.0	100
24	103.5	15.0	20.7	3.0	517.5	75.0	538.2	78.0	100
25	138.0	20.0	27.6	4.0	690.0	100.0	717.6	104.0	100
26	20.7	3.0	4.1	0.6	144.9	21.0	149.0	21.6	100
27	41.4	6.0	8.3	1.2	289.8	42.0	298.1	43.2	100
28	69.0	10.0	13.8	2.0	483.0	70.0	496.8	72.0	100
29	103.5	15.0	20.7	3.0	724.5	105.0	745.2	108.0	100
30	138.0	20.0	27.6	4.0	966.0	140.0	993.6	144.0	100

8.1.13. At the completion of this test, reduce the confining pressure to zero, and remove the sample from the triaxial chamber.

8.1.14. Remove the membrane from the specimen, and use the entire specimen to determine moisture content in accordance with T265.

8.2. Coarse-Grained Subgrade Soils

This procedure is used for all laboratory compacted specimens of subgrade soils for which the percent passing 75 μm (No. 200) sieve is less than 35 percent. Reconstructed specimens will usually be compacted directly on the pedestal of the triaxial cell.

Apparatus and Sample Preparation

8.2.1. Assembly of the triaxial cell: Refer to section 8.1.1.

8.2.2. Set up the axial displacement measurement system, and verify it is working properly.

8.2.3. If not already connected, connect the confining air pressure supply line to the triaxial chamber.

8.2.4. Open all valves on drainage lines leading to the inside of the specimen. This is necessary to develop confining pressure on the specimen.

8.2.5. Apply the specified conditioning confining pressure of 27.6 kPa (4.0 psi) to the test specimen. Apply a contact stress equal to 20 percent of the confining pressure to the specimen so that the load piston stays in contact with the top platen at all times.

8.2.6. Preconditioning: Apply 100 repetitions of a load equivalent to a maximum axial stress of 12.4 kPa (1.8 psi) and a corresponding cyclic stress of 6.9 kPa (1 psi) using a haversine-shaped, 0.2 second load pulse followed by 0.8 second rest period.

Permanent Deformation Test

8.2.7. Apply the haversine loading (P_{cyclic}) equivalent to a maximum axial stress of 60.7 kPa (8.8 psi) and a corresponding cyclic stress of 55.2 kPa (8 psi) using a haversine-shaped, 0.2 second load pulse followed by 0.8 second rest period, and continue until 10,000 cycles (2.8 hours) or until the specimen fails and/or the vertical permanent strain reaches 5 percent during the testing, whichever comes first. The total number of cycles or the testing time will depend on the stress levels applied.

8.2.8. During the load applications, record the load applied and the axial deformation measured from two LVDTs through the data acquisition system. All data should be collected in real time and collected/processed so as to minimize phase errors due to sequential channel sampling. In order to save storage space during data acquisition for 10,000 cycles, it is recommended to use the data acquisition of the cycles shown in Table C5.

Table C5. Suggested Data Collection for Triaxial Repeated Load Permanent Deformation Test for Granular Subgrades.

Data Collection During Cycles	Data Collection During Cycles	Data Collection During Cycles	Data Collection During Cycles
1-15	450	1300	4000
20	500	1400	4500
30	550	1500	5000
40	600	1600	5500
60	650	1700	6000
80	700	1800	6500
100	750	1900	7000
130	800	2000	7500
160	850	2200	8000
200	900	2400	8500
250	950	2600	9000
300	1000	2800	9500
350	1100	3000	10000
400	1200	3500	

Resilient Modulus Test

8.2.9. Specimen Testing–If the vertical permanent strain has neither reached 5 percent nor failed during permanent deformation test, use the same specimen to perform the resilient modulus test following the load sequence shown in Table C6. Begin by decreasing the maximum axial stress to 9.66 kPa (1.4 psi) (Sequence No. 1 Table C6), and set the confining pressure to 13.8 kPa (2 psi).

If the vertical permanent strain has reached 5 percent or failed during permanent deformation test, mold a new specimen, and then go back to section 8.2.1. In addition, reduce the load repetitions from 10,000 to 5,000 during the repeated load permanent deformation test. If the sample again reaches 5 percent total vertical permanent strain during the repeated load test, then terminate the test. No further testing of this material is necessary. If not, perform the resilient modulus test following the load sequence shown in Table C6. Begin by decreasing the maximum axial stress to 9.66 kPa (1.4 psi) (Sequence No. 1 Table C6), and set the confining pressure to 13.8 kPa (2 psi).

Table C6. Permanent Deformation and Resilient Modulus Test Sequence for Granular Subgrades.

Sequence	Confining Pressure		Contact Stress		Cyclic Stress		Maximum Stress		N_{rep}
	kPa	Psi	kPa	psi	kPa	Psi	kPa	psi	
Preconditioning	27.6	4.0	5.5	0.8	6.9	1.0	12.4	1.8	100
Permanent Deformation	27.6	4.0	5.5	0.8	55.2	8.0	60.7	8.8	10,000
1	13.8	2.0	2.8	0.4	6.9	1.0	9.7	1.4	100
2	27.6	4.0	5.5	0.8	13.8	2.0	19.3	2.8	100
3	41.4	6.0	8.3	1.2	20.7	3.0	29.0	4.2	100
4	55.2	8.0	11.0	1.6	27.6	4.0	38.6	5.6	100
5	82.8	12.0	16.6	2.4	41.4	6.0	58.0	8.4	100
6	13.8	2.0	2.8	0.4	13.8	2.0	16.6	2.4	100
7	27.6	4.0	5.5	0.8	27.6	4.0	33.1	4.8	100
8	41.4	6.0	8.3	1.2	41.4	6.0	49.7	7.2	100
9	55.2	8.0	11.0	1.6	55.2	8.0	66.2	9.6	100
10	82.8	12.0	16.6	2.4	82.8	12.0	99.4	14.4	100
11	13.8	2.0	2.8	0.4	27.6	4.0	30.4	4.4	100
12	27.6	4.0	5.5	0.8	55.2	8.0	60.7	8.8	100
13	41.4	6.0	8.3	1.2	82.8	12.0	91.1	13.2	100
14	55.2	8.0	11.0	1.6	110.4	16.0	121.4	17.6	100
15	82.8	12.0	16.6	2.4	165.6	24.0	182.2	26.4	100
16	13.8	2.0	2.8	0.4	41.4	6.0	44.2	6.4	100
17	27.6	4.0	5.5	0.8	82.8	12.0	88.3	12.8	100
18	41.4	6.0	8.3	1.2	124.2	18.0	132.5	19.2	100
19	55.2	8.0	11.0	1.6	165.6	24.0	176.6	25.6	100
20	82.8	12.0	16.6	2.4	248.4	36.0	265.0	38.4	100

8.2.10. Apply 100 repetitions of the corresponding cyclic axial stress using a haversine-shaped load pulse consisting of a 0.2 second load followed by a 0.8 second rest period. Record the average recovered deformations from each LVDT separately for the last five cycles.

8.2.11. Increase the maximum axial stress to 19.32 kPa (2.8 psi), and set the

confining pressure to 27.6 kPa (4 psi) (Sequence No. 2 Table C6), and repeat the previous step at this new stress level.

8.2.12. Continue the test for the remaining stress sequences in Table C6 (3 to 20) recording the vertical recovered deformation. If at any time the total permanent strain of the sample exceeds 5 percent, stop the test and report the result on the appropriate worksheet.

8.2.13. At the completion of this test, reduce the confining pressure to zero, and remove the sample from the triaxial chamber.

8.2.14. Remove the membrane from the specimen, and use the entire specimen to determine moisture content in accordance with T265.

8.3. Cohesive Subgrade Soils

This procedure is used for all laboratory compacted specimens of subgrade soils for which the percent passing 75 µm (No. 200) sieve is greater than 35 percent. Reconstructed specimens will usually be compacted directly on the pedestal of the triaxial cell.

Apparatus and Sample Preparation

8.3.1. Assembly of the Triaxial Cell: Refer to section 8.1.1.

8.3.2. Stiff to Very Stiff Specimens–For stiff and very stiff cohesive specimens ($S_u >$ 36 kPa (750 psf), here S_u designates the undrained shear strength of the soil), axial deformation should preferably be measured either directly on the specimen or between the solid end platens using grouted specimen ends.

8.3.3. Soft Specimens–The axial deformation of soft subgrade soils ($S_u <$ 36 kPa [750 psf]) should not be measured using a rubber band circled on the specimen. If the measured resilient modulus is less than 69,000 kPa (10,000 psi), axial deformation can be measured between top and bottom platens. An empirical correction is not required for irregular specimen end contacts for these low modulus soils. If the resilient modulus is greater than 69,000 kPa (10,000 psi), follow the procedure in section 8.3.2.

8.3.4. Install Axial Displacement Device: Carefully install the axial displacement instrumentation selected under 8.3.2 or 8.3.3. For top to bottom displacement measurement, attach the LVDTs or proximity gauges on steel or aluminum bars extending between the top and bottom platens. If the rubber band or clamps are used, place the rubber band or clamps at the quarter points of the specimen using two height gauges to ensure that clamps are positioned horizontally at the correct height. Each height gauge can consist of two circular aluminum rods machined to the correct length. These rods are placed on each side of the clamp to ensure proper location. Then ensure the displacement instrumentations are working properly by displacing each device and observing the resulting voltage output as shown by the data acquisition system.

8.3.5. Refer to section 8.1.1.

8.3.6. Set up the axial displacement measurement system, and verify it is working properly.

8.3.7. Open all valves on drainage lines leading to the inside of the specimen. This is necessary to develop confining pressure on the specimen.

8.3.8 If not already connected, connect the confining air pressure supply line to the triaxial chamber.

8.3.9 Apply the specified conditioning confining pressure of 27.6 kPa (4.0 psi) to the test specimen. Apply a contact stress equal to 20 percent of the confining pressure to the specimen so that the load piston stays in contact with the top platen at all times.

8.3.10. Preconditioning–Apply 100 repetitions of a load equivalent to a maximum axial stress of 12.4 kPa (1.8 psi) and a corresponding cyclic stress of 6.9 kPa (1 psi) using a haversine-shaped, 0.2 second load pulse followed by 0.8 second rest period.

Permanent Deformation Test

8.3.11. Apply the haversine-loading (P_{cyclic}) equivalent to a maximum axial stress of

53.8 kPa (7.8 psi) and a corresponding cyclic stress of 48.3 kPa (7 psi) using a haversine-shaped, 0.2 second load pulse followed by 0.8 second rest period and continue until 10,000 cycles (2.8 hours) or until the specimen fails and the vertical permanent strain reaches 5 percent during the testing, whichever comes first. The total number of cycles or the testing time will depend on the stress levels applied.

8.3.12. During the load applications, record the load applied and the axial deformation measured from all LVDTs through the data acquisition system. Signal-to-noise ratio should be at least 10. All data should be collected in real time and collected/processed so as to minimize phase errors due to sequential channel sampling. In order to save storage space during data acquisition for 10,000 cycles, it is recommended to use the data acquisition cycles shown in Table C7.

Table C7. Suggested Data Collection for Triaxial Repeated Load Permanent Deformation Test for Fine-Grained Subgrades.

Data Collection During Cycles	Data Collection During Cycles	Data Collection During Cycles	Data Collection During Cycles
1-15	450	1300	4000
20	500	1400	4500
30	550	1500	5000
40	600	1600	5500
60	650	1700	6000
80	700	1800	6500
100	750	1900	7000
130	800	2000	7500
160	850	2200	8000
200	900	2400	8500
250	950	2600	9000
300	1000	2800	9500
350	1100	3000	10000
400	1200	3500	

Resilient Modulus Test

8.3.13. Specimen Testing–If the vertical permanent strain has neither reached 5 percent nor failed during permanent deformation test, use the same specimen to perform the resilient modulus test following the load sequence shown in

Table C6. Begin by decreasing the maximum axial stress to 38.6 kPa (5.6 psi) (Sequence No. 1 Table C8), and set the confining pressure to 55.2 kPa (8 psi).

If the vertical permanent strain has reached 5 percent or failed during the permanent deformation test, mold a new specimen, and then go back to section 8.3.1. In addition, reduce the load repetitions from 10,000 to 5000 during the repeated load permanent deformation test. If the sample again reaches 5 percent total vertical permanent strain during the repeated load test, then terminate the test. No further testing of this material is necessary. If not, perform the resilient modulus test following the load sequence shown in Table C4. Begin by decreasing the maximum axial stress to 38.6 kPa (5.6 psi) (Sequence No. 1 Table C8), and set the confining pressure to 55.2 kPa (8 psi).

8.3.14. Apply 100 repetitions of the corresponding cyclic axial stress using a haversine-shaped load pulse consisting of a 0.2 second load followed by a 0.8 second rest period. Record the average recovered deformations from each LVDT separately for the last five cycles.

8.3.15. Decrease the maximum axial stress to 35.9 kPa (5.2 psi), set the confining pressure to 41.4 kPa (6 psi) (Sequence No. 2 Table C8), and repeat the previous step at this new stress level.

8.3.16. Continue the test for the remaining stress sequences in Table C8 (3 to 16) recording the vertical recovered deformation. If at any time the total permanent strain of the sample exceeds 5 percent, stop the test and report the result on the appropriate worksheet.

8.3.17. At the completion of this test, reduce the confining pressure to zero, and remove the sample from the triaxial chamber.

8.3.18. Remove the membrane from the specimen, and use the entire specimen to determine moisture content in accordance with T265.

Table C8. Permanent Deformation and Resilient Modulus Test Sequence for Fine-Grained Subgrades.

Sequence	Confining Pressure		Contact Stress		Cyclic Stress		Maximum Stress		$N_{rep.}$
	kPa	psi	kPa	psi	KPa	psi	kPa	Psi	
Preconditioning	27.6	4.0	5.5	0.8	6.9	1.0	12.4	1.8	100
Permanent Deformation	27.6	4.0	5.5	0.8	48.3	7.0	53.8	7.8	10,000
1	55.2	8.0	11.0	1.6	27.6	4.0	38.6	5.6	100
2	41.4	6.0	8.3	1.2	27.6	4.0	35.9	5.2	100
3	27.6	4.0	5.5	0.8	27.6	4.0	33.1	4.8	100
4	13.8	2.0	2.8	0.4	27.6	4.0	30.4	4.4	100
5	55.2	8.0	11.0	1.6	48.3	7.0	59.3	8.6	100
6	41.4	6.0	8.3	1.2	48.3	7.0	56.6	8.2	100
7	27.6	4.0	5.5	0.8	48.3	7.0	53.8	7.8	100
8	13.8	2.0	2.8	0.4	48.3	7.0	51.1	7.4	100
9	55.2	8.0	11.0	1.6	69.0	10.0	80.0	11.6	100
10	41.4	6.0	8.3	1.2	69.0	10.0	77.3	11.2	100
11	27.6	4.0	5.5	0.8	69.0	10.0	74.5	10.8	100
12	13.8	2.0	2.8	0.4	69.0	10.0	71.8	10.4	100
13	55.2	8.0	11.0	1.6	96.0	14.0	107.6	15.6	100
14	41.4	6.0	8.3	1.2	96.0	14.0	104.9	15.2	100
15	27.6	4.0	5.5	0.8	96.0	14.0	102.1	14.8	100
16	13.8	2.0	2.8	0.4	96.0	14.0	99.4	14.4	100

9. Calculations

Calculation of Permanent Strain

9.1. Calculate the average axial deformation for each specimen by averaging the readings from the two axial LVDTs. Convert the average deformation values to total axial strain by dividing by the gauge length, L (152 mm [6 inch] for 152 mm diameter sample; 102 mm (4 inch) for 102 mm diameter sample). Typical total axial strain versus time is shown in Figure C3.

9.2. Compute the cumulative axial permanent strain and resilient strain (ε_r) at 200th load repetition.

9.3. Plot the cumulative axial permanent strain versus the number of loading cycles in log space (shown in Figure C4). Determine the permanent deformation parameters, intercept (a) and slope (b), from the linear portion of the permanent strain curve (log-log scale), which is also demonstrated on Figure C4.

9.4. Compute the rutting parameters: Alpha, Mu

$$\mu = \frac{ab}{\varepsilon_r}$$

$$\alpha = 1 - b$$

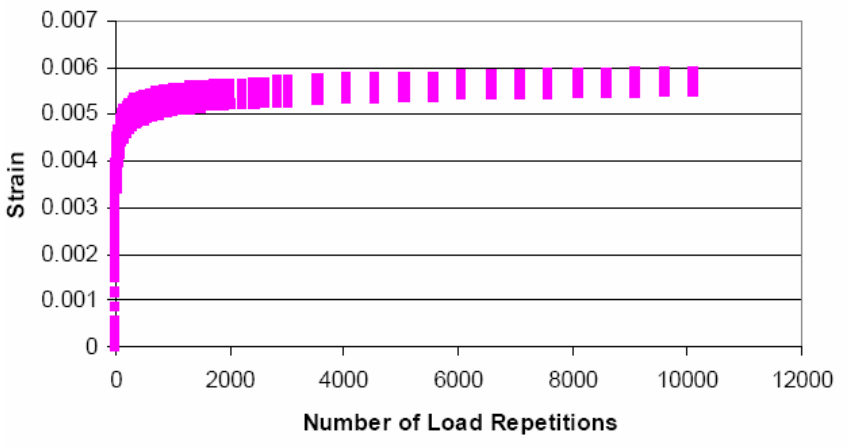

Figure C3. Triaxial Repeated Load Test Results: Strain vs. Number of Load Repetitions.

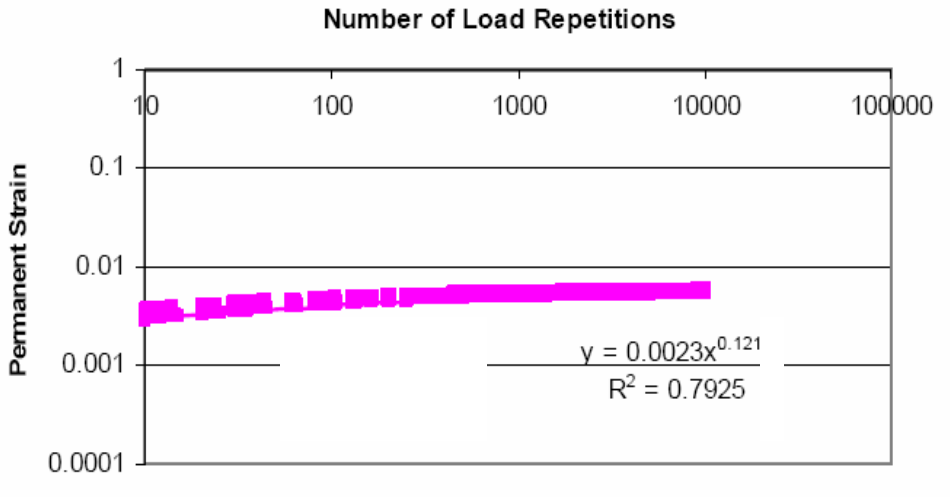

Figure C4. Permanent Strain vs. Number of Load Repetitions.

Calculation of Resilient Modulus

9.5. Perform the calculations to obtain resilient modulus values. The resilient modulus is computed from each of the last five cycles of each load sequence and then averaged. The data reduction processes should be fully automated to minimize the chance for human error.

9.6. Using nonlinear regression techniques fit the following resilient modulus model to the data obtained from the applied procedure. The equation for the normalized log-log k_1, k_2, k_3, k_6, and k_7 model is as follows:

$$M_R = k_1 p_a \left(\frac{\theta - 3k_6}{p_a} \right)^{k_2} \left(\frac{\tau_{oct}}{p_a} + k_7 \right)^{k_3}$$

$k_1, k_2 \geq 0$

$k_3, k_6 \leq 0$

$k_7 \geq 1$

where:

M_R = resilient modulus

θ = Bulk Stress, $\theta = \sigma_1 + \sigma_2 + \sigma_3$

τ_{oct} = Octahedral shear stress,

$$\tau_{oct} = \frac{1}{3}\sqrt{(\sigma_1 - \sigma_2)^2 + (\sigma_1 - \sigma_3)^2 + (\sigma_2 - \sigma_3)^2}$$

$\sigma_1, \sigma_2, \sigma_3$ = Principal Stresses

k = Regression constants

p_a = atmospheric pressure (14.7 psi)

Assign initial values of zero for k_6 and one for k_7; restrain all regression constants

according to the model. Report the constants k_1, k_2, k_3, k_6, and k_7, the ratio of the standard error of estimate, to the standard deviation and the square of the correlation coefficient.

10. Report

10.1. Permanent Deformation Test:

10.1.1. Report all specimen basic information including specimen identification, dates of manufacturing and testing, specimen diameter and length, confining pressure, stress levels used, and axial permanent deformation parameters: α, μ (or ε_r, a, and b).

10.2. Resilient Modulus Test:

10.2.1. Report all specimen basic information including specimen identification, dates of manufacturing and testing, specimen diameter, and length.

10.2.2. Report the average peak stress (σ_o) and strain (ε_o) for each confining pressure–cyclic stress combination tested.

10.2.3. For each confining pressure–cyclic stress combination tested, report the resilient modulus for each replicate test specimen.

10.2.4. Report nonlinear resilient modulus model and the model parameters: k_1, k_2, k_3, k_6, and k_7.